

INFORMATION TO USERS

This manuscript has been reproduced from the microfilm master. UMI films the text directly from the original or copy submitted. Thus, some thesis and dissertation copies are in typewriter face, while others may be from any type of computer printer.

The quality of this reproduction is dependent upon the quality of the copy submitted. Broken or indistinct print, colored or poor quality illustrations and photographs, print bleedthrough, substandard margins, and improper alignment can adversely affect reproduction.

In the unlikely event that the author did not send UMI a complete manuscript and there are missing pages, these will be noted. Also, if unauthorized copyright material had to be removed, a note will indicate the deletion.

Oversize materials (e.g., maps, drawings, charts) are reproduced by sectioning the original, beginning at the upper left-hand corner and continuing from left to right in equal sections with small overlaps.

**ProQuest Information and Learning
300 North Zeeb Road, Ann Arbor, MI 48106-1346 USA
800-521-0600**

UMI[®]

MULTICOMPONENT MULTIPHASE FLOW IN POROUS
MEDIA WITH TEMPERATURE VARIATION OR
ADSORPTION

A DISSERTATION
SUBMITTED TO THE DEPARTMENT OF PETROLEUM ENGINEERING
AND THE COMMITTEE ON GRADUATE STUDIES
OF STANFORD UNIVERSITY
IN PARTIAL FULFILLMENT OF THE REQUIREMENTS
FOR THE DEGREE OF
DOCTOR OF PHILOSOPHY

Jichun Zhu
March 2003

UMI Number: 3085248

**Copyright 2003 by
Zhu, Jichun**

All rights reserved.

UMI[®]

UMI Microform 3085248

**Copyright 2003 by ProQuest Information and Learning Company.
All rights reserved. This microform edition is protected against
unauthorized copying under Title 17, United States Code.**

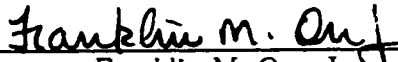
**ProQuest Information and Learning Company
300 North Zeeb Road
P.O. Box 1346
Ann Arbor, MI 48106-1346**

© Copyright 2003

by

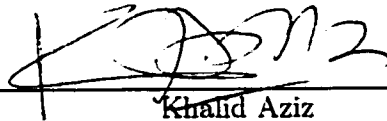
Jichun Zhu

I certify that I have read this thesis and that in my opinion it is fully adequate, in scope and in quality, as a dissertation for the degree of Doctor of Philosophy.



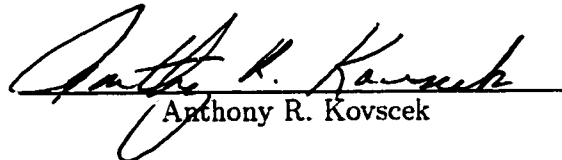
Franklin M. Orr, Jr.
(Principal Advisor)

I certify that I have read this thesis and that in my opinion it is fully adequate, in scope and in quality, as a dissertation for the degree of Doctor of Philosophy.



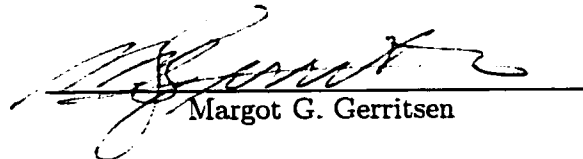
Khalid Aziz

I certify that I have read this thesis and that in my opinion it is fully adequate, in scope and in quality, as a dissertation for the degree of Doctor of Philosophy.



Anthony R. Kovscek

I certify that I have read this thesis and that in my opinion it is fully adequate, in scope and in quality, as a dissertation for the degree of Doctor of Philosophy.



Margot G. Gerritsen

Approved for the University Committee on Graduate Studies:

Abstract

Gas injection can serve as an effective enhanced recovery method for oil and gas production. With an assumption that the displacement is isothermal and without adsorption or desorption at the rock surfaces, an analytical theory has been established for solving the set of hyperbolic partial differential equations in one-dimension that describes the mass conservation of the individual fluid components using a method of characteristics approach. However, in some injection processes, the injection gas may be at a temperature that differs from that of the initial reservoir. In problems such as enhanced coal-bed methane recovery by CO_2 injection, adsorption and desorption play significant roles and are not negligible. The variation in temperature and adsorption and desorption of components changes the fluid properties and interacts with the propagation of the fluids.

In this work, the analytical theory is extended to consider the effects of variable temperature and adsorption and desorption of components from rock surfaces, and is applied to enhanced coal-bed methane and oil recovery separately. In both problems, the phase behavior is represented by the Peng-Robinson equation of state.

In enhanced coal-bed methane recovery by gas injection, we maintain the isothermal flow assumption and focus on the effect of adsorption/desorption of the gas components at the coal-bed surfaces. A mobile liquid phase is not considered in this section. The adsorption behavior is approximated by an extended Langmuir isotherm. Mixtures of CH_4 , CO_2 and N_2 are used to represent coal-bed and injection gases. Example solutions are presented for systems in which the initial gas has high CH_4 concentrations, and binary mixtures of CO_2 and N_2 are injected. The solutions obtained show that injection of N_2 - CO_2 mixtures rich in N_2 leads to relatively fast

initial recovery of CH_4 . Injection of mixtures rich in CO_2 gives slower initial recovery, increases breakthrough time, and decreases the injectant needed to sweep out the coal-bed.

When temperature is allowed to vary in enhanced oil recovery by gas injection, adsorption and desorption of fluid components at rock surfaces are neglected in the analysis. An energy balance is introduced to describe the flow of energy due to variation in temperature. Solution construction procedures are demonstrated through examples in one-component and binary systems. A careful examination of the solutions in binary systems reveals that for many cases the temperature fronts propagate slowly and separately from the composition fronts. The propagation of composition fronts is accompanied only by small temperature variation resulting from heat of condensation and vaporization. In this case, it is reasonable to assume isothermal flow at the downstream end, because the temperature variation occurs completely within the injected gas. However, under certain conditions, the temperature fronts catch up to and interact with trailing composition fronts. The simultaneous propagation of temperature and composition fronts is examined in detail for this scenario.

For both of the gas injection problems, a one-dimensional finite-difference scheme with single-point upstream weighting is developed to confirm the solutions obtained with the analytical approach, and yields satisfactory agreement. The computer time required for finite-difference simulations, however, is orders of magnitude higher than that of the analytical approach. More importantly, some of the subtle and fine structures revealed only by the analytical approach are obscured and become indistinguishable in finite-difference simulations due to numerical dispersion. Hence, the analytical solution method proves to be a useful tool to investigate individual aspects of multi-component multiphase flow through media without the effect of numerical dispersion at only a fraction of the computation cost of finite-difference simulations.

Acknowledgements

I would like to give thanks to my advisor, Professor Lynn Orr for his constant support, guidance, encouragement, tolerance and forgiveness over the years. If to this date I have accomplished anything, I couldn't have done it without him, and I owe it all to him.

I want to give thanks to Professor Tony Kovsky. I had very few opportunities to work with other faculty members besides my advisor, and I feel extremely lucky that working with Tony turned out to be very pleasant experience.

I want to thank Kristian Jessen for the enlightening discussion, and for letting me use some of his programs so I didn't have to reinvent the wheels.

I would also like to take this opportunity to thank Professor Khalid Aziz and Professor Margot Gerritsen for reading my dissertation, providing valuable comments, and serving on my defense committee, and Professor David Pollard for being the chairman of my defense committee.

Finally. I want to thank my family, and everyone else in my life, no matter my close friends, or those who make me sandwiches at the cafeteria, or the police officer who gave me speeding ticket. It is the people who lived through the days with me that made me the person I am today.

Contents

Abstract	iv
Acknowledgements	vi
1 Introduction	1
1.1 Theory of Two-Phase Multicomponent Flow in Porous Media at Constant Temperature	2
1.2 Gas Injection with Variable Temperature	3
1.3 Gas Injection for Enhanced Coal-Bed Methane Recovery	5
1.4 Summary	6
2 Mathematical Model	8
2.1 Assumptions and simplifications	8
2.2 Conservation of mass and energy	10
2.2.1 Eigenvalue problem and continuous solution	14
2.3 Continuous and discontinuous solutions	18
2.4 Solution construction procedure	20
3 Enhanced Coal Bed Methane Recovery	22
3.1 Introduction	22
3.2 Langmuir isotherm for adsorption and desorption	23
3.3 Mathematical Basis	25
3.4 Solution construction	26
3.4.1 Binary flow	27

3.4.2	Ternary flow	29
3.4.3	1D Finite-Difference Simulation	41
3.4.4	Example Solutions	44
3.4.5	Effect of Numerical Dispersion	55
3.5	Summary	55
4	Temperature Variation in One-Component Flow	59
4.1	Continuous Variation	60
4.2	Shocks	63
4.3	Examples of Single-Component Single-Phase Flow	65
4.3.1	Single-Component Single-Phase Flow of CH_4	65
4.3.2	Single-Component Single-Phase Flow of C_{10}	68
4.4	Summary	70
5	Temperature Variation in Binary Flow	73
5.1	Solutions in the Single-Phase Region	75
5.1.1	Continuous Variation in the Single-Phase Region	75
5.1.2	Discontinuous Solution in the Single-Phase Region	79
5.1.3	Examples in the Single-Phase Region	79
5.2	Solutions in the Two-Phase Region	84
5.2.1	Continuous Variation in the Two-Phase Region	84
5.2.2	Discontinuous Solution in the Two-Phase Region	93
5.2.3	Examples in the Two-Phase Region	94
5.3	Solutions across the Two-Phase Boundary	96
5.3.1	Continuous Variation across the Two-Phase Boundary	96
5.3.2	Phase-Change Shocks	102
5.4	Example Solutions	110
5.4.1	Solution Type I	111
5.4.2	Solution Type II	115
5.4.3	Solution Type III	117
5.4.4	Solution Type IV	124
5.4.5	Finite-Difference Simulation	124

5.4.6	Effect of Rock Heat Capacity	127
5.4.7	Effect of Injection Gas Solubility	129
5.5	Summary	134
6	Conclusions and Discussion	140
6.1	General Conclusions	140
6.1.1	Enhanced Recovery of Coal-Bed Methane	141
6.1.2	Enhanced Oil Recovery with Temperature Variation	142
6.2	Possible Improvements and Future Work	144
6.2.1	Enhanced Recovery of Coal-Bed Methane	144
6.2.2	Enhanced Oil Recovery with Temperature Variation	144
	Bibliography	146
	Bibliography	146
A	Miscellaneous Proofs and Derivations	151
A.1	Shock Solution in the Single-Phase Region of Binary Systems	151
A.2	Continuous Variation in the Two-Phase Region of Binary Systems	153
A.3	Isothermal Shock in the Two-Phase Region of Binary Systems	156
A.4	Solving Temperature Shocks	157

List of Tables

3.1	The thermodynamic properties of gas components in the example solutions.	26
3.2	Summary of breakthrough times and complete recovery of the initial CBM.	44
3.3	Analytical solution for ECBM in $CH_4 - CO_2 - N_2$ system, where the initial gas consists of 96% CH_4 , 3% CO_2 and 1% N_2 , and the injection gas 100% N_2	46
3.4	Analytical solution for ECBM in $CH_4 - CO_2 - N_2$ system, where the initial gas consists of 96% CH_4 , 3% CO_2 and 1% N_2 , and the injection gas 75% N_2 and 25% CO_2	48
3.5	Analytical solution for ECBM in $CH_4 - CO_2 - N_2$ system, where the initial gas consists of 96% CH_4 , 3% CO_2 and 1% N_2 , and the injection gas 50% N_2 and 50% CO_2	50
3.6	Analytical solution for ECBM in $CH_4 - CO_2 - N_2$ system, where the initial gas consists of 96% CH_4 , 3% CO_2 and 1% N_2 , and the injection gas 25% N_2 and 75% CO_2	50
3.7	Analytical solution for ECBM in $CH_4 - CO_2 - N_2$ system, where the initial gas consists of 96% CH_4 , 3% CO_2 and 1% N_2 , and the injection gas 100% CO_2	54
4.1	The thermodynamic properties of methane and decane.	61
4.2	The coefficients for ideal gas enthalpy calculation.	61
4.3	The properties of the porous medium.	61

5.1	Analytical solution for binary displacement with temperature variation in $CH_4 - C_{10}$ system, where the initial oil consists of 100% C_{10} at 530 °K, and the injection gas 85% CH_4 and 15% C_{10} at 550°K.	112
5.2	Analytical solution for binary displacement with temperature variation in $CH_4 - C_{10}$ system, where the initial oil consists of 100% C_{10} at 525.996 °K, and the injection gas 85% CH_4 and 15% C_{10} at 550°K. .	115
5.3	Analytical solution for binary displacement with temperature variation in $CH_4 - C_{10}$ system, where the initial oil consists of 100% C_{10} at 525.900 °K, and the injection gas 85% CH_4 and 15% C_{10} at 550°K. .	117
5.4	Analytical solution for binary displacement with temperature variation in $CH_4 - C_{10}$ system, where the initial oil consists of 100% C_{10} at 525.713 °K, and the injection gas 85% CH_4 and 15% C_{10} at 550°K. .	120
5.5	Analytical solution for binary displacement with temperature variation in $CH_4 - C_{10}$ system, where the initial oil consists of 100% C_{10} at 525.678 °K, and the injection gas 85% CH_4 and 15% C_{10} at 550°K. .	122
5.6	Analytical solution for binary displacement with temperature variation in $CH_4 - C_{10}$ system, where the initial oil consists of 100% C_{10} at 525.666 °K, and the injection gas 85% CH_4 and 15% C_{10} at 550°K. .	122
5.7	Analytical solution for binary displacement with temperature variation in $CH_4 - C_{10}$ system, where the initial oil consists of 100% C_{10} at 500.000 °K, and the injection gas 85% CH_4 and 15% C_{10} at 550°K. .	124
5.8	Analytical solution for Type I example with rock heat capacity reduced to 1/10 of its original value.	132

List of Figures

3.1	Experimental data for adsorption/desorption of pure CH_4 and CO_2 , and fitting with extended Langmuir isotherm.	25
3.2	Variation of normalized eigenvalue, local flow velocity and characteristic wave velocity along the $CH_4 - CO_2$ binary axis.	30
3.3	Solution profile for an example in the $CH_4 - CO_2$ system. The mixture of 95% CO_2 and 5% CH_4 is injected to displace an initial mixture of 3% CO_2 and 97% CH_4	31
3.4	Variation of normalized eigenvalue, local flow velocity and characteristic wave velocity along the $CH_4 - N_2$ binary axis.	32
3.5	Solution profile for an example in the $CH_4 - N_2$ system. The mixture of 95% N_2 and 5% CH_4 is injected to displace an initial mixture of 3% N_2 and 97% CH_4	33
3.6	Variation of normalized eigenvalue, local flow velocity and characteristic wave velocity along the $CO_2 - N_2$ binary axis.	34
3.7	Solution profile for an example in the $CO_2 - N_2$ system. The mixture of 95% N_2 and 5% CO_2 is injected to displace an initial mixture of 3% N_2 and 97% CO_2	35
3.8	Continuous solution paths for $CH_4 - CO_2 - N_2$ ternary system.	37
3.9	Variation of characteristic wave velocity following the fast and slow paths separately towards the CH_4 -rich zone. The initial composition (A) is the same for each path.	38
3.10	Type I solution, composed of upstream shock IC, and downstream continuous variation CO.	40

3.11	Type II solution paths, composed of upstream continuous variation IA , and downstream continuous variation AO	42
3.12	Type III solution paths, composed of upstream shock IC , and downstream shock CO	43
3.13	Solution paths for example solutions. The initial composition is fixed at 96% CH_4 , 3% CO_2 , and 1% N_2	45
3.14	Total recovery of CH_4 for the example solutions with different injection gas compositions.	45
3.15	Solution profile for example solution with an injection gas of 100% N_2	47
3.16	Solution profile for example solution with an injection gas of 25% CO_2 and 75% N_2	49
3.17	Solution profile for example solution with an injection gas of 50% CO_2 and 50% N_2	51
3.18	Solution profile for example solution with an injection gas of 75% CO_2 and 25% N_2	52
3.19	Solution profile for example solution with an injection gas of pure CO_2	53
3.20	Comparison of the analytical solution profiles with finite-difference simulation results. Injection gas consists of pure N_2	56
3.21	A study of the effect of numerical dispersion by a series of finite-difference simulations with various numbers of grid blocks.	57
4.1	The variation of rarefaction wave velocity and local flow velocity along the temperature path for single component displacement within the single-phase region of pure CH_4 system.	66
4.2	The variation of molar density and molar heat capacity of CH_4 with temperature. The results from calculation with Peng-Robinson Equation of State agree well with the data from the CRC Handbook of Physics and Chemistry.	67

4.3	In a pure CH_4 system, the velocities of all possible shocks and the rarefaction waves located at immediate downstream of the shocks. Each possible shock solution jumps from the injection temperature to an intermediate temperature between the initial and injection conditions.	69
4.4	The temperature profile for the example where pure CH_4 at 600 °K is injected into porous media saturated with 100% CH_4 at 250 °K. . . .	70
4.5	The variation of rarefaction wave velocity and local flow velocity along the temperature path for single component displacement within the single-phase region of pure C_{10} system.	71
4.6	In a pure C_{10} system, the velocities of all possible shocks from the injection temperature to an intermediate temperature, and the rarefaction waves located at immediate downstream of the shocks.	72
5.1	Composition space for CH_4 - C_{10} system.	74
5.2	Solution paths in the single-phase region of a binary system.	77
5.3	Variation of normalized temperature eigenvalue, local flow velocity and propagation velocity along a temperature path in the single-phase region of a binary system.	80
5.4	Example solution in single-phase region with initial mixture at A and injection mixture at C . The upstream continuous variation along isothermal path CD propagates faster than the downstream continuous variation along temperature path DA , violating the velocity rule.	82
5.5	Example solution in single-phase region with initial mixture at A and injection mixture at C	83
5.6	Example solution in single-phase region with initial mixture at C and injection mixture at A . The propagation velocity along path AB is higher than that along path BC . Along path BC , the propagation velocity decreases monotonically towards the downstream direction. .	85
5.7	Example solution in single-phase region with initial mixture at C and injection mixture at A . The propagation velocity along path AB is higher than that of the shock between B and C	86

5.8	Example solution in single-phase region with initial mixture at C and injection mixture at A . For continuous variation along temperature path AD , the propagation velocity decreases monotonically towards the downstream direction.	87
5.9	Example solution in single-phase region with initial mixture at C and injection mixture at A	88
5.10	Solution paths in the two-phase region of a binary system. The TL paths are isothermal or tie-line paths, and the T-paths are those for which temperature varies.	89
5.11	Variation of tie-line and temperature eigenvalues along an isothermal path at $500^{\circ}K$ in the $CH_4 - C_{10}$ system.	90
5.12	Variation of normalized temperature eigenvalue, local flow velocity and propagation velocity along a temperature path in the two-phase region of a binary system.	92
5.13	Examples with initial and injection mixtures both in the two-phase region.	95
5.14	Isothermal and temperature path near the equal-eigenvalue point. . .	97
5.15	Summary of possible switches between the continuous solution paths in the single-phase region and those in the two-phase region. The figure at the bottom is a magnified version of the one on top.	98
5.16	Switch between the continuous isothermal paths in the single-phase region and the two-phase region.	100
5.17	Switch between the continuous isothermal path in the two-phase region and continuous temperature path in the single-phase region.	101
5.18	Switch between the continuous temperature path in the two-phase region and continuous isothermal path in the single-phase region. . . .	103
5.19	Switch between the continuous temperature path in the two-phase region and continuous temperature path in the single-phase region. . .	104
5.20	All possible landing points of discontinuous variation with one side of the shock at G in the single-phase region.	105

5.21	All possible landing points of the near isothermal trailing shocks from the injection composition and temperature at G	107
5.22	Mixing pure CH_4 and C_{10} at identical initial temperature, with no heat added or removed from the mixture, results in two-phase mixtures at slightly different temperature at phase equilibrium.	108
5.23	All possible landing points of the temperature shocks from the injection composition and temperature at G	109
5.24	Solution paths and profile for Type I example.	113
5.25	Solution paths and profile for the critical case between Type I and II, where the phase envelope is crossed by a phase-change shock that begins on the phase envelope.	114
5.26	Solution paths and profile for the critical case between Type I and II, where the trailing temperature shock ends on the phase envelope and is followed by a continuous variation along temperature path.	116
5.27	Solution paths and profile for a Type II example.	118
5.28	Solution paths and profile for the critical case between Type II and III.	119
5.29	Solution paths and profile for a Type III example.	121
5.30	Solution paths and profile for the critical case between Type III and IV.	123
5.31	Solution paths and profile for a Type IV example.	125
5.32	Comparison of finite-difference solution and analytical solution for Type I example.	126
5.33	Comparison of finite-difference solution and analytical solution for Type IV example.	128
5.34	Type I example with rock heat capacity reduced to 1/10 of its original value. The temperature shock gc travels faster than the phase-change shock cb downstream, and hence violates the velocity rule.	130
5.35	Correct solution construction for the Type I example with rock heat capacity reduced to 1/10 of its original value.	131
5.36	A Type I example in the CO_2 - C_{16} system, where the initial oil is pure C_{16} at 600 °K. The injection gas consists of 95% CO_2 and 5% C_{16} at 650 °K.	133

- 5.37 A critical case between Type I and Type II in the CO_2-C_{16} system, where the phase envelope is crossed by a phase-change shock that begins on the phase boundary. The initial gas is pure C_{16} at 600 °K. The injection gas is composed of 91.8373% CO_2 and 8.1627% C_{16} at 650 °K. 135
- 5.38 A critical case between Type I and Type II in the CO_2-C_{16} system, where the two-phase region is entered by a continuous variation along a temperature path that begins from the two-phase envelope. The initial gas is pure C_{16} at 600 °K. The injection gas is composed of 91.8373% CO_2 and 8.1627% C_{16} at 650 °K. 136
- 5.39 A critical case between Type III and Type IV in the CO_2-C_{16} system, where the trailing tangent phase-change shock lands on the “initial” tie line directly. The initial gas is pure C_{16} at 600 °K. The injection gas is composed of 91.7981% CO_2 and 8.2029% C_{16} at 650 °K. 137
- 5.40 A Type IV example in the CO_2-C_{16} system, where the trailing tangent phase-change shock lands on an intermediate tie line, then to the “initial” tie line via a nontie-line shock within the two-phase region. The initial gas is pure C_{16} at 600 °K. The injection gas is composed of 90% CO_2 and 10% C_{16} at 650 °K. 138

Chapter 1

Introduction

Gas injection has been widely adopted in the oil industry as an efficient method of enhanced oil recovery. When applied to enhance the recovery of coal-bed methane, injection of CO_2 can also serve as a sequestration method for greenhouse gases.

The injected gases are compressed before arriving at the oil layers, often at a different temperature than that of the reservoir. The temperature difference is especially evident if the gas injection procedure is scheduled after waterflooding using cold sea water, as has been practiced in some of the North Sea and Alaskan oil fields. When the injected gas mixes with the reservoir fluids originally in place, two phases may form when local thermodynamic phase equilibrium is established. The reservoir fluids may exchange heat with the reservoir rock due to temperature difference and chemical species through adsorption and desorption at the reservoir rock surfaces. This process occurs repeatedly as the newly formed fluid phases propagate through the reservoir rocks at different rates and along different paths, according to the physical properties of the flowing phases and the heterogeneity of the reservoir rocks. Hence, the gas injection process is a problem of two-phase flow through a porous medium coupled with phase behavior of a multicomponent mixture.

Analytical solution methods can be used to isolate individual mechanisms that drive the gas injection process and provide a better understanding of the solution physics. Analytical solutions can also be used in combination with streamline methods

for reservoir simulation to yield very fast computational tools for modeling three-dimensional displacement [13]. However, in order to eliminate some of the complexity of the general flow, it is often assumed that flow occurs at constant temperature and without adsorption or desorption at the reservoir rock surfaces. The objective of this dissertation is to extend the analytical theory by including and studying the physical effects of variable temperature and adsorption or desorption on gas injection processes.

1.1 Theory of Two-Phase Multicomponent Flow in Porous Media at Constant Temperature

A general analytical theory for multicomponent multiphase gas displacements starts with material balances for individual components. When defined in a one-dimensional model in which dispersion is neglected, the material balances result in a series of quasi-linear, hyperbolic conservation equations. Furthermore, when the initial condition of the reservoir fluids is uniform and constant, and gas is injected at constant composition and rate, the flow problem is a Riemann problem that can be solved with the method of characteristics. Early study of gas/oil displacements using the method of characteristics was limited to systems with no more than three components and two phases. Welge *et al.* [39] presented the first analytical solution to the gas injection problem in ternary system where the volume change of components upon mixing was considered. Wachmann [36] studied alcohol flooding in ternary systems where the assumption of no volume change upon mixing seemed acceptable, which simplified the displacement problem significantly. Later, Larson *et al.* [23], Larson [22], Helfferich [10] and Hirasaki [11] investigated surfactant/oil/water displacements extensively. Helfferich [10] formulated the work into a general theory that described the underlying mathematics of multiphase multicomponent flow through porous media. The theory was then applied to gas injection problems in ternary systems by Dumoré *et al.* [6], where the effects of volume change upon mixing were again included.

Monroe *et al.* [27] reported the first solutions for systems with four components.

Johns *et al.* [17] [18] studied gas injection in four-component systems where molar density of the components remained constant in different phases. Dindoruk *et al.* [4] [5] tackled similar problems but considered the effect of volume change as components transfer between phases. The four-component theory was later applied to study the effect of gas enrichment by Johns *et al.* [19]. Orr *et al.* [28] studied the development of miscibility in gas/oil displacement processes using carbon dioxide as injection gases. Wang and Orr [37] [38] extended the solution method to systems with an arbitrary number of components, assuming only shock solution segments across a sequence of key tie-lines. The development of the analytical theory led to an efficient solution method for calculating the minimum miscible pressure (MMP). Jessen [12] and Ermakov [7] considered the effect of volume change on the analytical solutions for systems with arbitrary number of components. In the most recent development of the analytical theory, Jessen *et al.* [14] presented a systematic method to determine where a rarefaction solution segment would occur and introduced the concept of primary key tie line where the solution construction process should begin in a system with arbitrary number of components. The solutions presented by Jessen *et al.* included both rarefaction and shock solution segments across the key tie lines but neglected the volume change of components upon mixing. The analytical solutions reported by these investigations have been confirmed with finite-difference simulations for systems with both rarefaction and shock solution segments.

1.2 Gas Injection with Variable Temperature

While the analytical theory of multicomponent gas/oil displacement is now well developed, there still exist various restrictions. One of these requirements is that the temperature remain constant throughout the gas injection process. However, the reservoir temperature may not be uniform and identical to that of the injection fluids, especially when thermal recovery methods are employed in oil fields. Temperature changes may therefore accompany the displacement process. On one hand, the variations in temperature affect the phase behavior because thermodynamic equilibrium depends on temperature. On the other hand, temperature variation influences the

multiphase flow by altering the physical properties of the phases such as densities and viscosities. Limited efforts have been invested on the analytical solutions for flows with temperature variations. Fayers [8] analyzed the displacement of oil by hot water using the method of characteristics. He studied the cases where thermal capacities are constant or dependent on temperature and investigated the shock solutions across which both saturation and temperature may vary. Shutler and Boberg [34] presented an approximate solution for flow of steam, water and oil. Lake [20] provided an analysis of the propagation of temperature fronts for steam and hot water flooding. Later, Wingard [40] [41] studied the flow of steam, water and oil including the effect of temperature on phase density and condensation of steam into water phases. However, steam, water and oil were assumed to be immiscible, and the effect of hydrocarbon components transferring between phases was not considered. Wingard's analysis showed that three phases occur during the steam injection processes with a steam/oil zone near the injection end, an oil/water zone at the downstream end and a steam/water/oil zone in between. It was shown that as long as condensation of steam occurs, the Gibbs phase rule required that the steam/water/oil zone be at constant temperature, which simplified the problem significantly. Wingard focused on solving the shock balances where the temperatures are known on both sides of the shock. Wingard also discussed the problem of three-component, three-phase flow with temperature variation where the injected carbon dioxide and the reservoir oil are no longer immiscible. However, the complicated phase behavior posed one of the major obstacles to the solution construction for this problem and no attempt was made to solve the more complex problem.

Now with a better understanding of the physics underlying the multicomponent, multiphase flow from the dramatic improvement of the analytical theory, a theory can be constructed for displacements with temperature variation, where hydrocarbon components as well as heat in the system may transfer between phases and be carried downstream at variable local flow rates. In this study, the effects of hydrocarbon phase behavior are considered, but water or steam phases are not included. The temperature in the two-phase zone is variable depending on the heat concentration, phase composition and saturation. Since temperature has a strong effect on the

densities of the components, the effect of volume change that occurs when components transfer between phases are included. By extending the analytical theory to include temperature variation, we study the propagation of temperature fronts during gas injection processes, and examine the interaction between the temperature fronts and the composition waves.

1.3 Gas Injection for Enhanced Coal-Bed Methane Recovery

The effect of adsorption and desorption of fluid components at reservoir rock surfaces has been modeled in a global Riemann problem for single-component and multicomponent polymer flooding by Johansen *et al* [15] [16], where the aqueous phase containing polymer is assumed to be immiscible with the oleic phase. The specific adsorption behavior of the polymer is represented by a Langmuir isotherm and briefly discussed by Lake [21]. However, in the analytical theory of miscible gas injection, the effect of adsorption and desorption has been neglected, although it can be important in problems such as enhanced coalbed methane recovery (ECBM) by gas injection.

Coalbeds have large internal surface area and strong affinity for certain gas species such as CH_4 and CO_2 . In coal-bed methane (CBM) reservoirs, most of the total gas exists in an adsorbed state at liquid-like density. Only a small amount of the total gas is in a free gas phase. Primary recovery using depressurization techniques induces desorption of the CBM by lowering the overall pressure of the reservoir. Enhanced recovery of coal-bed methane (ECBM) makes use of injection of a second gas to maintain overall reservoir pressure while lowering the partial pressure of the CBM in the free gas. Injected gas also sweeps the desorbed gas through the CBM reservoir. Nitrogen is a natural choice as an injection gas because of its availability. Carbon dioxide, on the other hand, is also promising because of the additional benefit of greenhouse gas sequestration. When combusted, methane emits the least amount of CO_2 per unit of energy released among all the fossil fuels. Therefore, synergy exists between CO_2 sequestration and production of methane that leads to greater utilization of

coal-bed resources for both their sequestration ability and energy content. The first application of ECBM by CO_2 injection has been carried out in the San Juan Basin, and proved to be technically feasible [35].

One important aspect of ECBM is the adsorption and desorption behavior of gas mixtures on coalbeds. A significant amount of work has been invested on this issue as it is related to coal mine safety. However, transport of the desorbed gas through coalbeds has not been examined in detail. In this thesis, we extend the analytical theory to consider ECBM problems by gas injection where the effects of adsorption and desorption are not negligible. We study systems with up to three components that have different affinities for coal-bed surfaces, and investigate the interaction of the adsorption and desorption with the multicomponent flow through the porous coalbed.

1.4 Summary

In this chapter, the development of the analytical theory of two-phase multicomponent flow through porous media is reviewed. A brief introduction to the gas injection problem with temperature variation and component adsorption/desorption is given.

In Chapter 2, the assumptions and simplifications used in this study are stated, and a general mathematical model is established that describes the conservation of mass and energy during the gas displacement process. That system of equations is then converted to a general form of the eigenvalue problem. When the effect of volume change is considered, the local flow velocity is variable and must be solved together with the other dependent variables. Dindoruk [4] introduced a procedure that can be applied here to decouple the local flow velocity from the rest of the unknown variables. The eigenvalue problem with decoupled local flow velocity is derived, and the physical constraints are used to eliminate invalid solutions.

In Chapter 3, the ECBM problem in a $CH_4/N_2/CO_2$ system is solved. An extended Langmuir isotherm is used to represent the adsorption and desorption behavior of the gas components at the coal-bed surfaces. The eigenvalue problem is formulated and studied. A series of example solutions is presented and discussed in detail, and

the analytical solutions are confirmed by finite-difference simulations.

In Chapter 4, gas injection problems with temperature variation are solved for single-component system where phase behavior is simplified significantly. Then in Chapter 5, we provide a comprehensive study of solutions in binary systems.

Chapter 6 summarizes the results of this work and provides some insight into possible future research to extend the analytical theory.

Chapter 2

Mathematical Model

In this chapter, we present the mathematical background for solving the gas injection problems in 1D using the method of characteristics. The general assumptions and physical constraints are stated. For continuous variation of the state variables such as composition and temperature, the equations for conservation of mass and energy that describe the flow are established and converted to an eigenvalue problem. Discontinuous variation of the state variables must obey the conservation of mass and energy in an integral form across the discontinuity.

2.1 Assumptions and simplifications

The study of the gas injection problems using an analytical approach, to date, has been subject to the following general restrictions:

- The theory is established for one-dimensional flow.
- No diffusion or dispersion is included.
- The physical properties of the porous medium, such as porosity and permeability are homogeneous.
- The reservoir is initially at a uniform condition. Gas is injected at a constant rate and composition.

- For the purpose of evaluating phase behavior, pressure is assumed to be constant.
- The mixtures are at local thermodynamic equilibrium during the gas injection process.

When temperature is allowed to vary, energy transfer will take place as the phases move. Under constant pressure, we are only concerned with enthalpy or heat, hence in this work we use “heat” and “enthalpy” interchangeably. The flow of heat obeys a conservation equation that has a form very similar to those of the individual components. However, the flow of heat is not exactly the same as an individual component. Besides being contained by all the components in the reservoir fluids, heat can be absorbed and released by the reservoir rock matrix. When reservoir fluids flow, heat can be carried downstream by all of the components. The overall energy is still conserved, and there is only one heat balance equation. It is impossible to distinguish the contributions from individual components or rock matrix when we compute the heat concentration and heat flux.

In order for the method of characteristics to apply to a Riemann problem, it is required that the initial reservoir temperature be uniformly distributed and the injection fluid temperature be constant. Therefore, in this thesis, we will be solving gas injection problems where the initial reservoir temperature differs from that of the injection gas.

There are a few additional assumptions we must add to the gas injection problems with temperature variation. First, we assume that the system reaches thermodynamic equilibrium instantly. Secondly, heat transfer through conduction is neglected. The transportation of heat occurs primarily due to convective flow. A comparison between the heat transfer through convective flow and by conduction is presented in the next section where the mass and energy balance equations are established.

Another physical effect to be included in the analytical theory is adsorption and desorption. Similar to the exchange of heat between the flowing phases and the reservoir rock, when adsorption and desorption effects are significant, reservoir fluid components may partition between the flowing phases and the immobile reservoir

rock surfaces. However, including the effect of adsorption and desorption only affects the overall concentration of the components since it now includes contribution of the adsorbed gas species on the reservoir rock surfaces. The material balance equations that govern the fluid flow remain quasilinear in form. The adsorption and desorption behavior is determined by the thermodynamic properties of the flowing mixtures, as well as properties of the reservoir rock surfaces.

2.2 Conservation of mass and energy

In a system with n_c components and n_p phases, a general form of material balance equation for each component in the multicomponent multiphase mixture is

$$\frac{\partial}{\partial t} \left[\sum_{j=1}^{n_p} \phi x_{ij} \rho_j S_j + (1 - \phi) a_i \right] + \sum_{j=1}^{n_p} \nabla \cdot (\rho_j x_{ij} \vec{u}_j) = 0, \quad i = 1, n_c, \quad (2.1)$$

where ϕ is the porosity of the porous media, S_j is saturation of phase j , ρ_j is the molar density of phase j , x_{ij} is the mole fraction of component i in phase j , a_i is the adsorbed amount of gas component i per unit volume of reservoir rock matrix. \vec{u}_j is local flow velocity of phase j .

In a one dimensional problem, the overall concentrations and fractional flows are defined as

$$G_i = \phi \sum_{j=1}^{n_p} x_{ij} \rho_j S_j + (1 - \phi) a_i, \quad (2.2)$$

and

$$F_i = u \sum_{j=1}^{n_p} \rho_j x_{ij} f_j, \quad (2.3)$$

where $f_j \equiv u_j/u$ is the volumetric fractional flow of phase j , u is the overall local flow velocity.

Then, the material balance becomes

$$\frac{\partial G_i}{\partial t} + \frac{\partial F_i}{\partial x} = 0, \quad i = 1, n_c. \quad (2.4)$$

Similar to the material balance, a general form for the energy balance is

$$\frac{\partial}{\partial t} \left[\sum_{j=1}^{n_p} \phi \rho_j H_j S_j + (1 - \phi)(\rho_r H_r + \rho_a H_a) \right] + \sum_{j=1}^{n_p} \nabla \cdot (\rho_j H_j \vec{u}_j) = 0, \quad (2.5)$$

where H_j is the specific molar enthalpy of phase j , H_r is the specific enthalpy of the porous media, ρ_r is the density of the porous media, ρ_a is the overall density of the adsorbed components, and H_a is the overall specific enthalpy of the adsorbed components.

In the one-dimensional problem, define an overall energy content and flux as

$$\Gamma = \phi \sum_{j=1}^{n_p} \rho_j H_j S_j + (1 - \phi)(\rho_r H_r + \rho_a H_a), \quad (2.6)$$

and

$$\Theta = u \sum_{j=1}^{n_p} \rho_j H_j f_j. \quad (2.7)$$

Then the energy balance becomes

$$\frac{\partial \Gamma}{\partial t} + \frac{\partial \Theta}{\partial x} = 0. \quad (2.8)$$

Substitution of the following dimensionless variables into Eqs. 2.4 and 2.8.

$$\xi = \frac{x}{L}, \quad (2.9)$$

$$\tau = \frac{u_{inj} t}{\phi L}, \quad (2.10)$$

$$\rho_{jD} = \frac{\rho_j}{\rho_{ini}}, \quad (2.11)$$

$$u_D = \frac{u}{u_{inj}}, \quad (2.12)$$

$$\rho_{rD} = \frac{\rho_r}{\rho_{ini}}, \quad (2.13)$$

$$\rho_{aD} = \frac{\rho_a}{\rho_{ini}}, \quad (2.14)$$

$$H_{jD} = \frac{H_j}{H_{ini}}, \quad (2.15)$$

$$H_{rD} = \frac{H_r}{H_{ini}}, \quad (2.16)$$

$$H_{aD} = \frac{H_a}{H_{ini}}, \quad (2.17)$$

where

- L = system length,
- u_D = dimensionless total flow velocity,
- u_{inj} = injection velocity,
- ρ_{ini} = density of the original fluid in the system,
- ρ_{jD} = dimensionless molar density of phase j ,
- ρ_{rD} = dimensionless molar density of the rock.
- ρ_{aD} = dimensionless molar density of adsorbed phase.
- H_{ini} = molar enthalpy of the original fluid in the system,
- H_{jD} = dimensionless molar enthalpy of phase j ,
- H_{rD} = dimensionless molar enthalpy of the rock,
- H_{aD} = dimensionless molar enthalpy of the adsorbed phase,
- ξ = dimensionless distance,
- τ = dimensionless time,

yields the dimensionless form of the material balance and energy balance equations

$$\frac{\partial G_{iD}}{\partial \tau} + \frac{\partial F_{iD}}{\partial \xi} = 0, \quad (2.18)$$

$$\frac{\partial \Gamma_D}{\partial \tau} + \frac{\partial \Theta_D}{\partial \xi} = 0, \quad (2.19)$$

where

$$G_{iD} = \phi \sum_{j=1}^{n_p} x_{ij} \rho_{jD} S_j + (1 - \phi) a_{iD}, \quad (2.20)$$

$$F_{iD} = u_D \sum_{j=1}^{n_p} x_{ij} \rho_{jD} f_j, \quad (2.21)$$

$$\Gamma_D = \phi \sum_{j=1}^{n_p} \rho_{jD} H_{jD} S_j + (1 - \phi)(\rho_{rD} H_{rD} + \rho_{aD} H_{aD}), \quad (2.22)$$

$$\Theta_D = u_D \sum_{j=1}^{n_p} \rho_{jD} H_{jD} f_j. \quad (2.23)$$

The heat transfer via conduction, when included, contributes the following amount to the heat flux,

$$u_{\alpha x} = -\alpha_T \nabla T, \quad (2.24)$$

where $u_{\alpha x}$ is the rate of heat transfer by conduction per unit cross-sectional area, α_T is the thermal conductivity of the material. Hence the dimensionless form of the energy conservation becomes

$$\frac{\partial \Gamma_D}{\partial \tau} + \frac{\partial \Theta_D}{\partial \xi} - \frac{1}{P_{eH}} \frac{\partial^2 T_D}{\partial \xi^2} = 0. \quad (2.25)$$

where $P_{eH} = u_{inj} L \rho_{ini} H_{ini} / T_{ini} \alpha_T$ is the Peclet number. It describes a ratio of a characteristic time for heat conduction to a characteristic time for convection. When the Peclet number is large, the effect of thermal conduction is small, and convection dominates. Normally, the initial reservoir fluid has a molar density at the order of 10^{-2} gmol/cc and a heat capacity at the magnitude of 10^{-3} Btu/gmol \cdot $^{\circ}$ K. The typical thermal conductivity of a reservoir is in the order of 10 Btu/D \cdot ft \cdot $^{\circ}$ K, [31]. If we assume a one-dimensional model with a length of 1000 feet, and take a typical injection rate of 1 ft/D and a typical temperature difference of 100 $^{\circ}$ K. then the Peclet number is in the order of 100. This indicates that the heat flux by convective flow overwhelms the heat flux from conduction. With heavier fluids, higher injection rate, longer one-dimensional model and smaller temperature difference, the Peclet number can grow significantly larger. Therefore, neglecting the heat flux by thermal conduction is a reasonable assumption.

The Riemann problem requires uniform initial and constant boundary conditions

at the injection end that can be expressed as

$$z_i(x, 0) = z_i^{\text{ini}}, \quad x > 0, \quad (2.26)$$

$$z_i(0, t) = z_i^{\text{inj}}, \quad x = 0, i = 1, \dots, n_c, \quad (2.27)$$

$$u(x, 0) = 0, \quad x > 0, \quad (2.28)$$

$$u(0, t) = 1, \quad x = 0, \quad (2.29)$$

$$T(x, 0) = T^{\text{ini}}, \quad x > 0, \quad (2.30)$$

$$T(0, t) = T^{\text{inj}}, \quad x = 0. \quad (2.31)$$

In the following study of material and energy balances, we will use the dimensionless form of the equations and drop the subscript "D".

2.2.1 Eigenvalue problem and continuous solution

In a system with n_c components, there are n_c independent equations of material balance for the n_c components and one equation for the energy balance. Once we can solve for the overall molar compositions, local flow velocity u and temperature T , the other unknowns such as saturations and equilibrium phase compositions can be obtained through equilibrium calculations. There are $n_c - 1$ unknown independent overall molar compositions, one unknown local flow velocity u and one unknown temperature T . Therefore, we can choose a total number of these $n_c + 1$ unknowns that can be solved through the $n_c + 1$ material and energy balance equations.

The system of equations for the material and energy balances, together with the initial and injection conditions specified by two different composition and temperature states at $x = 0$ and $t = 0$, constitute a Riemann problem that yields self-similar solutions. Therefore, there exists a variable $\eta = \eta(x, t)$ such that the solution to the Riemann problem can be expressed in terms of η [24] [25], where

$$\eta = \xi/\tau. \quad (2.32)$$

Because G_i , F_i , Γ and Θ all depend on the unknown overall molar composition z_i

for $i = 1, n_c - 1$, the temperature T and local flow velocity u , we have

$$\frac{dG_i}{d\tau} = \left[\sum_{k=1}^{n_c-1} \frac{\partial G_i}{\partial z_k} \frac{\partial z_k}{\partial \eta} + \frac{\partial G_i}{\partial T} \frac{\partial T}{\partial \eta} \right] \frac{\partial \eta}{\partial \tau}, \quad (2.33)$$

$$\frac{dF_i}{d\xi} = \left[\sum_{k=1}^{n_c-1} \frac{\partial F_i}{\partial z_k} \frac{\partial z_k}{\partial \eta} + \frac{\partial F_i}{\partial T} \frac{\partial T}{\partial \eta} + \frac{\partial F_i}{\partial u} \frac{\partial u}{\partial \eta} \right] \frac{\partial \eta}{\partial \xi}, \quad (2.34)$$

$$\frac{d\Gamma}{d\tau} = \left[\sum_{k=1}^{n_c-1} \frac{\partial \Gamma}{\partial z_k} \frac{\partial z_k}{\partial \eta} + \frac{\partial \Gamma}{\partial T} \frac{\partial T}{\partial \eta} \right] \frac{\partial \eta}{\partial \tau}, \quad (2.35)$$

$$\frac{d\Theta}{d\xi} = \left[\sum_{k=1}^{n_c-1} \frac{\partial \Theta}{\partial z_k} \frac{\partial z_k}{\partial \eta} + \frac{\partial \Theta}{\partial T} \frac{\partial T}{\partial \eta} + \frac{\partial \Theta}{\partial u} \frac{\partial u}{\partial \eta} \right] \frac{\partial \eta}{\partial \xi}, \quad (2.36)$$

where

$$\frac{\partial \eta}{\partial \xi} = \frac{1}{\tau}, \quad (2.37)$$

$$\frac{\partial \eta}{\partial \tau} = -\frac{\xi}{\tau^2}. \quad (2.38)$$

Substitution of Eqs. 2.33, 2.34, 2.35, 2.36, 2.37 and 2.38 into Eqs. 2.4 and 2.8 yields the following system of equations,

$$\begin{aligned} & \left[\sum_{k=1}^{n_c-1} \frac{\partial G_i}{\partial z_k} \frac{\partial z_k}{\partial \eta} + \frac{\partial G_i}{\partial T} \frac{\partial T}{\partial \eta} \right] \frac{-\xi}{\tau^2} \\ & + \left[\sum_{k=1}^{n_c-1} \frac{\partial F_i}{\partial z_k} \frac{\partial z_k}{\partial \eta} + \frac{\partial F_i}{\partial T} \frac{\partial T}{\partial \eta} + \frac{\partial F_i}{\partial u} \frac{\partial u}{\partial \eta} \right] \frac{1}{\tau} = 0, \end{aligned} \quad (2.39)$$

$$\begin{aligned} & \left[\sum_{k=1}^{n_c-1} \frac{\partial \Gamma}{\partial z_k} \frac{\partial z_k}{\partial \eta} + \frac{\partial \Gamma}{\partial T} \frac{\partial T}{\partial \eta} \right] \frac{-\xi}{\tau^2} \\ & + \left[\sum_{k=1}^{n_c-1} \frac{\partial \Theta}{\partial z_k} \frac{\partial z_k}{\partial \eta} + \frac{\partial \Theta}{\partial T} \frac{\partial T}{\partial \eta} + \frac{\partial \Theta}{\partial u} \frac{\partial u}{\partial \eta} \right] \frac{1}{\tau} = 0. \end{aligned} \quad (2.40)$$

Eqs. 2.39 and 2.40 can be written as an eigenvalue problem where ξ/τ is the characteristic wave speed,

$$\eta = \frac{\xi}{\tau} = \lambda(\vec{U}(\eta)). \quad (2.41)$$

where $\vec{U}(\eta)$ is a vector of state variables.

The material and energy balance equations become an eigenvalue problem in the following matrix form,

$$\begin{aligned}
 & \begin{bmatrix} \frac{\partial F_1}{\partial z_1} & \frac{\partial F_1}{\partial z_2} & \dots & \frac{\partial F_1}{\partial z_{n_c-1}} & \frac{\partial F_1}{\partial T} & \frac{\partial F_1}{\partial u} \\ \frac{\partial F_2}{\partial z_1} & \frac{\partial F_2}{\partial z_2} & \dots & \frac{\partial F_2}{\partial z_{n_c-1}} & \frac{\partial F_2}{\partial T} & \frac{\partial F_2}{\partial u} \\ \vdots & \vdots & \dots & \vdots & \vdots & \vdots \\ \vdots & \vdots & \dots & \vdots & \vdots & \vdots \\ \frac{\partial F_{n_c}}{\partial z_1} & \frac{\partial F_{n_c}}{\partial z_2} & \dots & \frac{\partial F_{n_c}}{\partial z_{n_c-1}} & \frac{\partial F_{n_c}}{\partial T} & \frac{\partial F_{n_c}}{\partial u} \\ \frac{\partial \Theta}{\partial z_1} & \frac{\partial \Theta}{\partial z_2} & \dots & \frac{\partial \Theta}{\partial z_{n_c-1}} & \frac{\partial \Theta}{\partial T} & \frac{\partial \Theta}{\partial u} \end{bmatrix} \begin{bmatrix} \frac{dz_1}{d\eta} \\ \frac{dz_2}{d\eta} \\ \vdots \\ \vdots \\ \frac{dT}{d\eta} \\ \frac{du}{d\eta} \end{bmatrix} = \\
 & \lambda \begin{bmatrix} \frac{\partial G_1}{\partial z_1} & \frac{\partial G_1}{\partial z_2} & \dots & \frac{\partial G_1}{\partial z_{n_c-1}} & \frac{\partial G_1}{\partial T} & 0 \\ \frac{\partial G_2}{\partial z_1} & \frac{\partial G_2}{\partial z_2} & \dots & \frac{\partial G_2}{\partial z_{n_c-1}} & \frac{\partial G_2}{\partial T} & 0 \\ \vdots & \vdots & \dots & \vdots & \vdots & \vdots \\ \vdots & \vdots & \dots & \vdots & \vdots & \vdots \\ \frac{\partial G_{n_c}}{\partial z_1} & \frac{\partial G_{n_c}}{\partial z_2} & \dots & \frac{\partial G_{n_c}}{\partial z_{n_c-1}} & \frac{\partial G_{n_c}}{\partial T} & 0 \\ \frac{\partial \Gamma}{\partial z_1} & \frac{\partial \Gamma}{\partial z_2} & \dots & \frac{\partial \Gamma}{\partial z_{n_c-1}} & \frac{\partial \Gamma}{\partial T} & 0 \end{bmatrix} \begin{bmatrix} \frac{dz_1}{d\eta} \\ \frac{dz_2}{d\eta} \\ \vdots \\ \vdots \\ \frac{dT}{d\eta} \\ \frac{du}{d\eta} \end{bmatrix}. \tag{2.42}
 \end{aligned}$$

The flux terms for individual components and energy contain the local flow velocity. In order to separate the local flow velocity from the other dependent variables, we introduce the normalized flux terms that are independent of the local flow velocity as F_i^* and Θ^* ,

$$\alpha_i = \sum_{j=1}^{n_p} x_{ij} \rho_j f_j, \quad i = 1, n_c, \tag{2.43}$$

$$\beta = \sum_{j=1}^{n_p} \rho_j H_j f_j, \tag{2.44}$$

such that

$$F_i = u \alpha_i, \quad i = 1, \dots, n_c, \tag{2.45}$$

$$\Theta = u \beta. \tag{2.46}$$

Then Eq. 2.42 becomes

$$\begin{aligned}
 & \begin{bmatrix} u \frac{\partial \alpha_1}{\partial z_1} & u \frac{\partial \alpha_1}{\partial z_2} & \cdots & u \frac{\partial \alpha_1}{\partial z_{n_c-1}} & u \frac{\partial \alpha_1}{\partial T} & \alpha_1 \\ u \frac{\partial \alpha_2}{\partial z_1} & u \frac{\partial \alpha_2}{\partial z_2} & \cdots & u \frac{\partial \alpha_2}{\partial z_{n_c-1}} & u \frac{\partial \alpha_2}{\partial T} & \alpha_2 \\ \vdots & \vdots & \cdots & \vdots & \vdots & \vdots \\ \vdots & \vdots & \cdots & \vdots & \vdots & \vdots \\ u \frac{\partial \alpha_{n_c}}{\partial z_1} & u \frac{\partial \alpha_{n_c}}{\partial z_2} & \cdots & u \frac{\partial \alpha_{n_c}}{\partial z_{n_c-1}} & u \frac{\partial \alpha_{n_c}}{\partial T} & \alpha_{n_c} \\ u \frac{\partial \beta}{\partial z_1} & u \frac{\partial \beta}{\partial z_2} & \cdots & u \frac{\partial \beta}{\partial z_{n_c-1}} & u \frac{\partial \beta}{\partial T} & \beta \end{bmatrix} \begin{bmatrix} \frac{dz_1}{d\eta} \\ \frac{dz_2}{d\eta} \\ \vdots \\ \vdots \\ \frac{dT}{d\eta} \\ \frac{du}{d\eta} \end{bmatrix} = \\
 & \lambda \begin{bmatrix} \frac{\partial G_1}{\partial z_1} & \frac{\partial G_1}{\partial z_2} & \cdots & \frac{\partial G_1}{\partial z_{n_c-1}} & \frac{\partial G_1}{\partial T} & 0 \\ \frac{\partial G_2}{\partial z_1} & \frac{\partial G_2}{\partial z_2} & \cdots & \frac{\partial G_2}{\partial z_{n_c-1}} & \frac{\partial G_2}{\partial T} & 0 \\ \vdots & \vdots & \cdots & \vdots & \vdots & \vdots \\ \vdots & \vdots & \cdots & \vdots & \vdots & \vdots \\ \frac{\partial G_{n_c}}{\partial z_1} & \frac{\partial G_{n_c}}{\partial z_2} & \cdots & \frac{\partial G_{n_c}}{\partial z_{n_c-1}} & \frac{\partial G_{n_c}}{\partial T} & 0 \\ \frac{\partial \Gamma}{\partial z_1} & \frac{\partial \Gamma}{\partial z_2} & \cdots & \frac{\partial \Gamma}{\partial z_{n_c-1}} & \frac{\partial \Gamma}{\partial T} & 0 \end{bmatrix} \begin{bmatrix} \frac{dz_1}{d\eta} \\ \frac{dz_2}{d\eta} \\ \vdots \\ \vdots \\ \frac{dT}{d\eta} \\ \frac{du}{d\eta} \end{bmatrix}. \tag{2.47}
 \end{aligned}$$

Following a procedure similar to that introduced by Dindoruk [4] for decoupling the local flow velocity yields

$$\begin{pmatrix} [F] - \lambda^* [G] & \vec{0} \\ [\vec{F}^T] - \lambda^* [\vec{G}^T] & \frac{1}{u} \end{pmatrix} \begin{pmatrix} \vec{e} \\ \frac{du}{d\eta} \end{pmatrix} = \begin{pmatrix} \vec{0} \\ 0 \end{pmatrix}, \tag{2.48}$$

where

$$[F] = \begin{cases} \frac{\partial \alpha_i}{\partial z_j} - \frac{\alpha_i}{\beta} \frac{\partial \beta}{\partial z_j}, & i = 1, n_c; j = 1, n_c - 1, \\ \frac{\partial \alpha_i}{\partial T} - \frac{\alpha_i}{\beta} \frac{\partial \beta}{\partial T}, & i = 1, n_c; j = n_c, \end{cases} \tag{2.49}$$

$$[G] = \begin{cases} \frac{\partial G_i}{\partial z_j} - \frac{\alpha_i}{\beta} \frac{\partial \Gamma}{\partial z_j}, & i = 1, n_c; j = 1, n_c - 1, \\ \frac{\partial G_i}{\partial T} - \frac{\alpha_i}{\beta} \frac{\partial \Gamma}{\partial T}, & i = 1, n_c; j = n_c, \end{cases} \tag{2.50}$$

$$\vec{F}^T = \begin{cases} \frac{1}{\beta} \frac{\partial \beta}{\partial z_j}, & j = 1, n_c - 1, \\ \frac{1}{\beta} \frac{\partial \beta}{\partial T}, & j = n_c, \end{cases} \tag{2.51}$$

$$\vec{G}^T = \begin{cases} \frac{1}{\beta} \frac{\partial \Gamma}{\partial z_j}, & j = 1, n_c - 1, \\ \frac{1}{\beta} \frac{\partial \Gamma}{\partial T}, & j = n_c, \end{cases} \tag{2.52}$$

$$\vec{e}^T = \begin{cases} \frac{dz_j}{d\eta}, & j = 1, n_c - 1, \\ \frac{dT}{d\eta}, & j = n_c, \end{cases} \quad (2.53)$$

$$\lambda^* = \frac{\lambda}{u}. \quad (2.54)$$

Eq. 2.48 has a sub-matrix of order n_c that yields an eigenvalue problem of the form

$$[F - \lambda^* G] \vec{e} = \vec{0}. \quad (2.55)$$

Eq. 2.55 is completely independent of the local flow velocity because the velocity term is decoupled. The corresponding eigenvectors to the eigenvalues in Eq. 2.55 indicate the direction of the solution paths in the augmented composition space. Once the eigenvalues and the corresponding eigenvectors are solved from Eq. 2.55, the local flow velocity can be solved by integrating the last scalar equation of Eq. 2.48, *i.e.*,

$$(\vec{F}^T - \lambda^* \vec{G}^T) \vec{e} = -\frac{1}{u} \frac{du}{d\eta} \quad (2.56)$$

Eq. 2.56 must be integrated as a path is traced in the composition space. Taking small integration steps along the path, and assuming constant product of $(\vec{F}^T - \lambda^* \vec{G}^T)$ and \vec{e} , we have

$$u = u_0 \exp \left[-s (\vec{F}^T - \lambda^* \vec{G}^T) \vec{e} \right] \quad (2.57)$$

It must be pointed out that the last eigenvalue in Eq. 2.48 corresponds to the local flow velocity and has an infinite value. This tells us that, unlike the composition and temperature waves, any variation in the local flow velocity will propagate downstream instantly in the one-dimensional model.

2.3 Continuous and discontinuous solutions

In the 1D model, the solution to the Riemann problem consists of infinite number of states that are described by a set of dependent variables such as the molar compositions, temperature and local flow velocity. In an abstract space created by coordinates such as the molar compositions and temperature that will be called a “composition

space”, these states vary from the injection condition at upstream to the initial condition at downstream and form a path that will be called “solution path”. In a solution of the Riemann problem, each of these states propagates downstream at a fixed velocity, indicated by the eigenvalues of the eigenvalue problem, while the corresponding eigenvectors indicate the direction of the solution path in the composition space.

As can be seen from Eqs. 2.55 and 2.56, at any point in the composition space, there will exist n_c eigenvalues and eigenvectors. Each pair of the eigenvalues and corresponding eigenvectors gives a valid wave velocity and solution path direction. Taking a rarefaction solution along any of these solution paths satisfies Eqs. 2.55 and 2.56. However, when we trace the solution paths from the upstream condition to downstream, the corresponding wave velocity may not decrease monotonically. When this happens, the composition or temperature waves upstream may travel faster than those downstream. As a result, we may have multiple values for the state variables at the same time and same location. This behavior is non-physical and is a violation of the velocity rule that requires that fast traveling waves stay downstream of the slower traveling waves. When the velocity rule is violated, a discontinuous solution, called a “shock”, must be used to replace the rarefaction wave solution.

Across a shock, the material balance must be satisfied as well. This is the Rankine-Hugoniot condition. For each of the component, an integral balance across the shock yields

$$\Lambda_m = \frac{F_i^u - F_i^d}{G_i^u - G_i^d}, \quad i = 1, \dots, n_c, \quad (2.58)$$

where the superscripts “u” and “d” represent upstream and downstream conditions of the shock.

With variable temperature, energy is also conserved across the shock. Hence, the Rankine-Hugoniot conditions for mass balance must be augmented to accommodate the energy balance,

$$\Lambda_h = \frac{\Theta^u - \Theta^d}{\Gamma^u - \Gamma^d} = \Lambda_m, \quad i = 1, \dots, n_c. \quad (2.59)$$

In order for a shock solution to be stable, it must satisfy an entropy condition. A

shock may not be stable when the wave velocity at its immediate upstream side is lower than the shock velocity and that at the immediate downstream side is higher. An unstable shock not satisfying the entropy condition would collapse when given a small amount of perturbation. A stable shock, on the other hand, is a shock that moves faster than the waves immediately downstream and slower than those immediately upstream. Hence given a small amount of perturbation the shock is capable of sharpening itself back into a shock instead of spreading out and collapsing.

Besides the segments of continuous and discontinuous solutions, there also exist constant states in solutions to Riemann problems. In constant states, the dependent variables remain constant and propagate downstream together with the continuous and discontinuous solution segments.

Overall, the continuous solution, discontinuous solution and constant state segments for a complete solution to a Riemann problem must be arranged in such a way that the velocity rule is satisfied. When there is a slight change in the initial or injection condition, the solution structure must also change continuously corresponding to the change in input information.

2.4 Solution construction procedure

With the concepts of continuous and discontinuous solutions, we summarize the solution construction procedure as follows:

- Starting from the eigenvalue problem based on material balance and energy balance equations, find all possible continuous solution path combinations in the composition space that connect the initial and injection conditions.
- Apply the velocity rule on the solution segments, replace the continuous solution segments that violate the velocity rule with shock solutions. When constructing shock solutions, apply the entropy condition to find stable shocks. Overall, the whole solution structure must satisfy a continuity condition.
- Apply the velocity rule, entropy condition, and continuity condition recursively

and iteratively until all the non-physical solutions are excluded and a unique solution is found.

In the chapters that follow, these procedure are applied to the problem of coal-bed methane recovery and to the problem of gas injection with temperature variation.

Chapter 3

Enhanced Coal Bed Methane Recovery

3.1 Introduction

In this chapter, we concentrate on the effects of adsorption and desorption that are most evident in problems such as ECBM by gas injection. The temperature is assumed to remain constant during the gas displacement processes.

The ECBM problem is of interest because of the complex adsorption and desorption behavior, coupled with the phase equilibrium of the gas mixtures, and multiphase flow through the porous coal bed. Arri *et al.* [1] measured the adsorption isotherms using moist coal samples from the Fruitland coal seam of the San Juan Basin of Colorado. Measurements were performed on both pure gas components and binary mixtures, and were compared favorably with the prediction of the extended Langmuir isotherm at relatively low pressure. A black-oil simulator was adapted to accommodate the adsorption and desorption behavior of the gas components and model the CBM production. Up to three phases were introduced in the system, where the oil phase was set to be immobile and used to represent the coal. It adsorbed both gas components and moisture. The aqueous phase contained only water. The gas phase could contain both water and gas components. A new phase equilibrium model was developed and put in the simulator. The modified simulator was tested for primary

recovery of a single sorbing component and N_2 -ECBM.

In this study, we focus on the interaction of CH_4 , CO_2 , and N_2 with the method of characteristics approach. We neglect the mobile liquid phase, and use an extended Langmuir isotherm to approximate the adsorption and desorption of the gas components at the coalbed surfaces. When components transfer between flowing phases and coalbed surfaces, the effect of volume change is considered. However, we neglect the volume change of the adsorbed components at the coalbed surface. The thermodynamic behavior of the gas mixtures is represented by the Peng-Robinson equation of state.

3.2 Langmuir isotherm for adsorption and desorption

Most of the studies of multicomponent gas sorption on coal are limited to experimental work, where measurements of the adsorption isotherms were performed on dry coal and mostly at low pressures [32], [33]. As methane (CH_4), carbon-dioxide (CO_2) and nitrogen (N_2) are often the primary components in ECBM by gas injection, measurements were made on mixtures of these components. Rather than explore the effect of mixture composition on the adsorption behavior, most of the experimental work was carried out on mixtures with fixed molar composition but varying pressure. Hysteresis was observed when adsorption (pressure increasing) and desorption (pressure decreasing) isotherms are measured [2]. On the other hand, in a constant composition expansion and constant volume depletion sorption experiment by Chaback *et al.* [3], it was reported that the adsorption and desorption process is reversible and can be effectively described by extended Langmuir isotherm.

When applying the method of characteristics to the ECBM problem, we assume that the pressure remains constant for the purpose of evaluating the adsorption equilibrium. Therefore, adsorption and desorption occur when the molar composition of the flowing phases varies, resulting in variation in partial pressure of a given gas

species. We assume the adsorption and desorption process is reversible, and is described by a single set of isotherm constants.

Markham *et al.* [26] provided an extended Langmuir isotherm for a multicomponent mixture. It describes the fractional surface coverage of individual components, Θ_i , as

$$\Theta_i = \frac{B_i p_i}{1 + \sum_{j=1}^{n_c} B_j p_j}, \quad (3.1)$$

where B_i is a Langmuir constant at given temperature for adsorption of a pure species, and p_i is the partial pressure of component i that is approximated by the ideal gas relation as

$$p_i = z_i p, \quad (3.2)$$

where z_i is the mole fraction of species i . Hence, the molar concentration of the adsorbed components, a_i depends only on the molar composition of the free gas phase according to

$$a_i = \frac{\rho_i \rho_r V_{mi} B_i p_i}{1 + \sum_{j=1}^{n_c} B_j p_j}, \quad (3.3)$$

where ρ_r is the density of the coalbed, ρ_i is the molar density of component i at standard condition, and V_{mi} is a Langmuir constant for component i at given temperature.

The extended Langmuir isotherm constants based on the experiments of Greaves *et al.* [9] on adsorption and desorption of pure CH_4 , pure CO_2 , and mixtures of the two will be used in this work. Figure 3.1 illustrates the results of those experiments and the model fits. The Langmuir isotherm constants for pure N_2 are not readily available. However, since N_2 adsorbs less strongly to coal than either CH_4 or CO_2 , it is reasonable to assume that the extended Langmuir isotherm constants are about half as those of CO_2 . The results reported below will show that the competition among different gas species for coalbed surface is determined by the order of the affinity of the gas components, and hence the behavior of displacement can be investigated even if detailed N_2 data are not available.

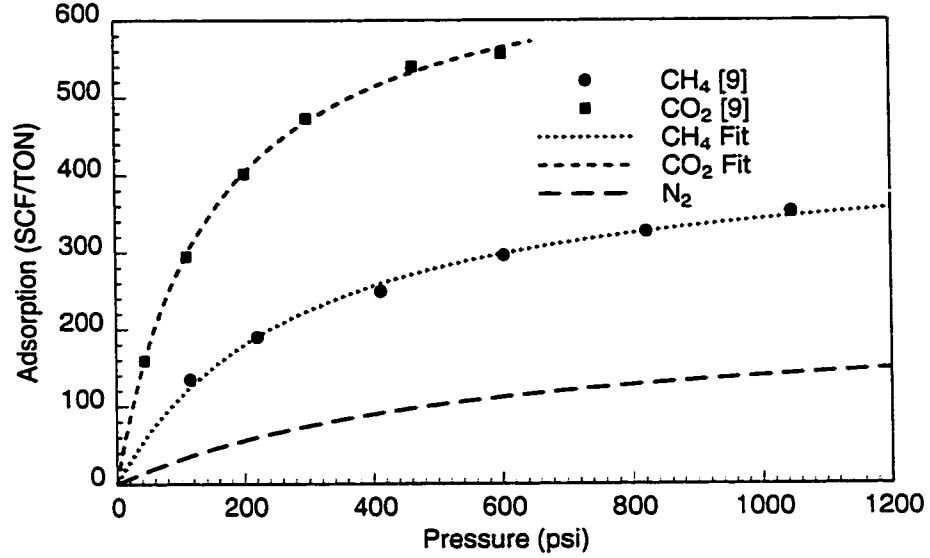


Figure 3.1: Experimental data for adsorption/desorption of pure CH_4 and CO_2 , and fitting with extended Langmuir isotherm.

3.3 Mathematical Basis

Since we only consider single-phase flow and assume constant temperature, the molar concentration and flux terms for the material balance of individual components simplify to

$$C_i = \phi \rho z_i + (1 - \phi) a_i, \quad (3.4)$$

and

$$F_i = u \alpha_i = u \rho z_i. \quad (3.5)$$

Instead of using the energy balance equation to perform the decoupling of the local flow velocity, we use the material balance equation for the last component. Accordingly, the sub-matrices for solving the normalized eigenvalue are evaluated as

$$[F] = \frac{\partial \alpha_i}{\partial z_j} - \frac{\alpha_i}{\alpha_{n_c}} \frac{\partial \alpha_{n_c}}{\partial z_j}, \quad (3.6)$$

$$[G] = \frac{\partial C_i}{\partial z_j} - \frac{\alpha_i}{\alpha_{n_c}} \frac{\partial C_{n_c}}{\partial z_j}, \quad (3.7)$$

$$\vec{F}^T = \frac{1}{\alpha_{n_c}} \frac{\partial \alpha_{n_c}}{\partial z_j}, \quad (3.8)$$

$$\vec{G}^T = \frac{1}{\alpha_{n_c}} \frac{\partial C_{n_c}}{\partial z_j}, \quad (3.9)$$

$$\vec{e} = \frac{dz_j}{d\eta}, \quad (3.10)$$

$$\lambda^* = \frac{\lambda}{u}, \quad (3.11)$$

$$\frac{\partial a_i}{\partial z_j} = V_{mi} \rho_i \rho_r B_i p \left[\frac{1}{1 + \sum_{k=1}^{n_c} B_k p_k} \frac{\partial z_i}{\partial z_j} - \frac{z_i \sum_{k=1}^{n_c} B_k p \frac{\partial z_k}{\partial z_j}}{(1 + \sum_{k=1}^{n_c} B_k p_k)^2} \right], \quad (3.12)$$

where the subscripts i and j vary from 1 to $n_c - 1$.

3.4 Solution construction

Construction of the analytical solution for ECBM with gas injection varies for systems with different numbers of components. Solution in a single-component system is trivial because the injected gas and initial gas are at dynamic equilibrium, and hence the local flow velocity remains constant, that is, identical to the injection rate. In this section, we will first discuss solutions in binary system, and then continue to ternary systems. Specifically, three components are used, CH_4 , CO_2 , and N_2 . The thermodynamic properties of these components are summarized in Table 3.1. If not stated otherwise, the pressure is 1600 psi, and temperature 160 °F for all calculations.

Table 3.1: The thermodynamic properties of gas components in the example solutions.

	P_c (atm)	T_c (°F)	M_w (g/gmol)	Ω	V_m (SCF/ton)	B (psi ⁻¹)	κ		
							CH_4	CO_2	N_2
CH_4	667.2	-116.6	16.043	0.008	444.0	0.0034	0.0	0.103	0.031
CO_2	1069.9	87.9	44.01	0.225	707.5	0.0066	0.103	0.0	0.0
N_2	493.0	-232.4	28.01	0.04	222.0	0.0017	0.031	0.0	0.0

3.4.1 Binary flow

Consider first the continuous solution. The composition space is the binary axis, because only one of the molar compositions varies independently. The problem for the normalized eigenvalue and the corresponding eigenvector is of first order, and yields

$$\lambda^* = \frac{\phi \rho}{\phi \rho + (1 - \phi) \left(z_2 \frac{\partial a_1}{\partial z_1} - z_1 \frac{\partial a_2}{\partial z_1} \right)}, \quad (3.13)$$

and

$$\vec{e} = \left[\frac{\partial z_1}{\partial \eta} \right] = 1. \quad (3.14)$$

Substitution of the normalized eigenvalue and eigenvector to the local flow velocity problem yields

$$\frac{1}{u} \frac{du}{d\eta} = - \left[\left(\frac{1}{\rho} \frac{\partial \rho}{\partial z_1} - \frac{1}{z_2} \right) - \lambda^* \left(\frac{1}{\rho} \frac{\partial \rho}{\partial z_1} - \frac{1}{z_2} + \frac{1 - \phi}{\phi} \frac{1}{\rho z_2} \frac{\partial a_2}{\partial z_1} \right) \right]. \quad (3.15)$$

In a continuous solution, the composition varies continuously along the binary axis from the injection gas composition to the initial composition. At each intermediate state, the molar composition is associated with a normalized eigenvalue and local flow velocity. If the wave velocity increases monotonically as the solution path is traced from the injection condition upstream to the initial condition downstream, then the velocity rule is satisfied. The solution is a continuous variation from the injection composition to the initial composition.

On the other hand, if the continuous solution violates the velocity rule, a shock solution is needed. If the molar compositions on the upstream and downstream sides of the shock are both known, and the injection gas flow rate is a given constant, then the only unknowns are the local flow velocity on the downstream side of the shock u^d and the shock velocity Λ . Solving the Rankine-Hugoniot conditions

$$\Lambda = \frac{F_1^u - F_1^d}{C_1^u - C_1^d} = \frac{F_2^u - F_2^d}{C_2^u - C_2^d} \quad (3.16)$$

yields

$$u^d = u^u \frac{\alpha_1^u (C_2^u - C_2^d) - \alpha_2^u (C_1^u - C_1^d)}{\alpha_1^d (C_2^u - C_2^d) - \alpha_2^d (C_1^u - C_1^d)}, \quad (3.17)$$

and

$$\Lambda = u^u \frac{\alpha_1^d \alpha_2^u - \alpha_1^u \alpha_2^d}{\alpha_1^d (C_2^u - C_2^d) - \alpha_2^d (C_1^u - C_1^d)}. \quad (3.18)$$

We use the $CH_4 - CO_2$ system to demonstrate the solution construction procedure. Figure 3.2 illustrates the variation of the normalized eigenvalue, local flow velocity as the molar composition varies continuously. The propagation velocity of a composition is the product of the normalized eigenvalue and the local flow velocity. As the CO_2 concentration decreases continuously, both the normalized eigenvalue and local flow velocity decrease. Therefore, if a binary mixture with high CO_2 content is injected at a unit rate into a coalbed initially saturated with a binary mixture rich in CH_4 , the propagation velocity of the composition wave decreases as CH_4 concentration increases. This variation violates the velocity rule. A shock solution must be constructed instead as indicated by the Rankine-Hugoniot condition. Figure 3.3 shows the single shock profile for an example solution in the binary CH_4-CO_2 system, where the injection gas consists of 95% CO_2 and 5% CH_4 , and the initial gas 3% CO_2 and 97% CH_4 .

In the $CH_4 - N_2$ system, when the N_2 composition increase continuously. its corresponding normalized eigenvalue and local flow velocity decrease monotonically. The resulting propagation velocity of the composition is shown in Fig. 3.4. When a N_2 -rich mixture is injected to displace an initial mixture rich in CH_4 , the propagation velocity increases as the composition of N_2 decreases continuously from upstream to downstream. Therefore, the solution is a continuous variation of molar composition from upstream to downstream. The solution profiles for the molar compositions, molar density and adsorption are summarized in Fig. 3.5.

Similar analysis can be applied to the CO_2-N_2 system. The the variation of eigenvalues and local flow velocity with the continuous variation of molar composition can be seen in Fig. 3.6. In an example solution, when a mixture rich in N_2 is injected to displace an initial mixture with high CO_2 concentration, there exists a continuous solution that satisfies the velocity rule, as shown in Fig. 3.7.

In general, it can be observed that a shock solution occurs when a gas rich in a component with higher affinity for coal is injected to displace a coalbed gas that is rich in a component that adsorbs less strongly. Continuous solutions result during injection of gas rich in a weakly adsorbing component, N_2 displacing CO_2 , for example.

3.4.2 Ternary flow

Consider a mixture of CH_4 , CO_2 , and N_2 as an example for systems with three components. The composition space is described by a ternary diagram that represents the molar compositions. In order to construct a continuous solution, the 2 by 2 submatrices in Eq. 3.6 through Eq. 3.9 that determine the normalized eigenvalues are evaluated as

$$F_{11} = \rho \left(1 + \frac{z_1}{z_3} \right), \quad (3.19)$$

$$F_{12} = \rho \frac{z_1}{z_3}, \quad (3.20)$$

$$F_{21} = \rho \frac{z_2}{z_3}, \quad (3.21)$$

$$F_{22} = \rho \left(1 + \frac{z_2}{z_3} \right), \quad (3.22)$$

$$G_{11} = \rho \left(1 + \frac{z_1}{z_3} \right) + \frac{1-\phi}{\phi} \left(\frac{\partial a_1}{\partial z_1} - \frac{z_1}{z_3} \frac{\partial a_3}{\partial z_1} \right), \quad (3.23)$$

$$G_{12} = \rho \frac{z_1}{z_3} + \frac{1-\phi}{\phi} \left(\frac{\partial a_1}{\partial z_2} - \frac{z_1}{z_3} \frac{\partial a_3}{\partial z_2} \right), \quad (3.24)$$

$$G_{21} = \rho \frac{z_2}{z_3} + \frac{1-\phi}{\phi} \left(\frac{\partial a_2}{\partial z_1} - \frac{z_2}{z_3} \frac{\partial a_3}{\partial z_1} \right), \quad (3.25)$$

$$G_{22} = \rho \left(1 + \frac{z_2}{z_3} \right) + \frac{1-\phi}{\phi} \left(\frac{\partial a_2}{\partial z_2} - \frac{z_2}{z_3} \frac{\partial a_3}{\partial z_2} \right), \quad (3.26)$$

$$\vec{F}^T = \begin{bmatrix} \frac{1}{\rho} \frac{\partial \rho}{\partial z_1} - \frac{1}{z_3} \\ \frac{1}{\rho} \frac{\partial \rho}{\partial z_2} - \frac{1}{z_3} \end{bmatrix}, \quad (3.27)$$

$$\vec{G}^T = \begin{bmatrix} \frac{1}{\rho} \frac{\partial \rho}{\partial z_1} - \frac{1}{z_3} + \frac{1-\phi}{\phi} \frac{1}{\rho z_3} \frac{\partial a_3}{\partial z_1} \\ \frac{1}{\rho} \frac{\partial \rho}{\partial z_2} - \frac{1}{z_3} + \frac{1-\phi}{\phi} \frac{1}{\rho z_3} \frac{\partial a_3}{\partial z_2} \end{bmatrix}. \quad (3.28)$$

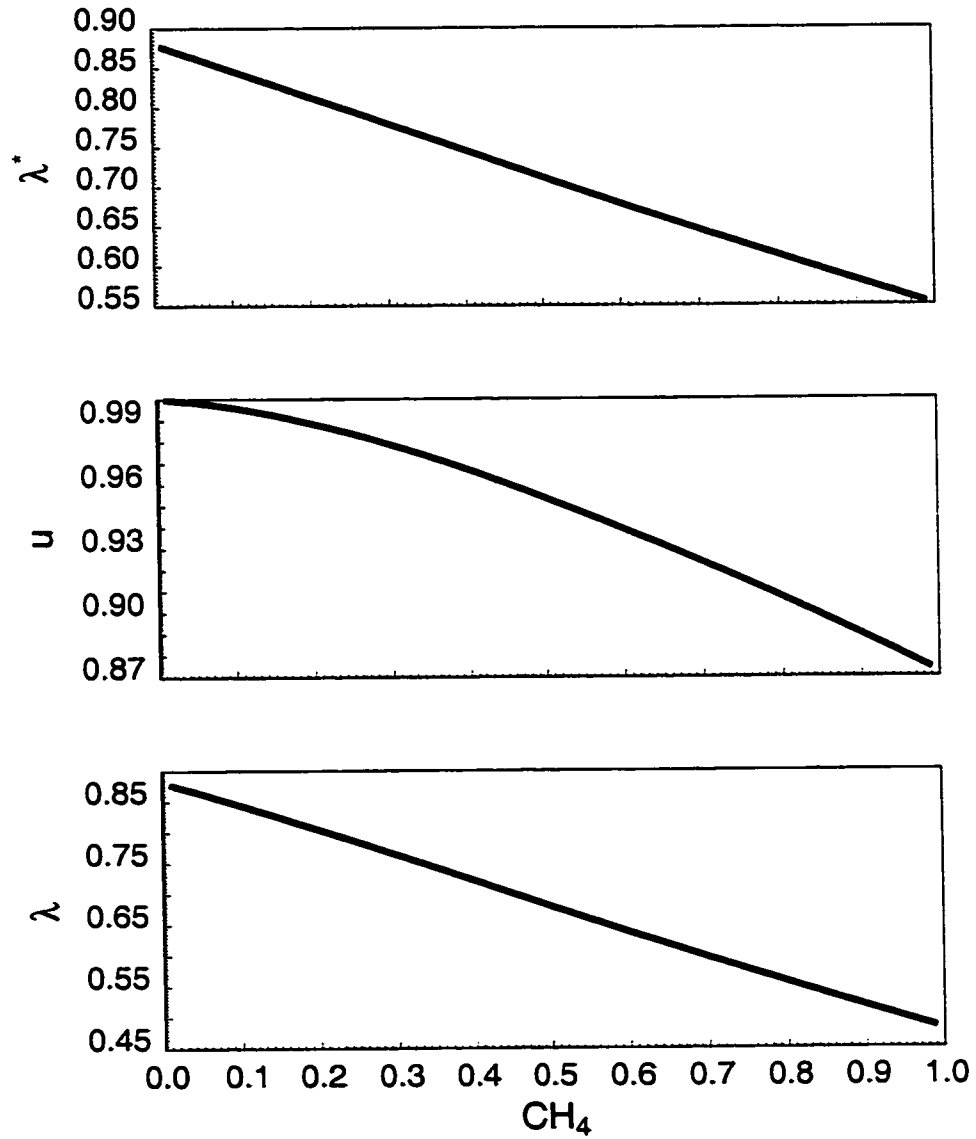


Figure 3.2: Variation of normalized eigenvalue, local flow velocity and characteristic wave velocity along the $CH_4 - CO_2$ binary axis.

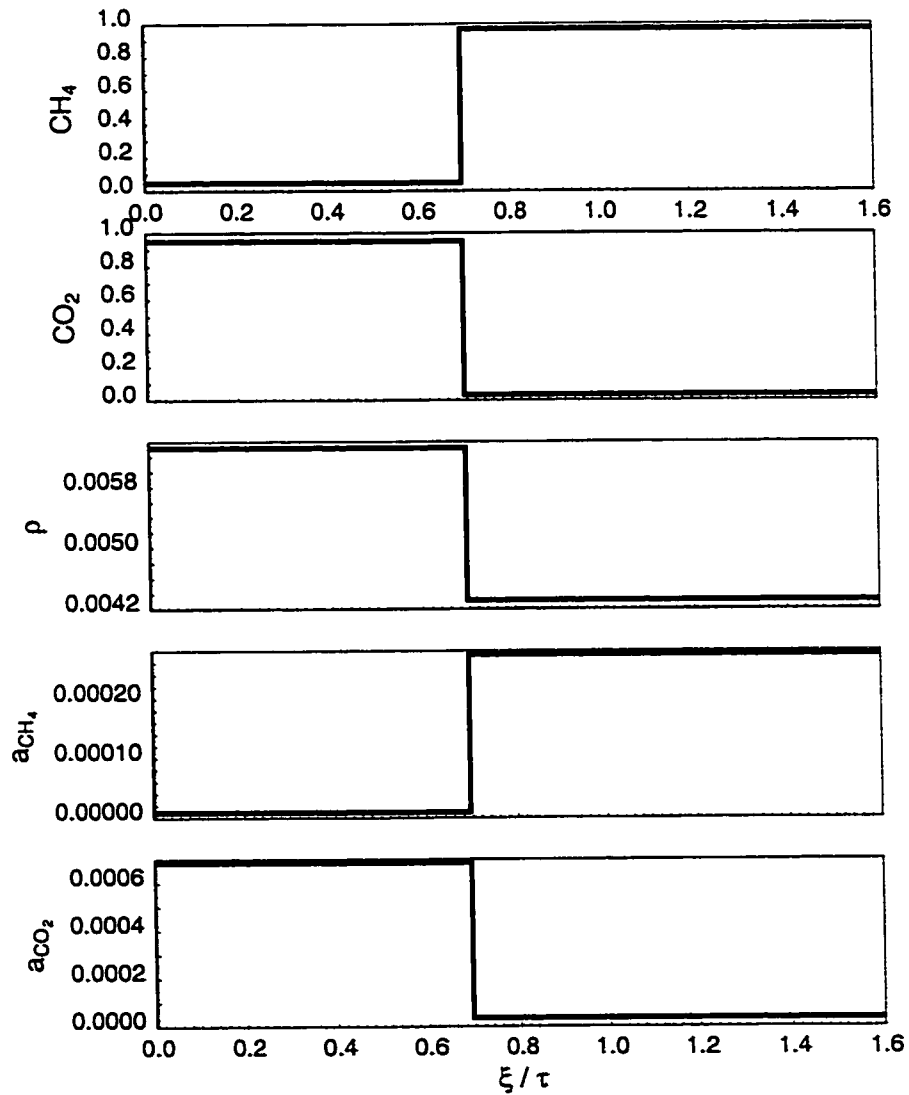


Figure 3.3: Solution profile for an example in the $CH_4 - CO_2$ system. The mixture of 95% CO_2 and 5% CH_4 is injected to displace an initial mixture of 3% CO_2 and 97% CH_4 .

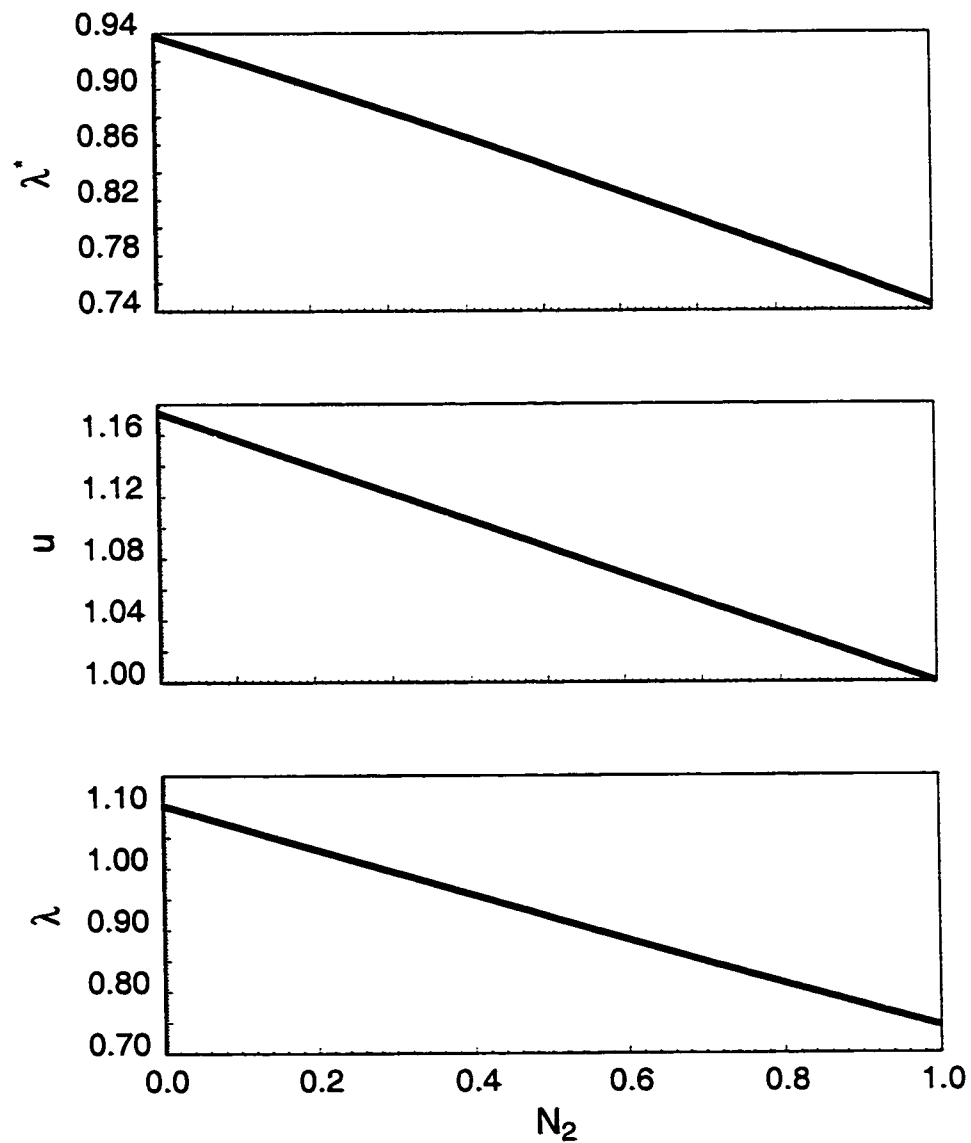


Figure 3.4: Variation of normalized eigenvalue, local flow velocity and characteristic wave velocity along the $CH_4 - N_2$ binary axis.

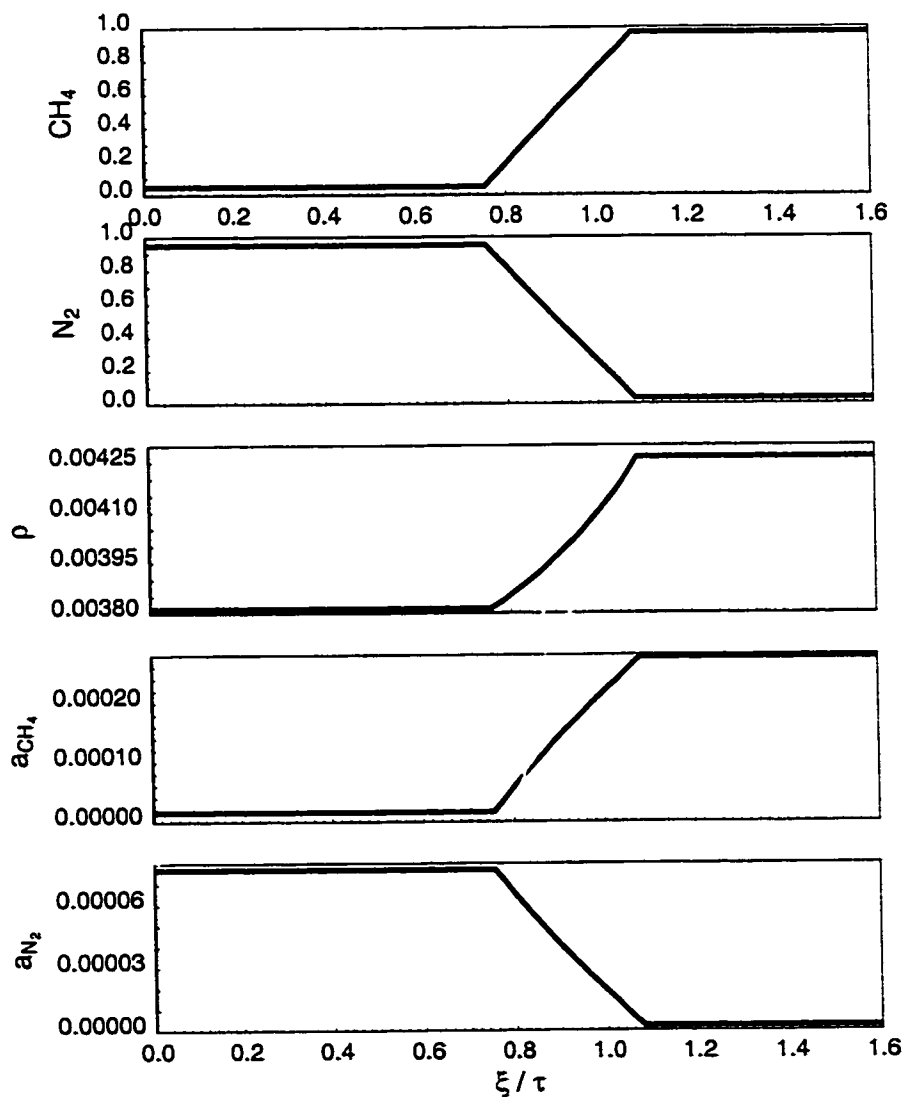


Figure 3.5: Solution profile for an example in the $CH_4 - N_2$ system. The mixture of 95% N_2 and 5% CH_4 is injected to displace an initial mixture of 3% N_2 and 97% CH_4 .

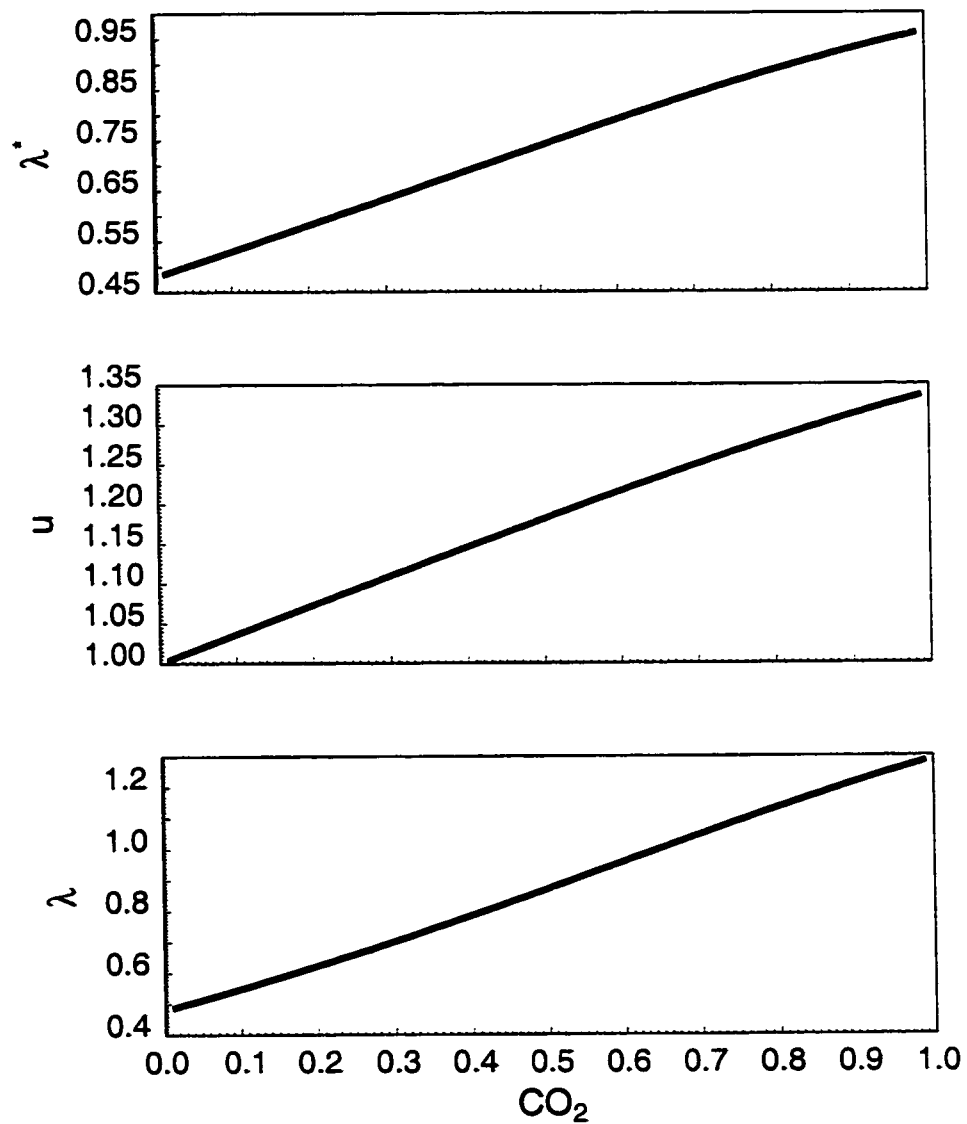


Figure 3.6: Variation of normalized eigenvalue, local flow velocity and characteristic wave velocity along the $CO_2 - N_2$ binary axis.

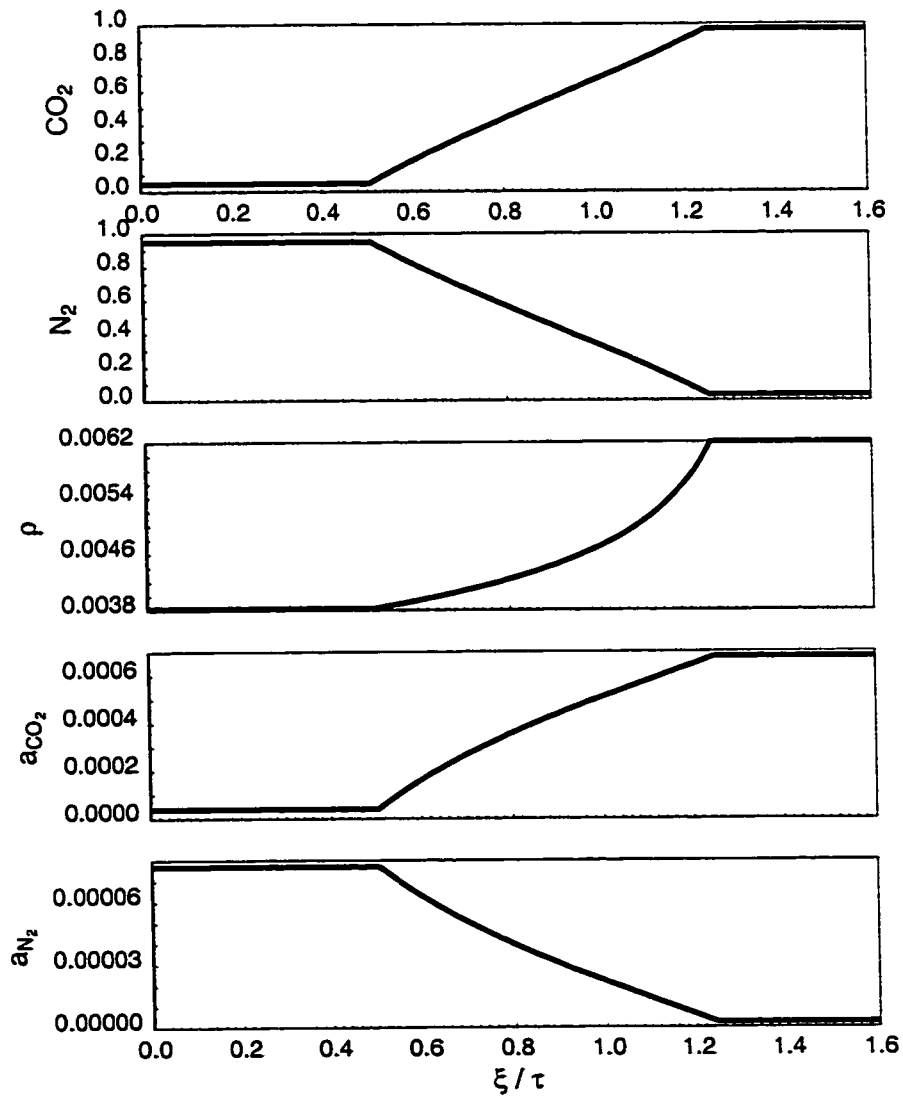


Figure 3.7: Solution profile for an example in the $CO_2 - N_2$ system. The mixture of 95% N_2 and 5% CO_2 is injected to displace an initial mixture of 3% N_2 and 97% CO_2 .

At each point in the ternary composition space, there are two normalized eigenvalues that can be found as the two roots of

$$\lambda^{*2}(G_{11}G_{22} - G_{12}G_{21}) + \lambda^*(F_{12}G_{21} + F_{21}G_{12} - F_{11}G_{22} - F_{22}G_{11}) + (F_{11}F_{22} - F_{12}F_{21}) = 0, \quad (3.29)$$

$$\vec{e} = \begin{pmatrix} \frac{dz_1}{d\eta} \\ \frac{dz_2}{d\eta} \end{pmatrix} = \begin{pmatrix} F_{12} - \lambda^*G_{12} \\ -F_{11} + \lambda^*G_{11} \end{pmatrix} \quad (3.30)$$

There are two sets of paths, each corresponding to one of the two normalized eigenvalues and its corresponding eigenvector. The two sets of paths form a mesh-like pattern, as shown in Fig. 3.8. The paths are not necessarily straight lines but a result from an integration in the composition space along directions given by the eigenvectors. To illustrate the path-mapping procedure, we start from a point **A** in the ternary composition space as the upstream condition (Fig. 3.9), and assume a local flow velocity at this point. The eigenvalue problem yields two normalized eigenvalues with different magnitudes, each with its own eigenvector. Following the direction indicated by the eigenvector corresponding to the larger eigenvalue, we take a small step towards the region with higher CH_4 concentration, and solve the eigenvalue problem for the normalized eigenvalue, its corresponding eigenvector, and the local flow velocity at the new composition. The process is repeated until we arrive at the boundary of the ternary composition space at **C**. The variation of the composition, normalized eigenvalue, and local flow velocity is recorded along the path. Path **AC** is sloped upward to the right, and the wave velocity increases monotonically as the path is traced towards the CH_4 -rich region, as Fig. 3.9 shows. Similarly, following path **AB** that slopes upward to the left, given by the eigenvector corresponding to the smaller eigenvalue, the wave velocity decreases as the path is traced towards the region with higher CH_4 content (Fig. 3.9). We refer to the paths sloping upward to the left as “slow paths”, and those sloping upward to the right as “fast paths”.

Now consider solutions for ECBM processes where the initial gases are richer in CH_4 than the injected gases. Given initial and injection gas compositions, and a fixed injection rate, the displacement is solved by finding a solution path, consisting of either continuous segments or shock segments, that connects the injection and initial

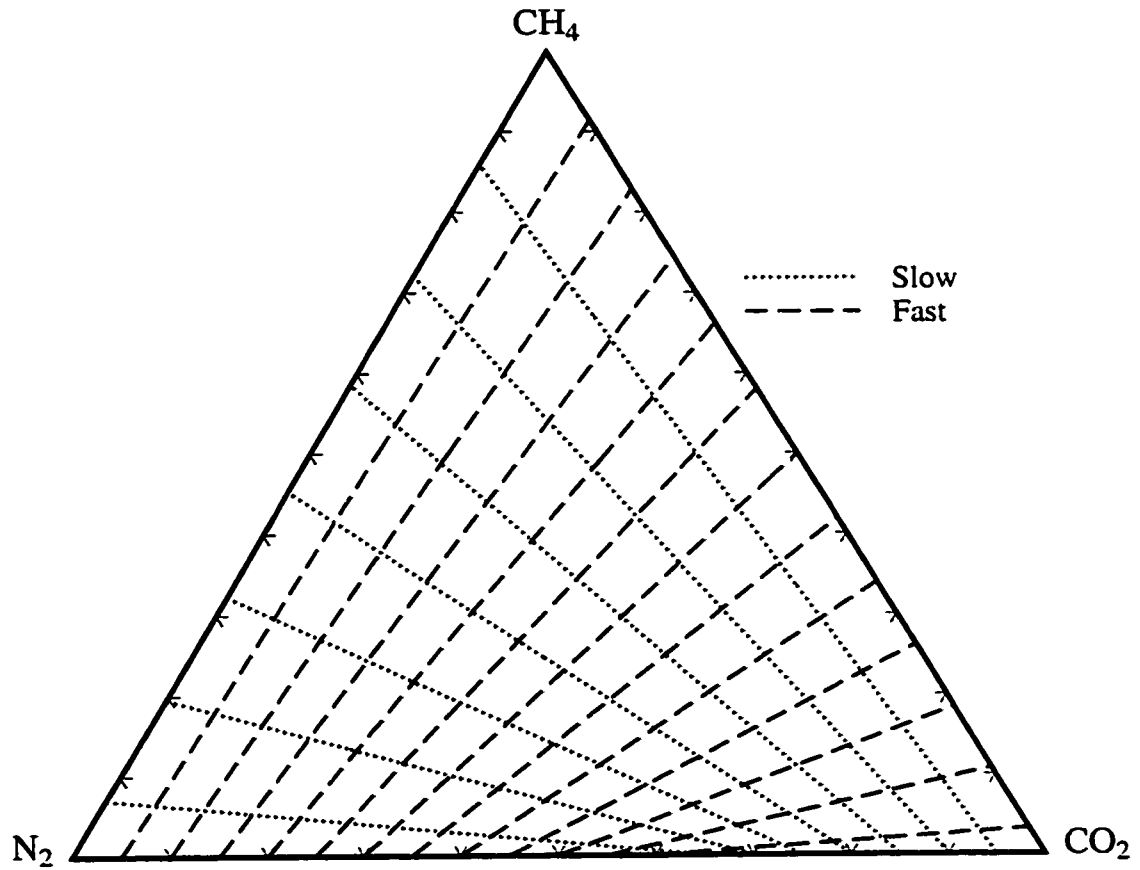


Figure 3.8: Continuous solution paths for $CH_4 - CO_2 - N_2$ ternary system.

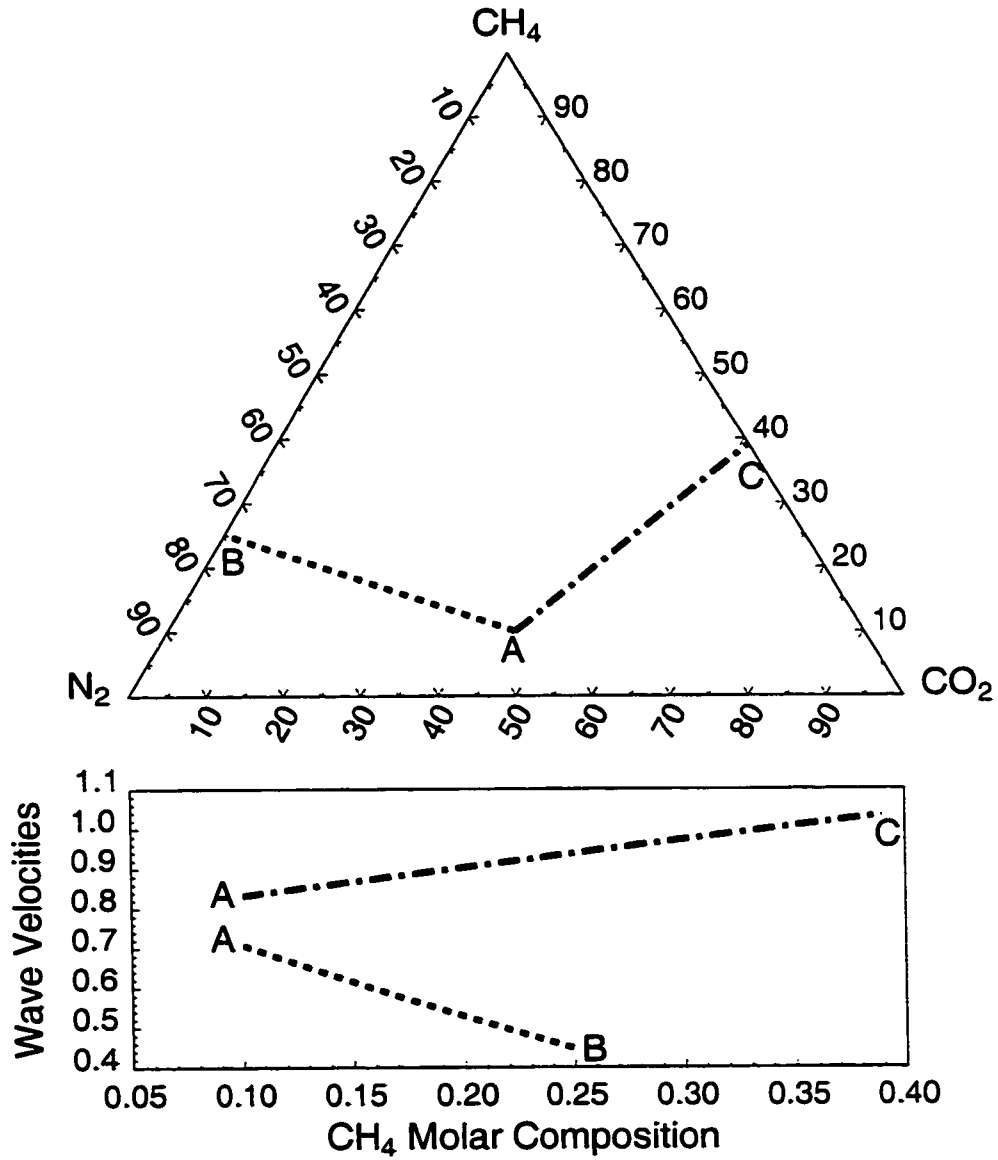


Figure 3.9: Variation of characteristic wave velocity following the fast and slow paths separately towards the CH_4 -rich zone. The initial composition (A) is the same for each path.

gas compositions in the ternary composition space. Each intermediate stage along the solution path represents an intermediate molar composition with a normalized eigenvalue and local flow velocity. The product of the two is the wave velocity at which the composition wave propagates downstream. Depending on the injected gas composition, the solutions can be classified into three types.

It is more likely that CO_2 -rich gases will be used to displace CH_4 -rich gases than the reverse. Figure 3.10 shows the most commonly seen configuration of initial and injection compositions. We name this scenario Type I. Two sets of paths connect the initial composition, represented by point **O** in the ternary composition space, and injection composition, represented by point **I**. A continuous solution path connecting the injection and initial compositions could follow the path $I \rightarrow A \rightarrow O$ or path $I \rightarrow B \rightarrow O$. The path $I \rightarrow B \rightarrow O$ requires a switch from a fast path to a slow path at point **B** as the composition path is traced from upstream to downstream. This switch violates the velocity rule. Hence, this path configuration is unphysical and must be excluded. On the other hand, following path **IA** with a switch to path **AO** requires a switch from a slower path upstream to a fast path downstream, which does not violate the velocity rule. However, as the slow path is traced from **I** to **A**, the wave velocity decreases in the downstream direction. This is a violation of the velocity rule, and hence this composition variation must be replaced by a shock solution. The shock solution satisfies the material balances in an integral form, and does not necessarily follow the path for a continuous solution,

$$\Lambda = \frac{F_1^u - F_1^d}{C_1^u - C_1^d} = \frac{F_2^u - F_2^d}{C_2^u - C_2^d} = \frac{F_3^u - F_3^d}{C_3^u - C_3^d}. \quad (3.31)$$

All the variables at the upstream side of the shock are known. The molar composition and local flow velocity can be obtained from the Rankine-Hugoniot condition, Eq. 3.31. The shock landing point is fully determined and must lie on the fast path through the initial composition at point **C**. Therefore, the final solution consists of a shock between **I** and **C**, a constant state at **C**, and a continuous variation **CO**, Fig. 3.10.

As the injection composition is moved closer to the fast path through the initial

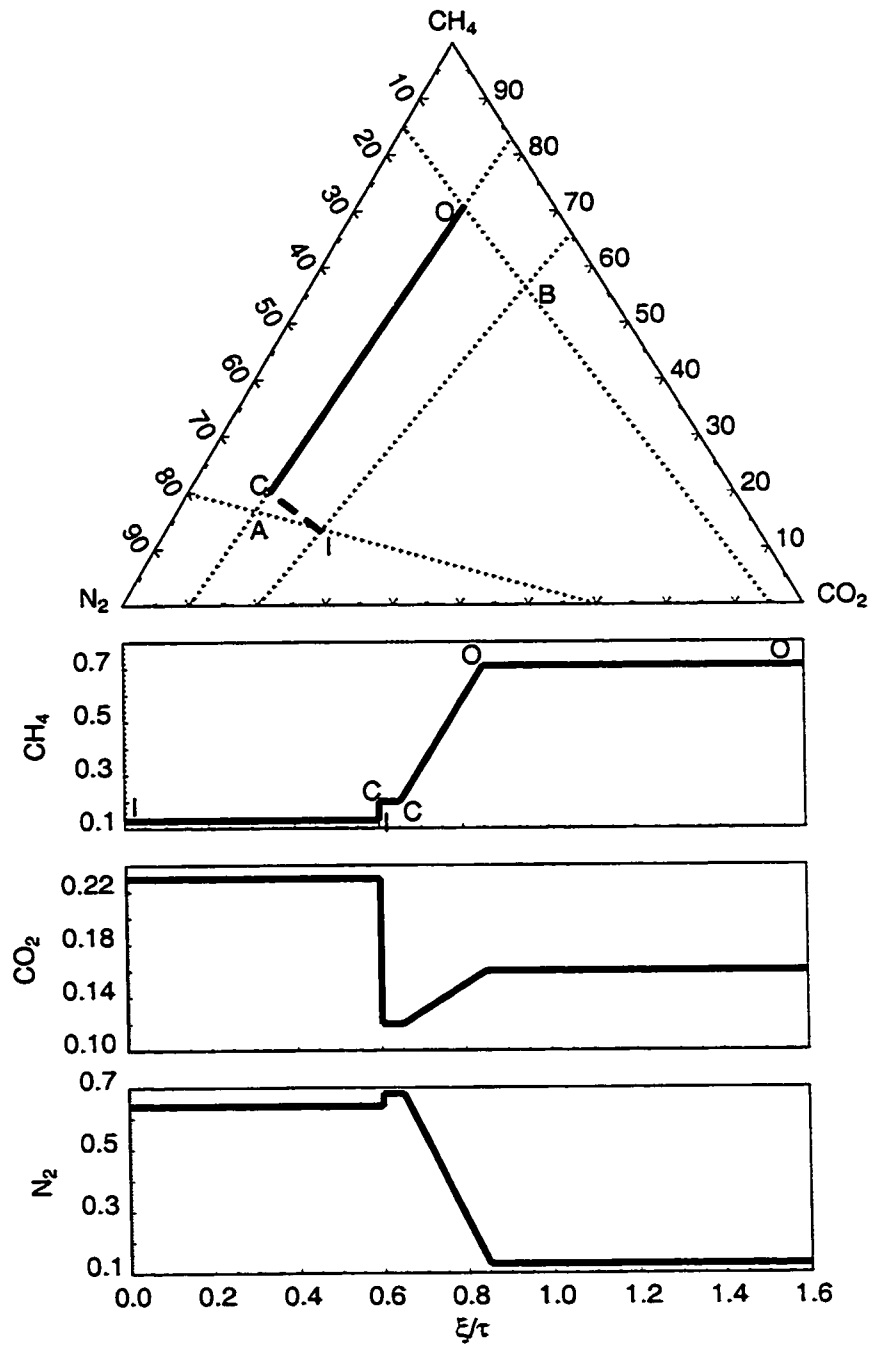


Figure 3.10: Type I solution, composed of upstream shock IC, and downstream continuous variation CO.

composition, the upstream shock segment becomes shorter. In the limit when the injection composition falls on the fast path through **O**, the upstream shock segment disappears. The solution is a continuous wave between the initial and injection compositions. On the other hand, when the injection composition moves towards the CO_2 vertex, the shock landing point **C** moves closer to the initial composition **O**, with a shorter downstream continuous wave segment. The limiting case takes place when point **C** and **O** overlap, resulting in complete disappearance of the downstream continuous wave. The solution is a single shock between the initial and injection compositions.

The second type of solution (Type II) occurs when the injection composition moves to the left of the fast path through the initial composition, as shown in Fig. 3.11. Similar analysis using the velocity rule indicates that the solution must be composed of an upstream continuous wave along the slow path from injection composition **I** to point **A**, where there is a switch to the fast path and a continuous variation from **A** to initial composition **O**.

The third type of solution (Type III) occurs when the shock landing point **C** goes beyond point **O**, as Fig. 3.12 shows. Tracing a path from **C** back to **O** violates the velocity rule, and hence a shock is required between **C** and **O**. The shock solution does not necessarily occur along paths for continuous solutions. Therefore, a shock point **C** must be found such that shocks **CO** and **CI** both satisfy the Rankine-Hugoniot condition.

3.4.3 1D Finite-Difference Simulation

A one-dimensional finite-difference scheme was used to simulate the ECBM process by gas injection and to confirm the analytical solutions. With single-point upstream weighting, the finite-difference form of the material balance equation is

$$C_{i,k}^{n+1} = C_{i,k}^n - \frac{\Delta t}{\Delta x} [F_{i,k}^n - F_{i,k-1}^n]. \quad (3.32)$$

At each time step, a calculation similar to a multiphase equilibrium calculation was performed. Given an overall molar composition in a cell, the components were

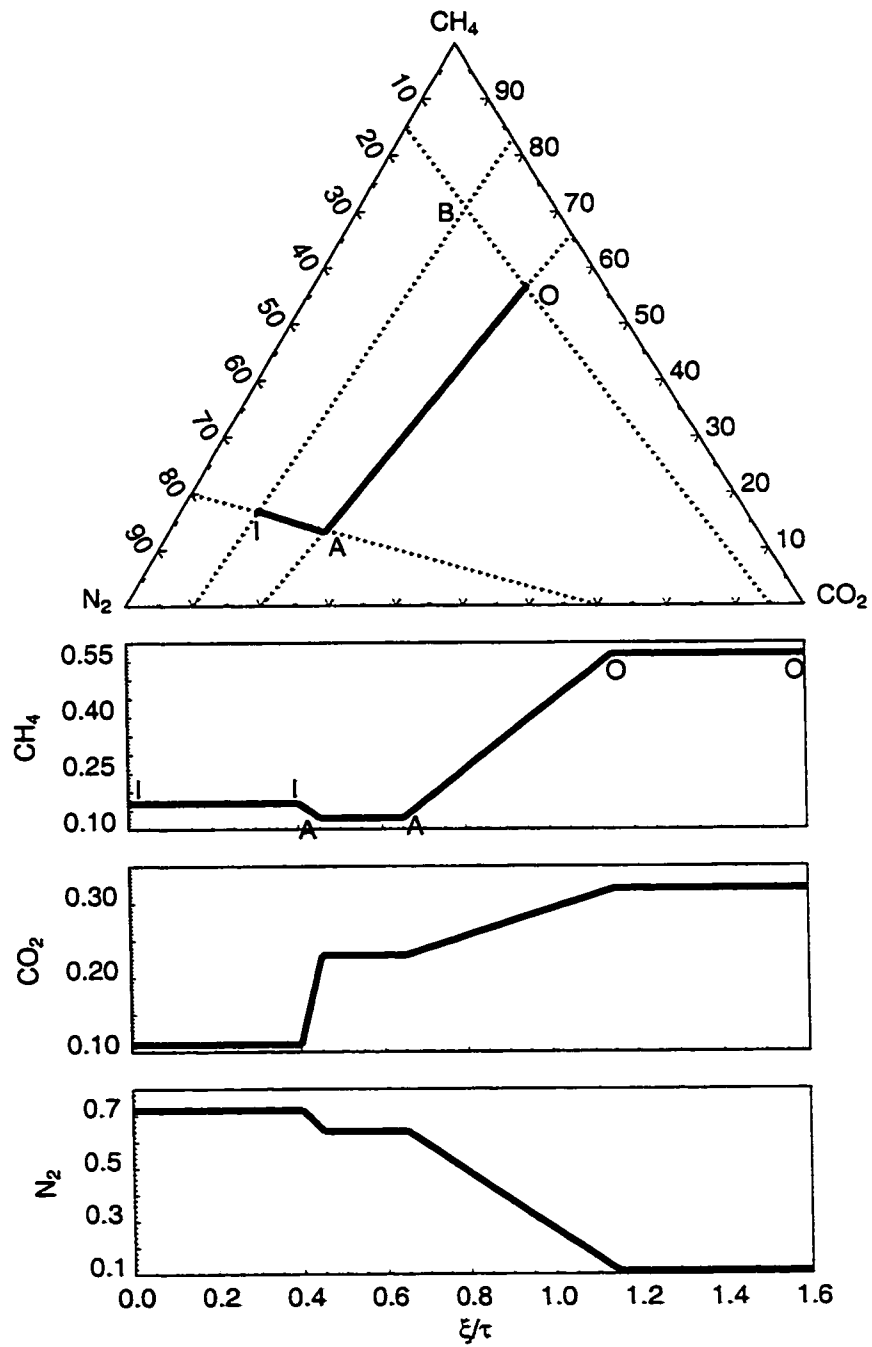


Figure 3.11: Type II solution paths, composed of upstream continuous variation IA, and downstream continuous variation AO.

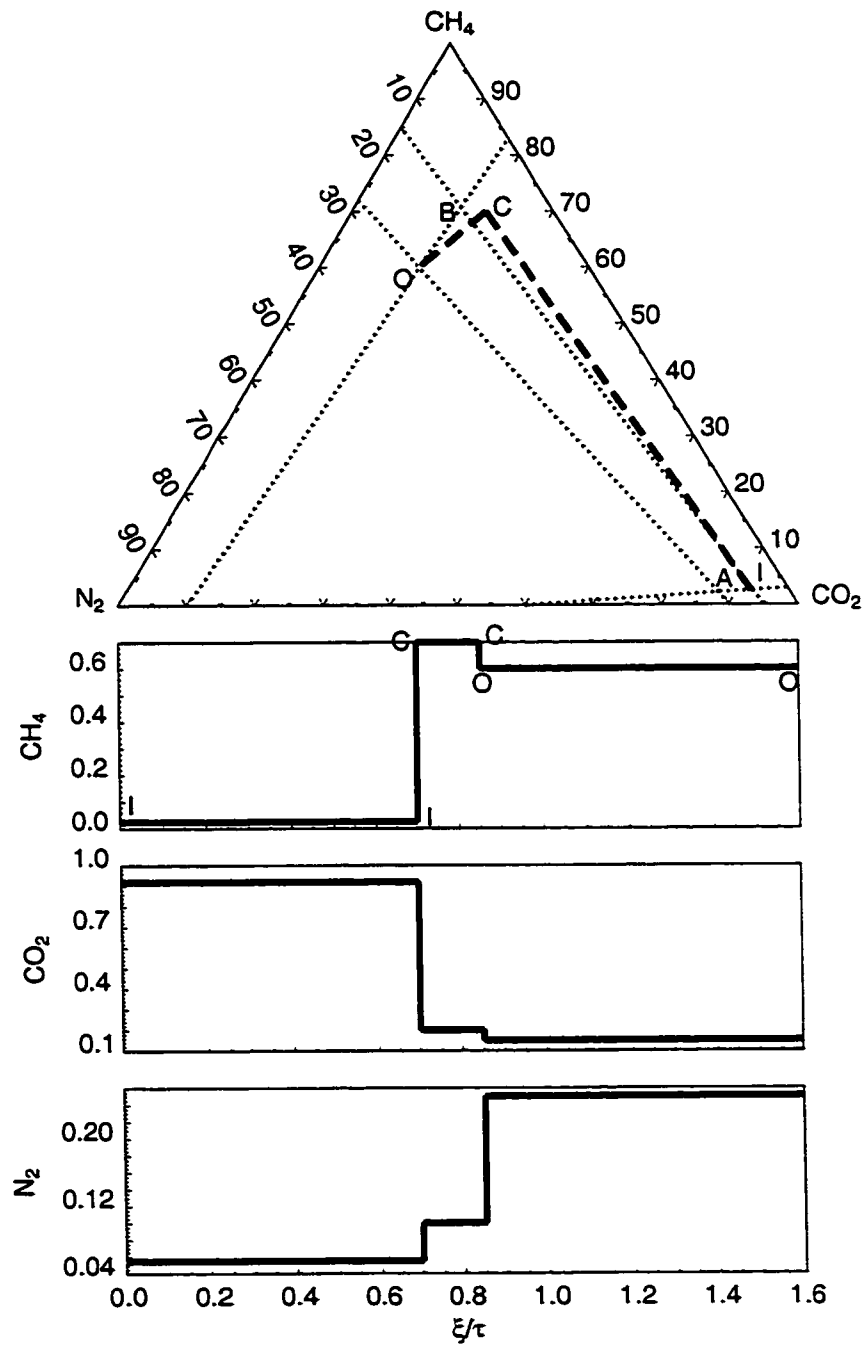


Figure 3.12: Type III solution paths, composed of upstream shock IC, and downstream shock CO.

distributed between the pore space as free gas and coalbed as adsorbed gas with the equilibrium compositions determined by the extended Langmuir isotherm for adsorption. The local flow velocity at each cell is computed corresponding to the variation in molar density due to mixing of the components.

3.4.4 Example Solutions

The analytical solution procedure was applied to study injection of N_2/CO_2 mixtures into coalbeds. The initial gas composition is fixed as 96% CH_4 , 3% CO_2 and 1% N_2 , and the injection gases are binary mixtures composed of CO_2 and N_2 . Five injection compositions were considered containing 0%, 25%, 50%, 75% and 100% mole fraction of CO_2 , with the remainder being N_2 . These compositions yield analytical solutions of the three different types. For each of these sample cases, a 1D finite-difference simulation was run to confirm the analytical solutions. The number of grid blocks was 5000, and the Courant number ($\Delta t/\Delta x$) was fixed at 0.1.

The solution paths for the examples are summarized in Fig. 3.13. The arrival times of the leading edge and trailing shocks for the example solutions are summarized in Table 3.2. The recovery curves of CH_4 are shown in Fig. 3.14.

A Type II solution results when the injection gas consists of pure N_2 , as Fig. 3.15 shows. The solution includes an upstream continuous variation from the injection gas composition to the path switch point **A**, and a downstream continuous wave along the fast path from **A** to the initial composition **O**. The composition waves arrive at the producing end at a time given by $1/\lambda$ or $1/\Lambda$, where the producing end corresponds to

Table 3.2: Summary of breakthrough times and complete recovery of the initial CBM.

	Injection Gas		PVI at breakthrough	PVI at complete recovery
	CO_2 (%)	N_2 (%)		
1	0	100	0.91	2.08
2	25	75	0.99	1.90
3	50	50	1.08	1.75
4	75	25	1.15	1.60
5	100	0	1.16	1.43

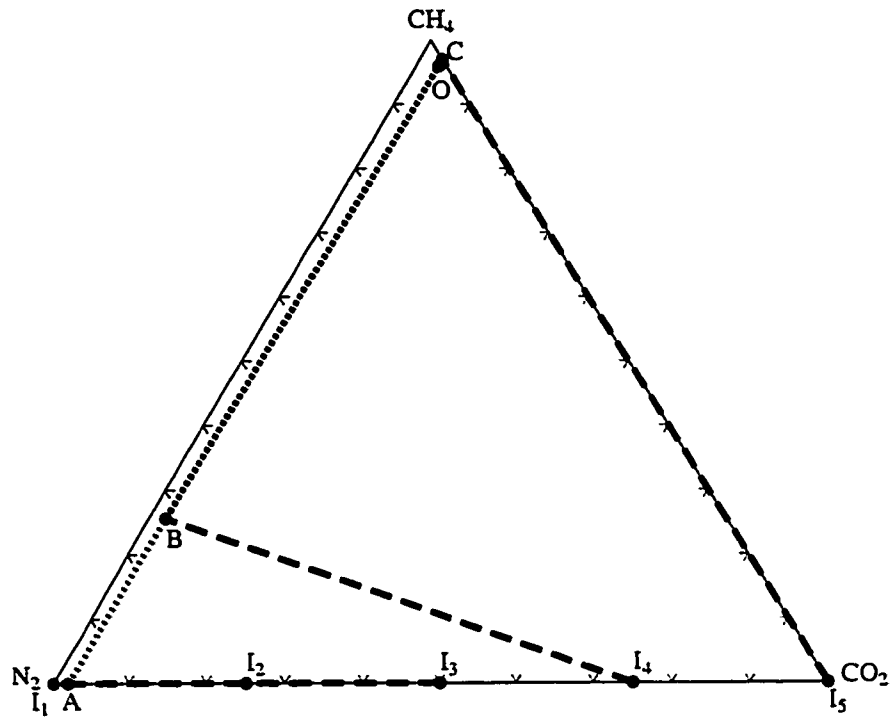


Figure 3.13: Solution paths for example solutions. The initial composition is fixed at 96% CH_4 , 3% CO_2 , and 1% N_2 .

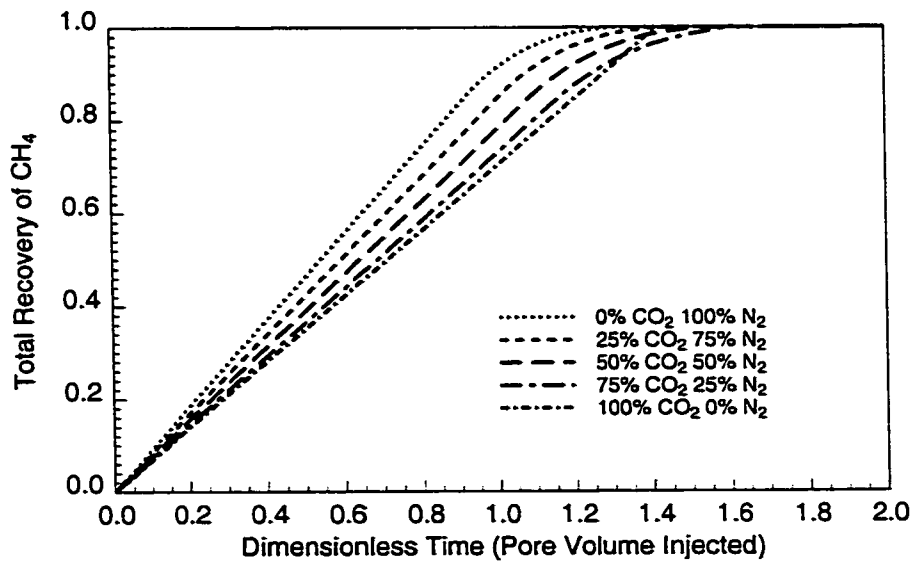


Figure 3.14: Total recovery of CH_4 for the example solutions with different injection gas compositions.

a location $\xi = 1$ in the one-dimensional model, and λ and Λ stand for the propagation velocity of continuous and discontinuous variations respectively. The solution profile in Fig. 3.15 indicates that at the producing end the CH_4 concentration starts to decline after about 0.91 pore volume (PV) has been injected, corresponding to the arrival of the leading front of the continuous variation segment **AO**. When the end of the upstream segment of continuous waves arrives at about 2.08 PV injected, all of the CH_4 originally in place is completely recovered. The values of the compositions and propagation velocities at the key points in the solution profile are given in Table. 3.3.

A Type I solution occurs when the injection gas consists of 75% N_2 and 25% CO_2 , as shown in Fig. 3.16. The compositions and propagation velocities at the key points in the solution profile are summarized in Table. 3.4. An upstream shock occurs along the $CO_2 - N_2$ axis and ends at point **A**. At point **A**, a constant state exists. The solution then switches to the fast path and follows a continuous variation to the initial composition **O**. Due to the strongest affinity of CO_2 for the coal surfaces among the three components, most of the variation in the composition of CO_2 occurs at the upstream edge of the variation zone where CO_2 adsorbs strongly and sweeps out both N_2 and CH_4 , forming a trailing step change. At the downstream end, the interaction of N_2 and CH_4 adsorption/desorption is evidenced by a continuous variation because the injection gas has a higher concentration of N_2 that adsorbs less strongly than CH_4 , a major component of the initial gas. A bank of N_2 forms between the leading continuous variation and trailing step change, (see Fig. 3.16). At the producing end, the CH_4 concentration starts to decline after 0.99 PV has been injected. After 1.90

Table 3.3: Analytical solution for ECBM in $CH_4 - CO_2 - N_2$ system, where the initial gas consists of 96% CH_4 , 3% CO_2 and 1% N_2 , and the injection gas 100% N_2 .

Composition Label	Composition (Mole Fraction)			Wave Velocity (λ)
	CH_4	CO_2	N_2	
I_1	0.0	0.0	1.0	0.0-0.481
A	0.0	0.02	0.98	0.487
O	0.96	0.03	0.01	1.103

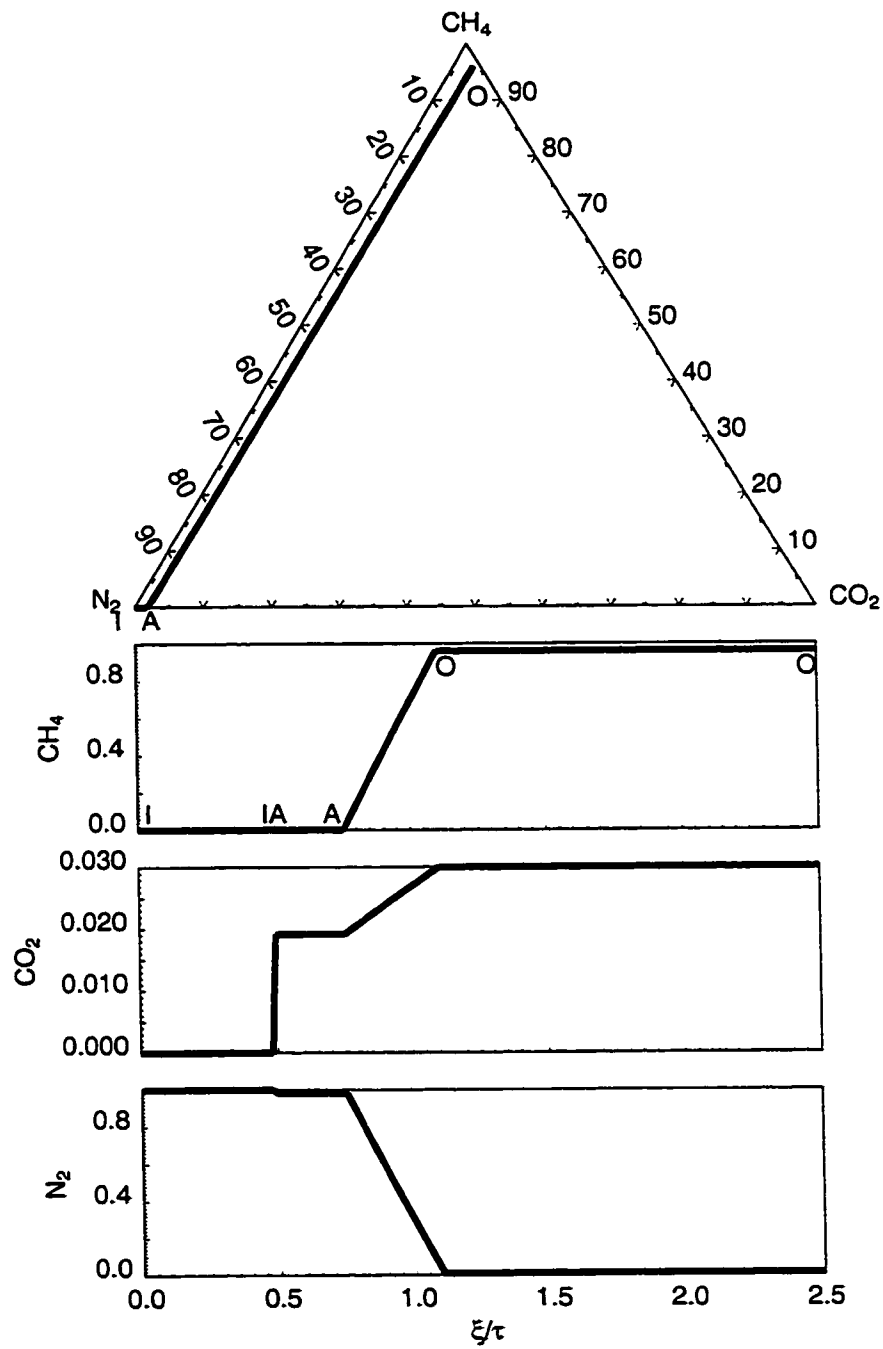


Figure 3.15: Solution profile for example solution with an injection gas of 100% N₂.

PV has been injected, the CH_4 originally in place is recovered completely.

The solution structure remains rather similar for the next two examples as the injection gas consists 50% N_2 and 50% CO_2 , and 25% N_2 and 75% CO_2 , except that when 50% N_2 and 50% CO_2 is used as injection gas, the trailing shock occurs along the $N_2 - CO_2$ axis, whereas the trailing shock goes to the interior of the ternary composition space for the later case. The solution profiles for these two examples are presented in Fig. 3.17 and Fig. 3.18. The compositions and propagation velocities at the key points are summarized in Table. 3.5 and Table. 3.6. It can be seen that with 25% N_2 and 75% CO_2 in the injection gas, the leading front is slower, and the trailing shock becomes faster, resulting in a more compressed solution profile. A general observation is that for Type I solutions, as the CO_2 fraction in the injection gas increases, the trailing shock is "stronger", *i.e.*, spans greater difference in gas composition, and the leading continuous variation becomes "weaker". A stronger shock propagates faster, but has lower local flow velocity on the downstream side. This is the result of volume change as CO_2 adsorbs. The loss of CO_2 volume is greater than the volume of the CH_4 released from the coalbed surfaces. Along a downstream continuous variation, the local flow velocity increases, but less strongly with a weaker continuous variation. Therefore, the wave velocity furthest downstream is a combined effect of the trailing shock and the leading continuous variation. As the CO_2 content in the injection gas increases, the trailing shock dominates, and the leading continuous variation becomes less significant, resulting in a slower moving

Table 3.4: Analytical solution for ECBM in $CH_4 - CO_2 - N_2$ system, where the initial gas consists of 96% CH_4 , 3% CO_2 and 1% N_2 , and the injection gas 75% N_2 and 25% CO_2 .

Composition Label	Composition (Mole Fraction)			Wave Velocity (λ)
	CH_4	CO_2	N_2	
I_2	0.0	0.25	0.75	0.0-0.527
A	0.0	0.02	0.98	0.527-0.685
O	0.96	0.03	0.01	1.007

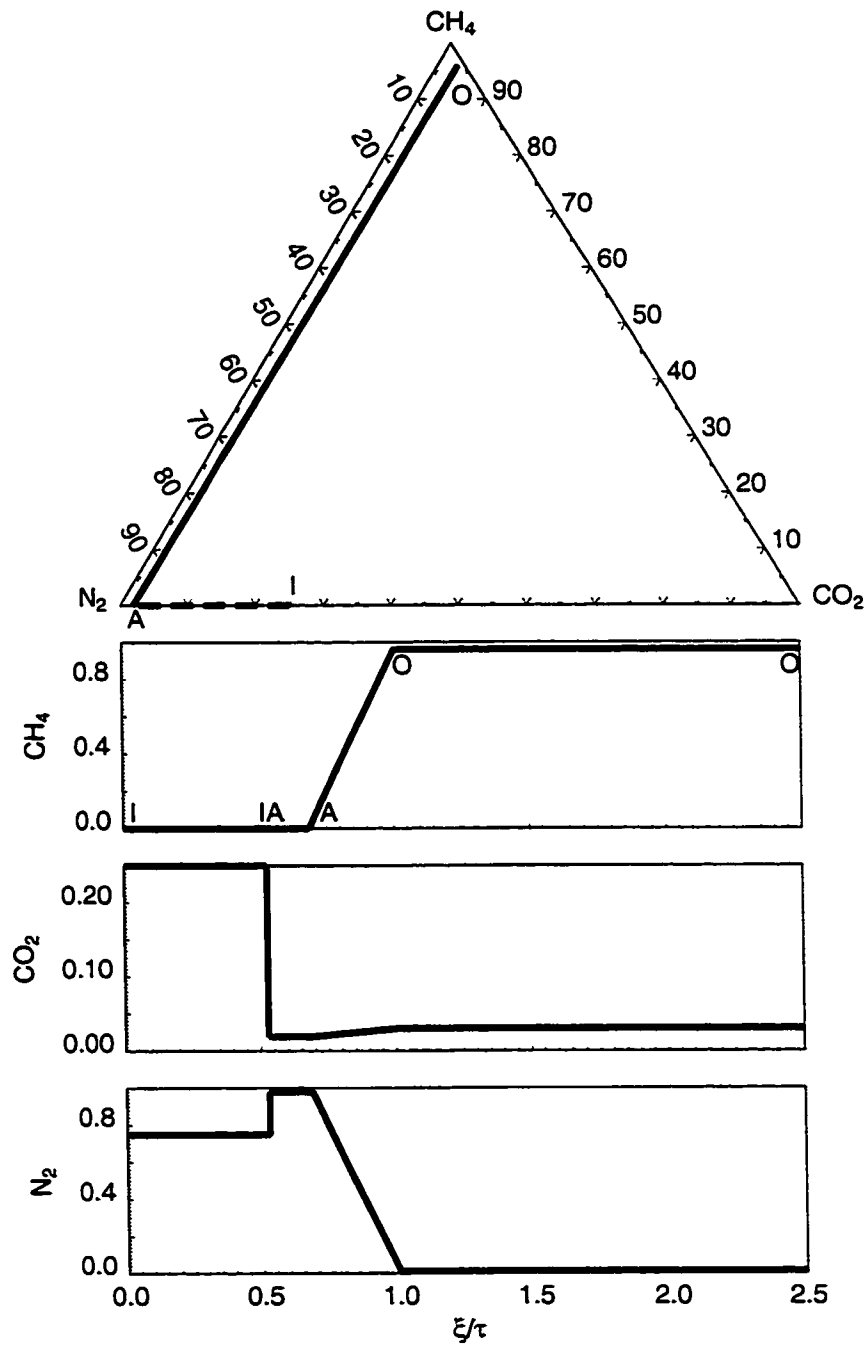


Figure 3.16: Solution profile for example solution with an injection gas of 25% CO_2 and 75% N_2 .

Table 3.5: Analytical solution for ECBM in $CH_4 - CO_2 - N_2$ system, where the initial gas consists of 96% CH_4 , 3% CO_2 and 1% N_2 , and the injection gas 50% N_2 and 50% CO_2 .

Composition Label	Composition (Mole Fraction)			Wave Velocity (λ)
	CH_4	CO_2	N_2	
I_3	0.0	0.50	0.50	0.0-0.572
A	0.0	0.02	0.98	0.572-0.632
O	0.96	0.03	0.01	0.929

Table 3.6: Analytical solution for ECBM in $CH_4 - CO_2 - N_2$ system, where the initial gas consists of 96% CH_4 , 3% CO_2 and 1% N_2 , and the injection gas 25% N_2 and 75% CO_2 .

Composition Label	Composition (Mole Fraction)			Wave Velocity (λ)
	CH_4	CO_2	N_2	
I_4	0.0	0.75	0.25	0.0-0.626
B	0.26	0.02	0.72	0.626-0.661
O	0.96	0.03	0.01	0.868

leading front and faster moving trailing shock, (see Fig. 3.18).

In the last example, an injection gas of pure CO_2 is used. The solution is of Type III, as shown in Fig. 3.19. It consists of two discontinuous waves. Starting from the injection gas I_5 , the trailing shock occurs along the $CH_4 - CO_2$ axis, ending at point C . After a constant state at C , there is a downstream shock, and a jump to the initial composition O . The leading shock is relatively insignificant compared to the trailing shock. It arrives at the exit after 1.16 PV has been injected, followed by a short period of production of $CH_4 - CO_2$ binary mixture that has slightly higher CH_4 content than the initial gas. The CH_4 originally in place is completely recovered when the trailing shock arrives at 1.42 PV.

Since the gases are injected at a fixed volumetric rate, for a solution of Type II, the local flow velocity increases along the upstream continuous path and also the downstream continuous path, resulting in a high local flow velocity at the leading

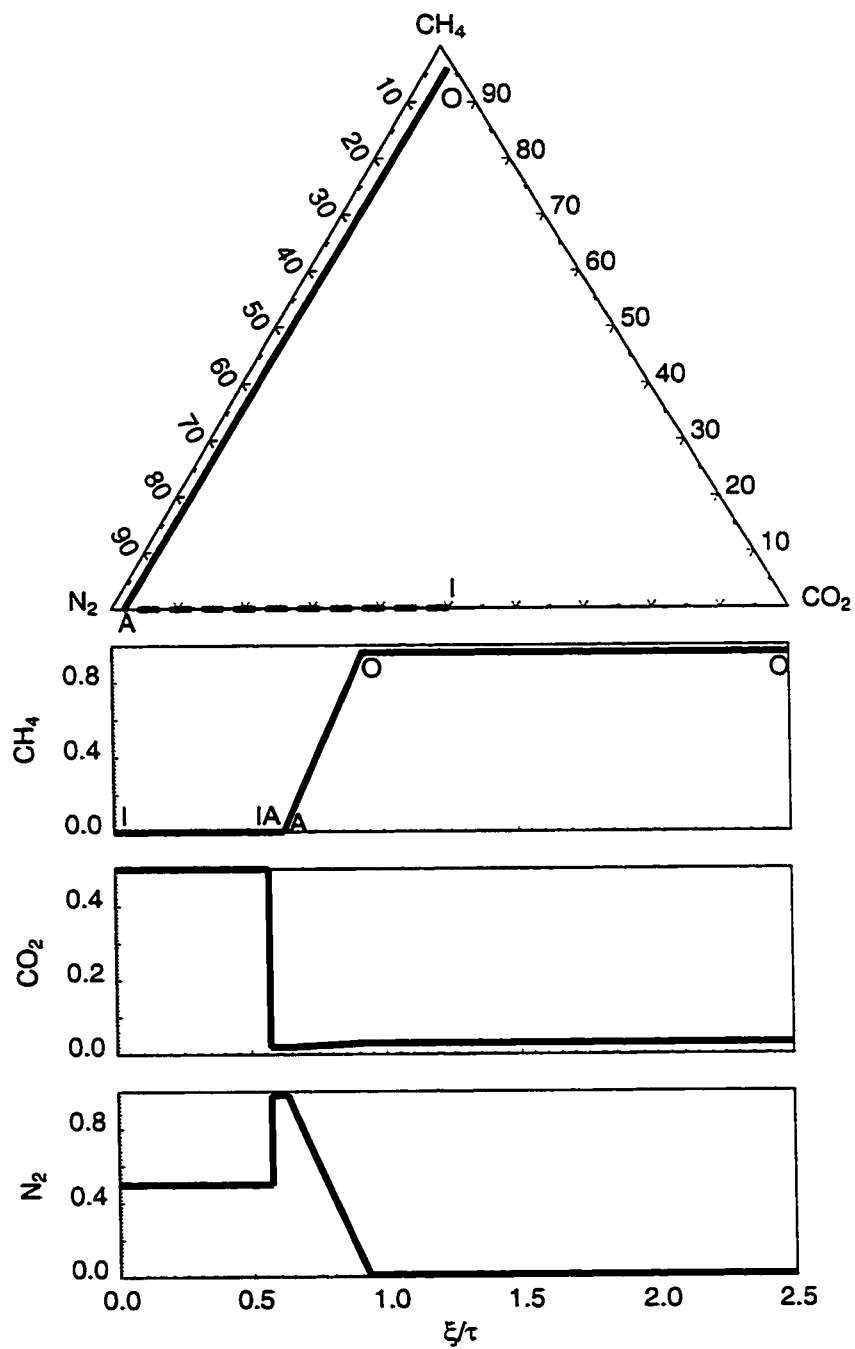


Figure 3.17: Solution profile for example solution with an injection gas of 50% CO_2 and 50% N_2 .

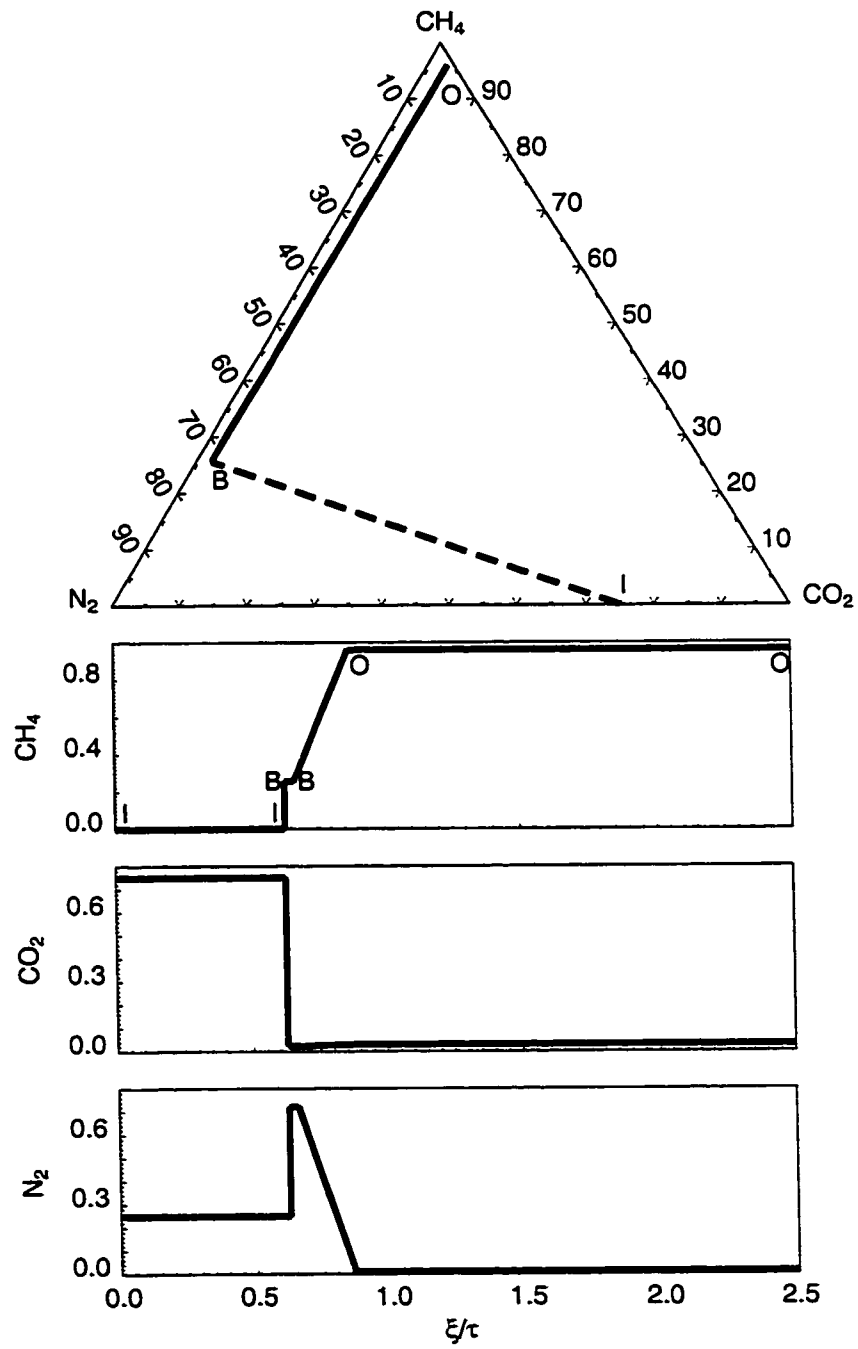


Figure 3.18: Solution profile for example solution with an injection gas of 75% CO_2 and 25% N_2 .

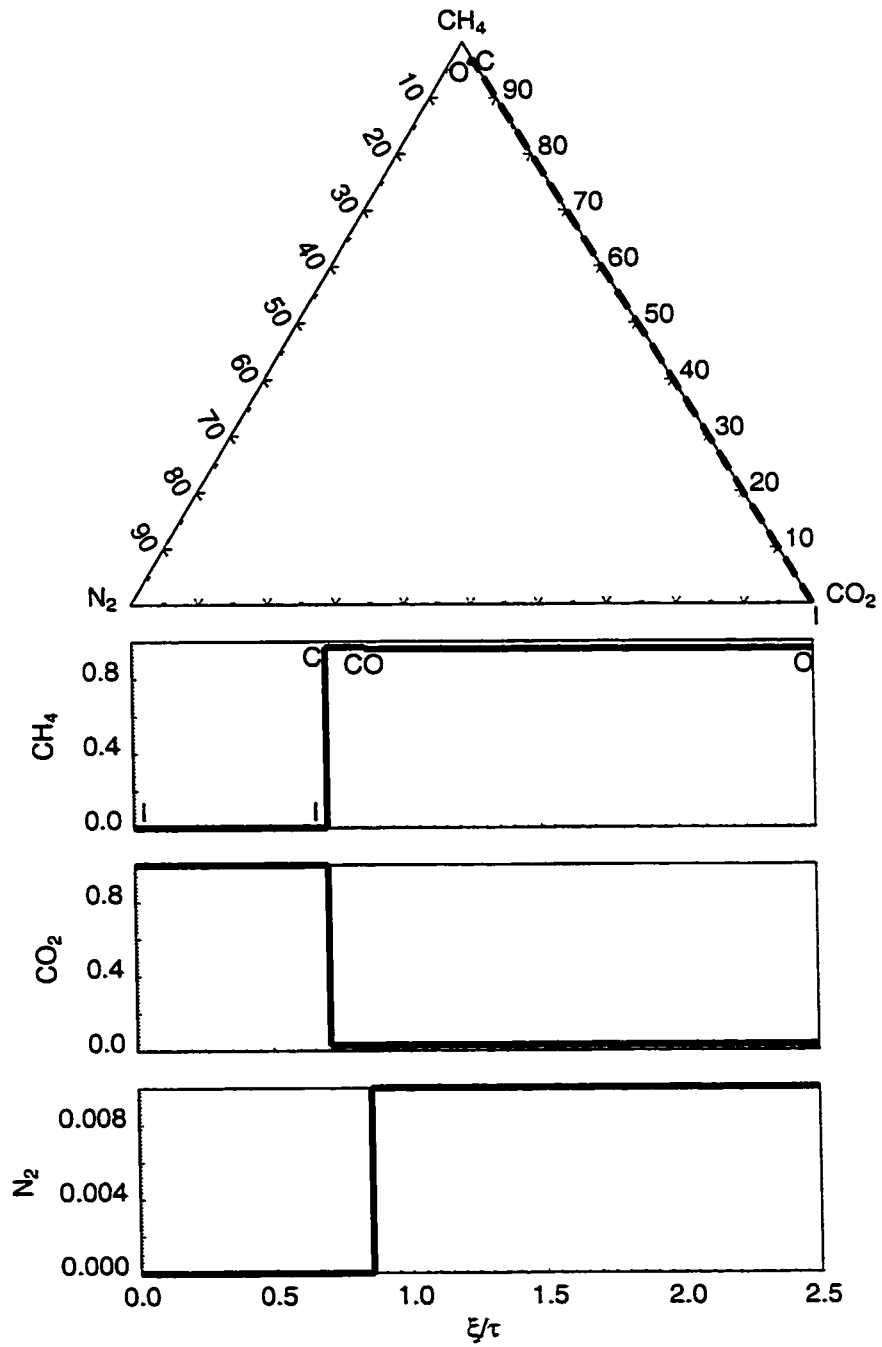


Figure 3.19: Solution profile for example solution with an injection gas of pure CO_2 .

front. Hence, the recovery curve of the initial gas is steeper. This is consistent with current ECBM practice where N_2 is the injectant of choice because enhanced CH_4 production occurs sooner. By the time the leading front arrives at the producing end, and the CH_4 composition starts declining, most of the CH_4 originally in place has been recovered. The remaining CH_4 is produced as its concentration in the produced gas declines continuously. Hence, it takes an extended period to produce the remaining CH_4 and also requires separation of the CH_4 from the produced gas.

In a Type I solution, the local flow velocity shows a dramatic decline across the upstream shock. Although the flow velocity increases along the fast path towards downstream, the local flow velocity at the leading front is lower than it is in a Type II solution. Within this solution type, the higher CO_2 composition in the injection gas results in a stronger upstream shock, a weaker downstream continuous variation, a slower leading front, and a faster upstream shock. Therefore, if there is more CO_2 in the injection gas, the recovery of gas is initially slower, but the total recovery of the CH_4 originally in place occurs earlier. Separation of CH_4 from the produced gas is still required because the CH_4 composition keeps declining for an extended period until the upstream shock arrives.

When an injection gas very rich in CO_2 is used, a Type III solution occurs. The upstream shock spans a large difference of concentration. The downstream shock, on the other hand, is relatively insignificant, as can be seen from the sample solution on Fig. 3.13. There is a fast moving upstream shock but low local flow velocity at the leading front, resulting in a lower production rate of the initial gas, compared to the

Table 3.7: Analytical solution for ECBM in $CH_4 - CO_2 - N_2$ system, where the initial gas consists of 96% CH_4 , 3% CO_2 and 1% N_2 , and the injection gas 100% CO_2 .

Composition Label	Composition (Mole Fraction)			Wave Velocity (λ)
	CH_4	CO_2	N_2	
I_5	0.0	1.0	0.0	0.0-0.705
C	0.97	0.03	0.0	0.705-0.852
O	0.96	0.03	0.01	0.852

Type I and Type II examples. The duration of initial gas production is longer, and it takes less time to recover the remaining CH_4 originally in place.

3.4.5 Effect of Numerical Dispersion

The analytical solutions for the examples were confirmed with solutions obtained from finite-difference simulation. Figure 3.20 shows a comparison of the analytical and finite-difference solutions for the example where pure N_2 is used as injection gas. The number of grid blocks used in the finite-difference simulation is 5000. Very good agreement between the two solutions is observed with only small difference due to numerical dispersion in the finite-difference solution. Similar agreement between the analytical and numerical solutions was obtained for the remaining examples.

For the example solution where the initial mixture consists of 75% CO_2 and 25% CO_2 , a series of finite-difference simulations was carried out. The solution paths are summarized in Fig. 3.21. When an inadequate number of grid blocks is used, a strong effect of numerical dispersion is observed that forces the solution paths to differ from the dispersion-free analytical solution and approach a dilution line that connects the initial and injection mixture compositions. In order to have a satisfactory match with the analytical solution, the number of grid blocks must be as high as 5000 that requires a large amount of computational time. The convergence of the numerical solution to the analytical solution confirms the correctness of the analytical solution.

3.5 Summary

We describe an analytical theory of three-component flow for ECBM processes where adsorption and desorption of gas components on coal play important roles. The theory and examples presented lead to the following conclusions:

1. In binary systems, shock solutions occur when a more strongly adsorbing gas mixture is injected. Continuous variation occurs when the injection gas is less strongly adsorbing than the initial gases.

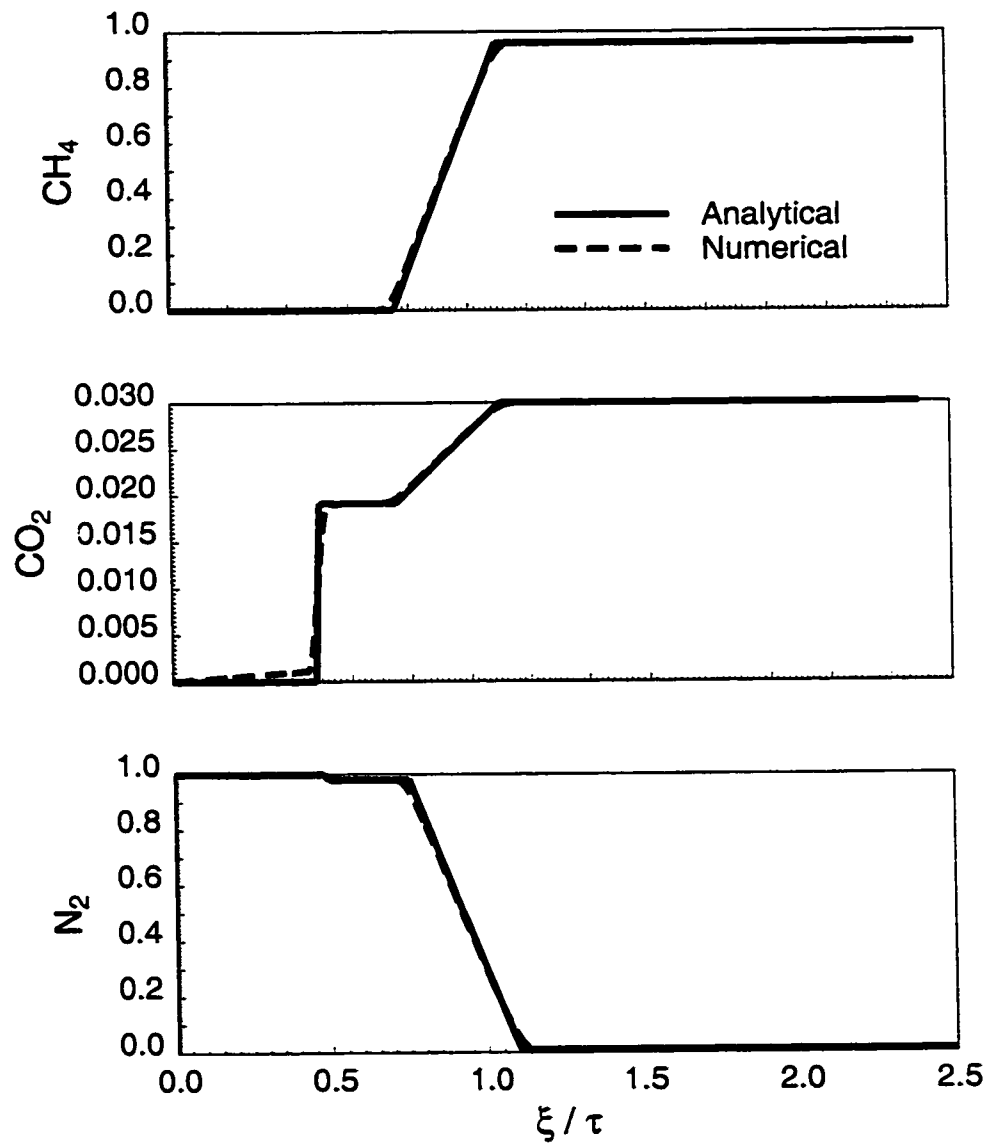


Figure 3.20: Comparison of the analytical solution profiles with finite-difference simulation results. Injection gas consists of pure N_2 .

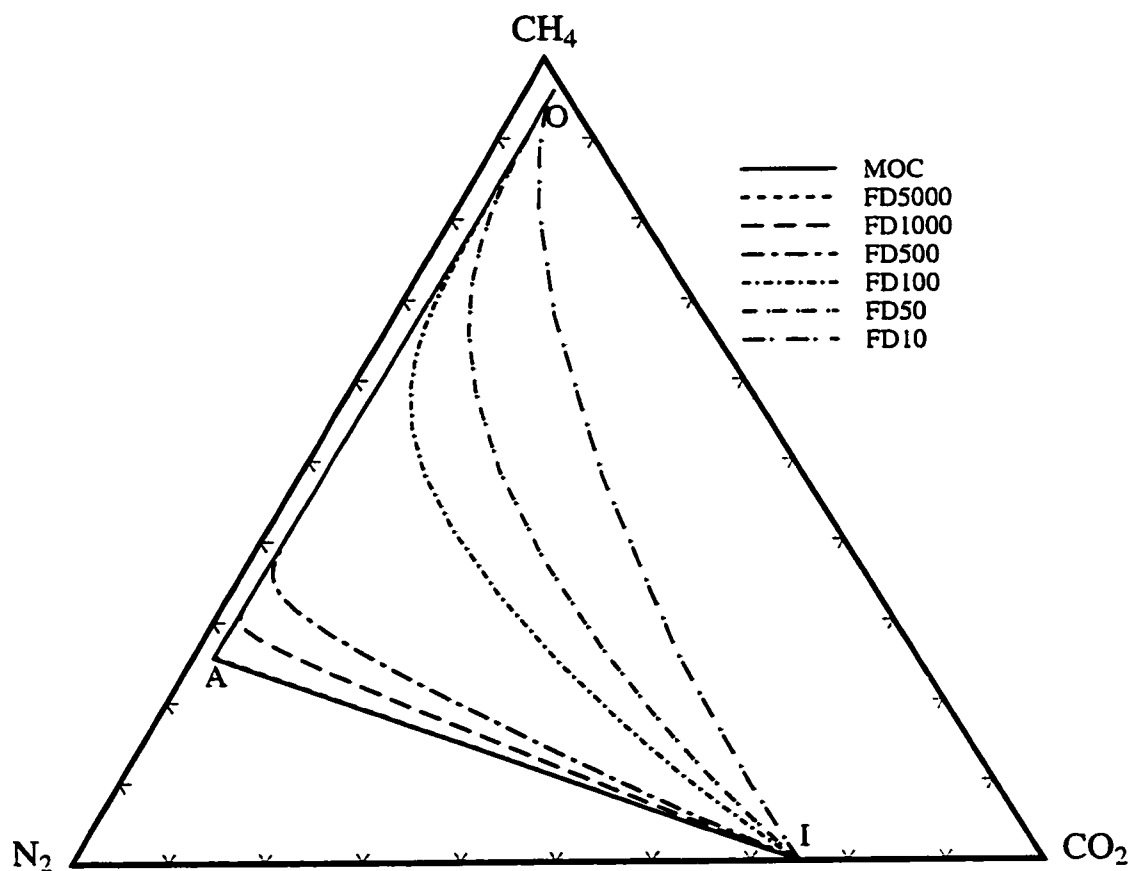


Figure 3.21: A study of the effect of numerical dispersion by a series of finite-difference simulations with various numbers of grid blocks.

2. In ternary systems, the composition of injection gas has small effect on the amount of time to recover all CH_4 originally in place. However, injection gas composition has significant effect on the produced gas composition and the time to breakthrough of the injection gas. An injection gas rich in N_2 yields a greater initial recovery rate, but earlier breakthrough of injected gas. Thus, N_2 must be separated from produced gas for a substantial period of time. On the other hand, an injection gas rich in CO_2 yields recovery of CH_4 -rich gas for a greater period of time.

Chapter 4

Temperature Variation in One-Component Flow

In this chapter we study gas injection problems with temperature variation using the method of characteristics. The mathematical model and general approach are summarized in Chapter 2. The adsorption and desorption of gas components at rock surfaces are not considered here. The phase equilibrium behavior is represented by the Peng-Robinson equation of state [30]. A few components are chosen as the sample systems where solutions are sought, and the parameters used for computing the thermodynamic properties with Peng-Robinson equation of state are listed in Table 4.1. In order to calculate the enthalpy of pure components at ideal state, Passut and Danner's correlation [29] is used,

$$H^* = A + BT + CT^2 + DT^3 + ET^4 + FT^5, \quad (4.1)$$

where A , B , C , D , E , and F are derived coefficients, with the enthalpy in Btu/lb and the temperature in $^{\circ}R$. For the heat capacity, ($C_p^* = dH^*/dT$):

$$C_p^* = B + 2CT + 3DT^2 + 4ET^3 + 5FT^4. \quad (4.2)$$

The coefficients for enthalpy calculation using this correlation in the examples are summarized in Table 4.2. The porosity, density and heat capacity of the porous

medium are assumed to be constant and listed in Table 4.3.

However, for single-component systems with temperature variation, the eigenvalue problem established for multi-component systems is not applicable. In this chapter, we consider the special case of single-component systems.

When a gas is injected at a temperature different from that of the original fluids in the reservoir, mass transfer, as well as heat transfer, occurs. While the injected gas participates in the multicomponent multiphase flow through the porous medium, the temperature of the injected component, as well as that of the original fluids and the porous medium varies due to the heat exchange between the fluids and porous medium. Without losing generality, we assume that the injection gas is at higher temperature than the porous medium and the original fluids in place. Then, the injected gas will heat up the porous medium and the original fluids in place, as well as displacing the original fluids through the porous medium. Generally, the injection gas has a much lower heat capacity than the rock. At the upstream end, the injected gas may first experience changes in temperature before it contacts the reservoir fluids. The injected gas at the leading edge will mix with the fluids downstream and participate in the multiphase flow. The injected gas near the inlet remains at the same composition while moving downstream, being displaced by newly injected gases. Therefore, there exists a sub-problem at the upstream end where the injected gas displaces the same injected gas, but at different temperature. We can further simplify the problem by choosing the injection gas to be a pure component. The solution to single-component gas drive is useful, and we will be studying this problem using methane as an example. For the temperature range we consider, the methane remains as a single gas phase, and no phase behavior calculation is needed. We will concentrate on the resulting temperature profile and local flow velocity.

4.1 Continuous Variation

The eigenvalue problem of general form, Eq. 2.48, however, does not apply to this single component gas displacement example, since the molar composition is always 100% methane. Hence, single component gas displacement with temperature variation

Table 4.1: The thermodynamic properties of methane and decane.

	P_c (atm)	T_c (°K)	M (g/gmol)	ω
CH_4	45.4	190.6	16.0	0.008
CO_2	72.8	304.2	44.0	0.225
C_{10}	20.8	617.6	142.3	0.490
C_{16}	14.0	717.0	226.4	0.742
δ_{ij}				
	CH_4	CO_2	C_{10}	C_{16}
CH_4	0.000	0.100	0.052	0.035
CO_2	0.100	0.000	0.094	0.120
C_{10}	0.052	0.094	0.000	0.000
C_{16}	0.035	0.120	0.000	0.000

Table 4.2: The coefficients for ideal gas enthalpy calculation.

	CH_4	CO_2	C_{10}	C_{16}
A	-5.58114	4.77805	28.48990	26.19390
B	0.564834	0.114433	-0.023837	-0.022825
$C(\times 10^{-3})$	-0.282973	0.101132	0.461164	0.459024
$D(\times 10^{-6})$	0.417399	-0.026494	-0.099786	-0.100021
$E(\times 10^{-10})$	-1.525576	0.034706	0.108353	0.108912
$F(\times 10^{-14})$	1.958857	-0.013140	-0.033074	-0.033390

Table 4.3: The properties of the porous medium.

Rock properties	
ϕ	0.2
ρ_r (g/cc)	1.2
C_{pm} (J/g · °K)	1.0

is a special case. We start again from the material balance and energy balance equations as follows:

$$\frac{\partial \rho}{\partial t} + \frac{1}{\phi} \frac{\partial(\rho u)}{\partial x} = 0, \quad (4.3)$$

and

$$\frac{\partial(\rho u h)}{\partial x} + \phi \frac{\partial(\rho h)}{\partial t} + (1 - \phi) \frac{\partial(\rho_r h_r)}{\partial t} = 0, \quad (4.4)$$

where ρ is the molar density of the fluid, u is the local flow velocity, h is the molar enthalpy of the fluid, ρ_r is the rock density, and h_r is the heat contained in the rock.

Since pressure is assumed to be constant, the molar density and molar enthalpy of the gas depend on temperature only, *i.e.*, $\rho = \rho(T)$ and $h = h(T)$. If we assume constant porosity, density and heat capacity for the rock, then the heat contained in the rock is only a linear function of temperature. Therefore, for the material balance and energy balance equations, the two unknown variables are u and T .

Substituting the mass balance equation into the heat balance equation and using temperature as the dependent variable yields

$$\frac{\partial T}{\partial t} + \left(\frac{u}{\phi}\right) \left(\frac{1}{1 + \frac{1-\phi}{\phi} \frac{\rho_r C_r}{\rho C_f}}\right) \frac{\partial T}{\partial x} = 0, \quad (4.5)$$

where C_r and C_f are the solid and fluid heat capacity defined as

$$C_r = \frac{dh_r}{dT}, \quad (4.6)$$

and

$$C_f = \frac{dh}{dT}. \quad (4.7)$$

Eq. 4.5 has the general form for applying the method of characteristics. It is easily seen that the propagation velocity of the temperature wave is

$$\lambda = \frac{dx}{dt} = \left(\frac{u}{\phi}\right) \lambda^*, \quad (4.8)$$

where λ^* is the normalized eigenvalue, and

$$\lambda^* = \left(\frac{1}{1 + \frac{1-\phi}{\phi} \frac{\rho_r C_r}{\rho C_f}} \right). \quad (4.9)$$

The rock heat capacity is normally much larger than that of the fluid in the reservoir. Hence, from Eq. 4.8 it can be seen that the normalized eigenvalue is of small value, and the propagation velocity of the temperature is reduced significantly due to the large heat capacity of the rock.

Rearranging the mass balance equation using the fact that gas density ρ is only function of temperature T results in

$$\frac{d\rho}{dT} \frac{\partial T}{\partial t} + \frac{\rho}{\phi} \frac{\partial u}{\partial x} + \frac{u}{\phi} \frac{d\rho}{dT} \frac{\partial T}{\partial x} = 0. \quad (4.10)$$

Substituting Eq.4.10 into Eq.4.5 yields an expression for the flow velocity:

$$\frac{1}{u} \frac{\partial u}{\partial x} + \frac{1}{\rho} \frac{d\rho}{dT} \frac{1}{1 + \frac{\phi}{1-\phi} \frac{\rho C_f}{\rho_r C_r}} \frac{\partial T}{\partial x} = 0. \quad (4.11)$$

Note in Eq. 4.11 that the variables in the coefficient for the temperature term are functions of temperature only. Since the solution for the temperature profile is single-valued with respect to the spatial variable x , u can be solved by integrating Eq. 4.11 with respect to x and applying the boundary condition at $x = 0$.

4.2 Shocks

The rarefaction solutions constructed in the last section satisfy the material and energy balance equations but are not necessarily physical. When the characteristic velocity of the temperature waves at upstream locations is higher than those downstream, the velocity rule is violated. Shock solutions are needed in order to maintain a single-valued solution under such circumstances. In this section, we will describe the construction of shock solutions.

Although the shock solutions are discontinuities, material balance and energy

balance are still honored across the shocks. In order to construct a shock solution, we start from the conservation equations of mass and energy. Denote the shock velocity by Λ . The shock sweeps a finite distance $\Delta x = \Lambda \Delta t$ in finite time Δt . We take the small element of finite length $\Delta x = \Lambda \Delta t$ and study the material and energy balances. The conditions upstream and downstream of the shock are known. Hence the density of the gas can easily be computed because it depends on the temperature only. The unknowns are the shock velocity Λ and the local velocity downstream of the shock. The change of the mass in the control element before and after the shock sweeps by is $\phi A \Delta x (\rho^u - \rho^d)$. The net inflow of mass in the control element when the shock sweeps by is $\rho^u A u^u \Delta t - \rho^d A u^d \Delta t$. Therefore, across the shock the material balance equation becomes

$$\rho^u (u^u - \phi \Lambda) = \rho^d (u^d - \phi \Lambda). \quad (4.12)$$

Similarly, the change of enthalpy before and after the shock sweeps by the control element is $\phi A \Delta x (\rho^u h^u - \rho^d h^d) + (1 - \phi) A \Delta x \rho_r C_r (T^u - T^d)$. The net inflow of enthalpy into the control element when the shock sweeps by is $\rho^u h^u A u^u \Delta t - \rho^d h^d A u^d \Delta t$. Therefore, across the shock the energy balance equation becomes

$$\rho^u h^u (u^u - \phi \Lambda) = \rho^d h^d (u^d - \phi \Lambda) + (1 - \phi) \Lambda \rho_r C_r (T^u - T^d) \quad (4.13)$$

Combining Eq. 4.12 and Eq. 4.13 and solving for Λ and u^d gives

$$\Lambda = \frac{1}{\phi} = \left(\frac{u^u}{\phi} \right) \left(\frac{1}{1 + \frac{1 - \phi}{\phi} \frac{\rho_r C_r (T^u - T^d)}{\rho^u (h^u - h^d)}} \right) \quad (4.14)$$

and the local flow velocity downstream of the shock

$$u^d = u^u \left(\frac{1 + \frac{1 - \phi}{\phi} \frac{\rho_r C_r (T^u - T^d)}{\rho^d (h^u - h^d)}}{1 + \frac{1 - \phi}{\phi} \frac{\rho_r C_r (T^u - T^d)}{\rho^u (h^u - h^d)}} \right). \quad (4.15)$$

4.3 Examples of Single-Component Single-Phase Flow

In this section, we use CH_4 and C_{10} to illustrate the solution construction for single-component single-phase flow. For the following examples, the pressure is at 98.7 atm, and the temperature range is between 250 °K and 600 °K.

4.3.1 Single-Component Single-Phase Flow of CH_4

For a single-component single-phase system consisting of CH_4 , we start the solution construction process by assuming that the solution consists of rarefaction waves. The eigenvalues and the local flow velocity can be solved from Eqs. 4.14 and Eq. 4.15. In Fig. 4.1, starting upstream where temperature is higher, the eigenvalue that stands for the propagation velocity of the temperature waves first decreases as the temperature declines and then starts increasing after arriving at a minimum value. The behavior of the eigenvalue is completely determined by the thermodynamic properties of the gas, as can be seen from Eq. 4.8 and the special behavior of molar density and heat capacity of CH_4 at temperatures around 200 °K, confirmed by both calculations using the Peng-Robinson Equation of State and data from the CRC Handbook of Physics and Chemistry (see Fig. 4.2). Starting from upstream when the eigenvalue decreases, the velocity rule is violated. A shock solution must be constructed instead. However, at the downstream part when the eigenvalue starts to increase, the velocity rule is satisfied and the rarefaction solution is allowed. The remaining problem is to determine the intermediate temperature where the upstream shock ends and the downstream rarefaction begins.

For each possible value for this intermediate temperature, the shock velocity and local flow velocity at the immediate downstream side of the shock can be calculated based on Eqs. 4.14 and 4.15. With the local flow velocity at the immediate downstream side of the shock solved, the wave velocity of the rarefaction can be computed according to Eq. 4.8. The velocities for shocks between the injection condition and

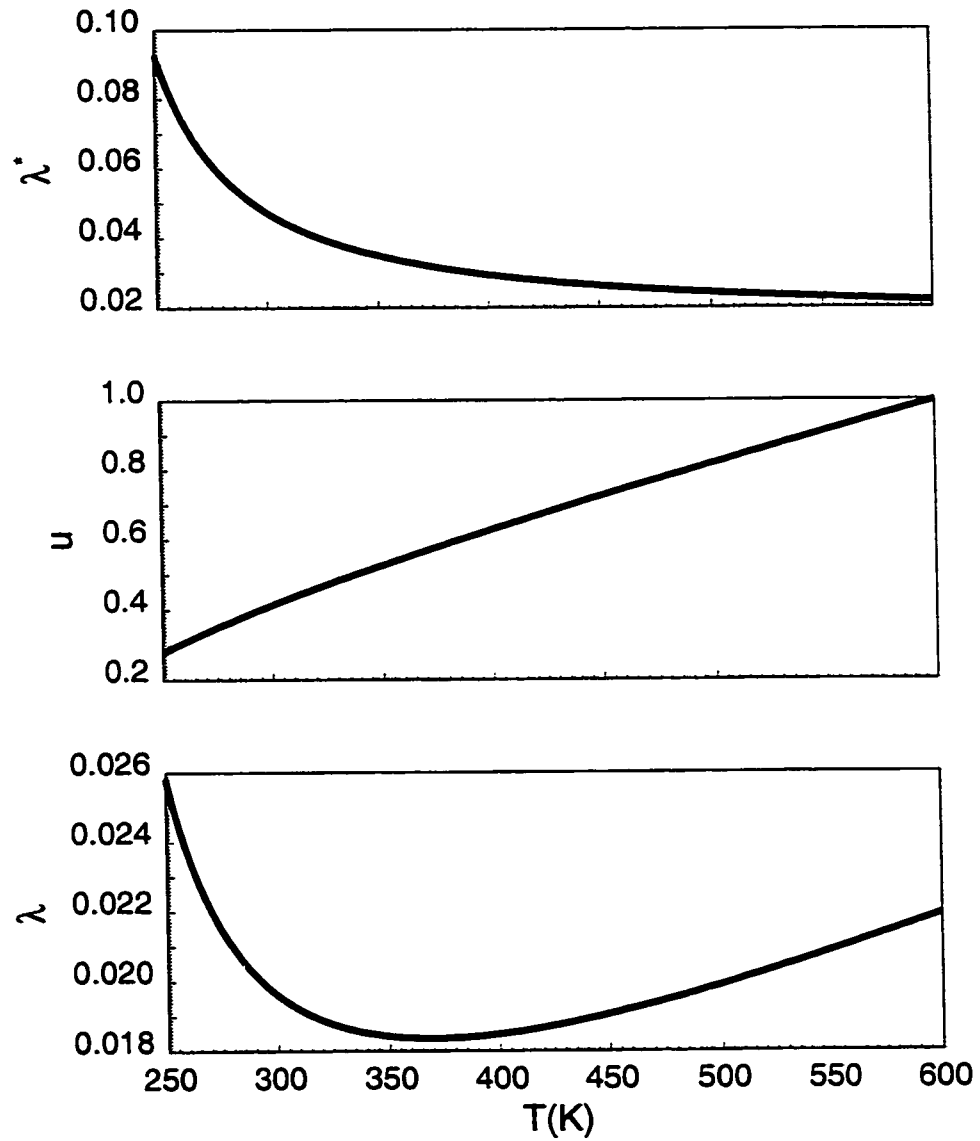


Figure 4.1: The variation of rarefaction wave velocity and local flow velocity along the temperature path for single component displacement within the single-phase region of pure CH_4 system.

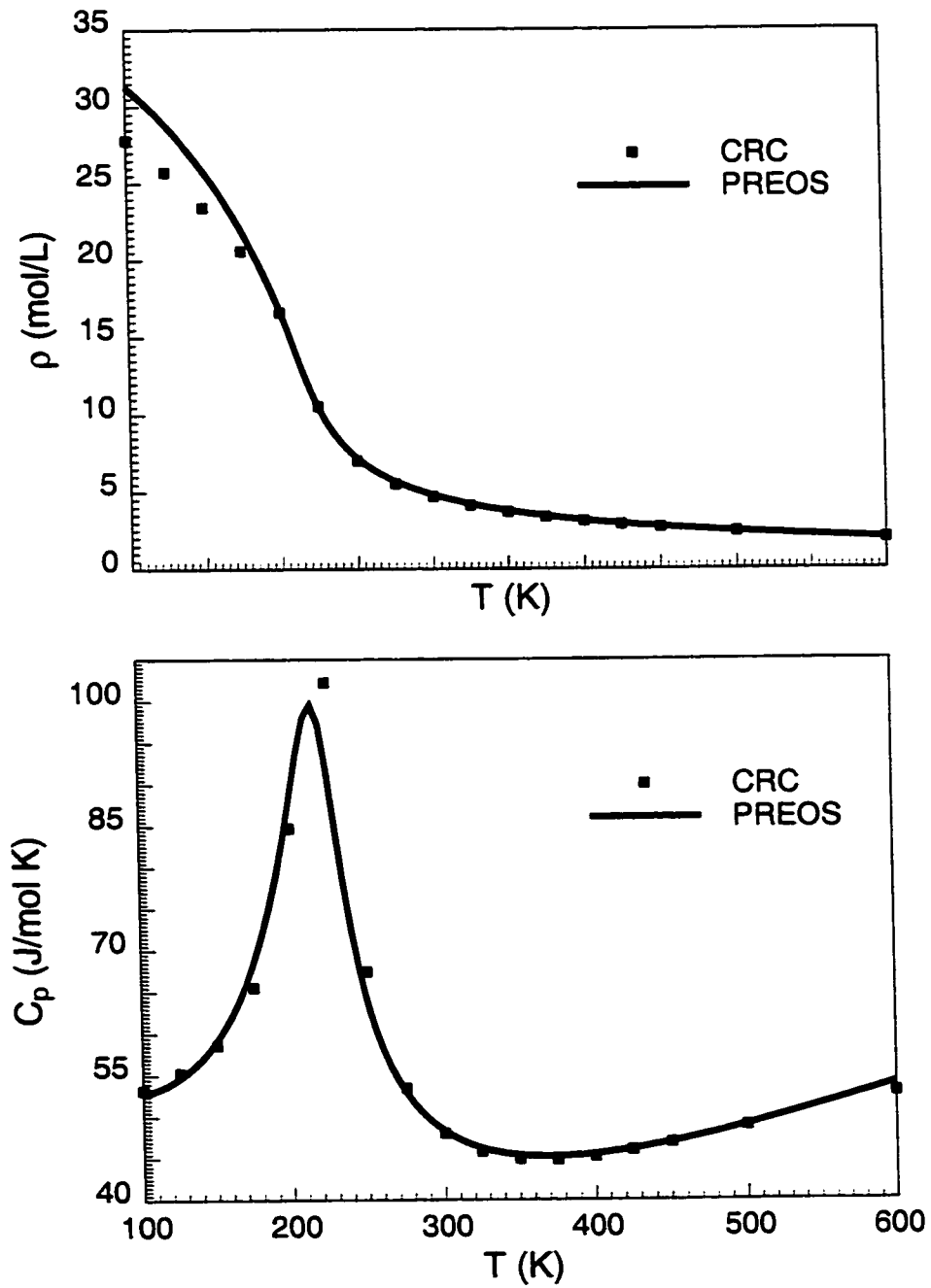


Figure 4.2: The variation of molar density and molar heat capacity of CH_4 with temperature. The results from calculation with Peng-Robinson Equation of State agree well with the data from the CRC Handbook of Physics and Chemistry.

possible intermediate temperatures are shown as a function of the intermediate temperature in Fig. 4.3. The rarefaction wave velocity at the immediate downstream side of the shock is also calculated as a function of the immediate temperature values. If the rarefaction wave velocity immediately downstream of the shock is lower than that of the shock, the shock will overtake the rarefaction wave, which results in a violation of the velocity rule. If the rarefaction wave velocity immediately downstream of the shock is higher than the shock velocity, the velocity rule is satisfied. However, the shock is not stable since the entropy condition is not satisfied. Given a small amount of perturbation, the shock will collapse and spread out as increasingly fast moving rarefaction waves towards downstream. Therefore, the intermediate temperature should be such a point that the shock velocity is equal to the rarefaction wave velocity immediately downstream of the shock. In this example, the intermediate temperature is solved as 301 °K, and the shock velocity is 0.01955. Therefore, the final solution for the example is a temperature shock from the injection temperature to an intermediate temperature at 301 °K, followed by a rarefaction downstream of the shock. The temperature profile is shown in Fig. 4.4. The analytical solution is verified by a good match against a one-dimensional finite difference simulation, shown in Fig. 4.4. In the finite-difference simulation, a single point upstream weighting scheme is used. The number of grid blocks is 10000, and the dimensionless time step size is 0.0001. It takes computer time on the order of several hours to produce a well developed solution. In comparison, the construction of analytical solution only requires less than a second of computer time.

4.3.2 Single-Component Single-Phase Flow of C_{10}

In a single-component, single-phase system of C_{10} , the variation of the wave velocity of the continuously varying temperature is shown in Fig. 4.5, in which case, for the whole temperature range, the continuous wave velocity decreases monotonically with temperature.

Therefore, it is easy to conclude that in this system, when pure C_{10} at a higher temperature is injected to displace pure C_{10} at a lower temperature, the temperature

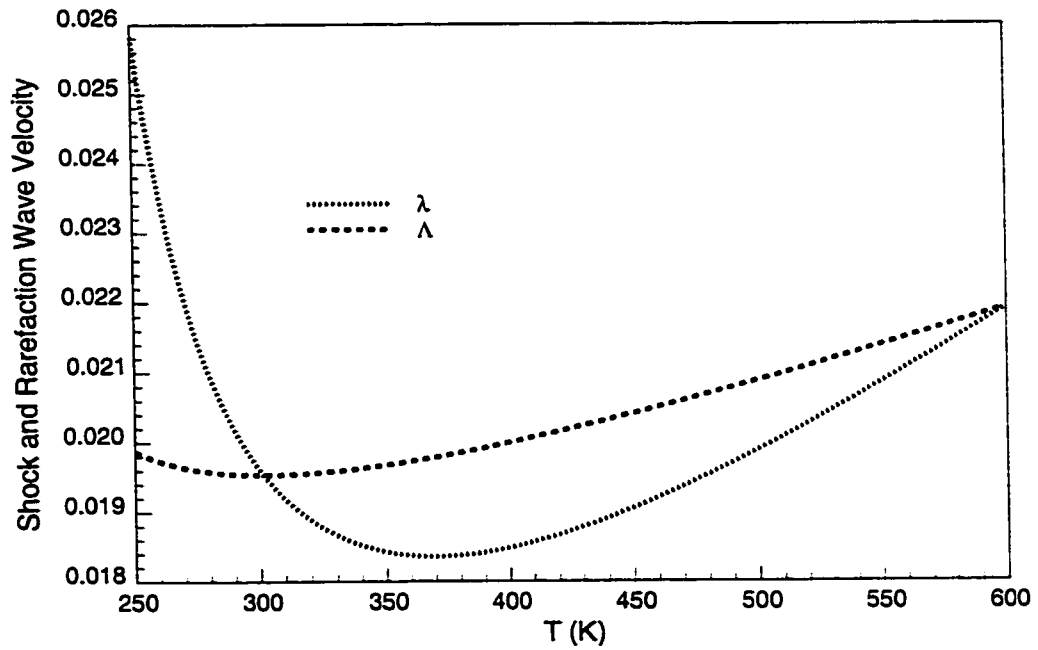


Figure 4.3: In a pure CH_4 system, the velocities of all possible shocks and the rarefaction waves located at immediate downstream of the shocks. Each possible shock solution jumps from the injection temperature to an intermediate temperature between the initial and injection conditions.

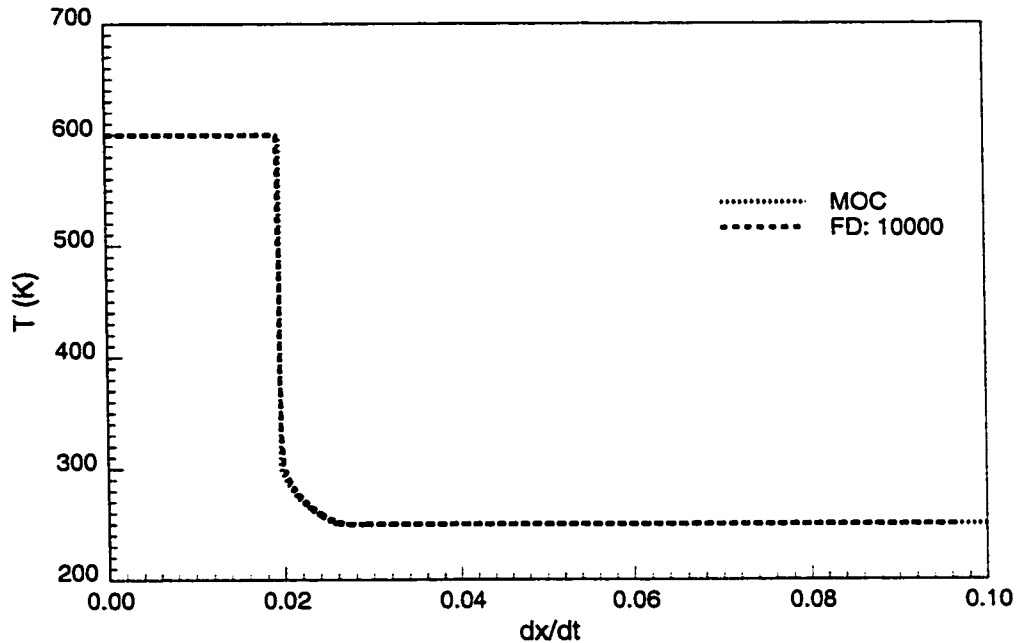


Figure 4.4: The temperature profile for the example where pure CH_4 at 600 °K is injected into porous media saturated with 100% CH_4 at 250 °K.

waves upstream travel faster than those downstream, and hence violate the velocity rule and result in discontinuous solutions. It can be confirmed from Fig. 4.6 where for each possible shock from the injection temperature to an intermediate temperature, the shock velocity is higher than the continuous wave located immediately downstream of the shock. The final solution is simply a shock jump directly from the injection temperature to the initial temperature, of which the velocity can be computed easily from the conservation of mass and energy.

On the other hand, when the injected pure C_{10} is at lower temperature than that of the initial pure C_{10} , a continuous variation of the temperature suffices.

4.4 Summary

Gas injection problems for pure component systems with temperature variation serve as building blocks for more complicated ones. In these scenarios, compositional effects are only limited to the volume change caused by variation in temperature. The

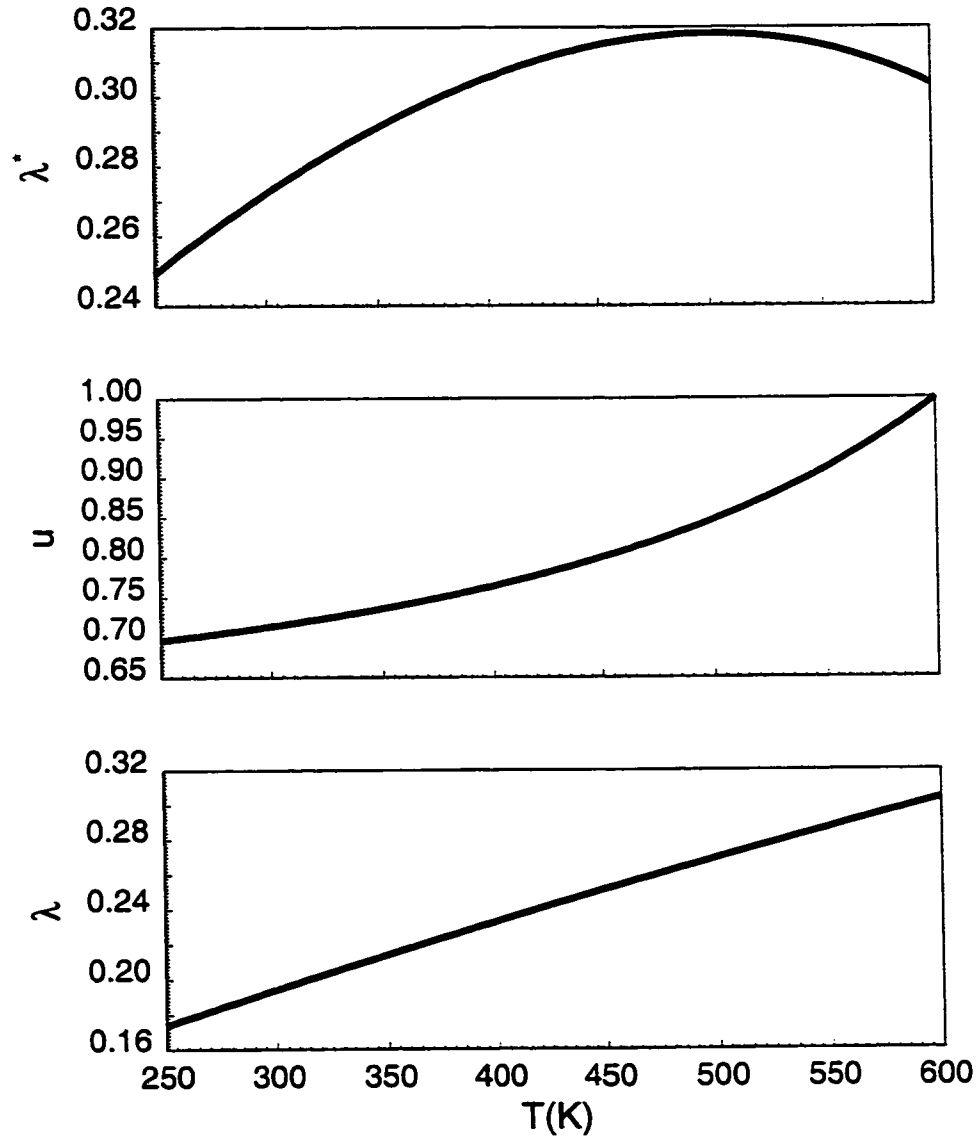


Figure 4.5: The variation of rarefaction wave velocity and local flow velocity along the temperature path for single component displacement within the single-phase region of pure C_{10} system.

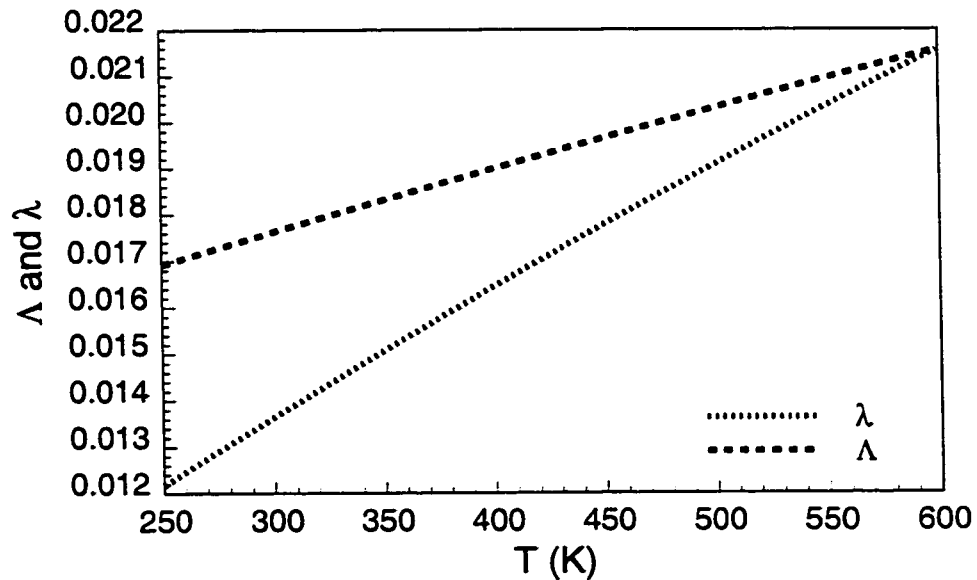


Figure 4.6: In a pure C_{10} system, the velocities of all possible shocks from the injection temperature to an intermediate temperature, and the rarefaction waves located at immediate downstream of the shocks.

propagation of temperature, on the other hand, is determined by the fluid flow velocity that varies due to the volume change. For the temperature range we considered, the molar volume of the pure components increases with temperature, resulting in increasing propagation velocity of the temperature waves. The continuous solution suffices if the injection temperature is lower than that of the initial fluids as the velocity rule is satisfied. When the temperature of the injected fluids is higher than that of the initial reservoir, shock solutions are needed as the high temperature waves upstream travel faster and violate the velocity rule.

However, the heat capacity of a pure component does not vary monotonically with the temperature, as can be observed in pure CH_4 system at very low temperature. Instead of a simple continuous variation or shock solution, a combination of both solution segments is needed.

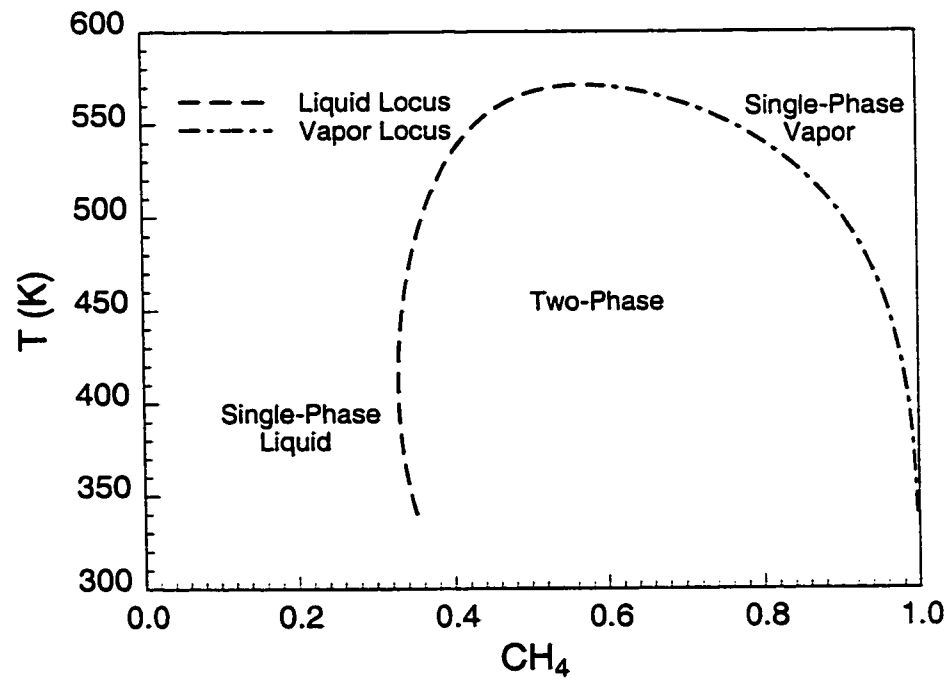
Chapter 5

Temperature Variation in Binary Flow

In this chapter, we consider gas injection problems with temperature variation in binary systems and study the effect of temperature variation on the solution behavior. When temperature and molar composition are chosen as the dependent variables, the composition space can be divided into single-phase liquid, single-phase vapor and two-phase regions by the phase envelope, as illustrated in Fig. 5.1. In common practice, single-phase gases are injected in order to displace the original single-phase liquid oil. Hence, the variation of molar composition and temperature from the initial condition to the injection condition can be decomposed as solution segments within the single-phase regions and the two-phase region, and transitions between single and two-phase regions.

Therefore, in this chapter, we first analyze possible solutions within the single-phase and two-phase regions, including both continuous and discontinuous solutions, and solutions that occur across the two-phase envelope. At the end, we will combine these solution segments and construct example solutions for various initial and injection conditions of gas injection problems in binary system.

For all the example solutions in this study, pressure is fixed at 10 MPa, and temperature varies between 250 °K and 600 °K. The phase behavior is described by the Peng-Robinson equation of state. The multiphase flow behavior is represented by

Figure 5.1: Composition space for CH_4-C_{10} system.

a fractional flow function as follows:

$$f_v = \frac{S_v^2}{S_v^2 + \frac{\mu_v}{\mu_l} S_l^2}, \quad (5.1)$$

where the subscripts “*l*” and “*v*” stand for liquid and vapor phases.

5.1 Solutions in the Single-Phase Region

5.1.1 Continuous Variation in the Single-Phase Region

In a gas injection problem where both the initial and injection mixtures are in the single-phase region and on the same side of the two-phase region, the eigenvalue problem represented by Eq. 2.55 becomes

$$\begin{vmatrix} (1 - \lambda^*) \left(\rho - \frac{Z_1}{H} \frac{\partial(\rho H)}{\partial Z_1} \right) & Z_1 \left[(1 - \lambda^*) \left(-\frac{\rho}{H} \frac{\partial H}{\partial T} \right) + \lambda^* \frac{1-\phi}{H} \rho_m C_{pm} \right] \\ (1 - \lambda^*) \left(-\rho - \frac{Z_2}{H} \frac{\partial(\rho H)}{\partial Z_1} \right) & Z_2 \left[(1 - \lambda^*) \left(-\frac{\rho}{H} \frac{\partial H}{\partial T} \right) + \lambda^* \frac{1-\phi}{H} \rho_m C_{pm} \right] \end{vmatrix} = 0, \quad (5.2)$$

which yields two eigenvalues

$$\lambda_1^* = 1, \quad (5.3)$$

and

$$\lambda_2^* = \frac{\rho \frac{\partial H}{\partial T}}{\rho \frac{\partial H}{\partial T} + \frac{1-\phi}{\phi} \rho_m C_{pm}}, \quad (5.4)$$

with two corresponding eigenvectors

$$\vec{e}_1 = \begin{pmatrix} \frac{dZ_1}{d\eta} \\ \frac{dT}{d\eta} \end{pmatrix}_1 = \begin{pmatrix} 1 \\ 0 \end{pmatrix}, \quad (5.5)$$

and

$$\vec{e}_2 = \begin{pmatrix} \frac{dZ_1}{d\eta} \\ \frac{dT}{d\eta} \end{pmatrix}_2 = \begin{pmatrix} 0 \\ 1 \end{pmatrix}. \quad (5.6)$$

The eigenvalues and corresponding eigenvectors describe two sets of solution paths. Along a solution path indicated by eigenvector \vec{e}_1 , the temperature remains constant.

and only the molar composition varies. Hence we call this path an isothermal path, and the corresponding eigenvalue, the isothermal eigenvalue. A set of such isothermal paths is illustrated in in Fig. 5.2, where the binary system is composed of CH_4 and C_{10} .

Along the isothermal path in the single-phase region, the local flow velocity can be computed from Eq. 2.56 as

$$\frac{1}{\beta} \frac{\partial \beta}{\partial Z_1} \frac{dZ_1}{d\eta} + \frac{1}{u} \frac{du}{d\eta} - \left(\frac{1}{\beta} \frac{\partial \Gamma}{\partial Z_1} \frac{dZ_1}{d\eta} \right) = 0. \quad (5.7)$$

Recalling the definition of overall heat concentration and heat flux in the single-phase region as

$$\Gamma = \phi \rho H + (1 - \phi) \rho_r H_r, \quad (5.8)$$

and

$$\Theta = u\beta = u\rho H, \quad (5.9)$$

we obtain

$$\frac{du}{d\eta} = 0, \quad (5.10)$$

since the heat contained in the rock, H_r , is fixed at constant temperature and independent of the gas composition.

Therefore, along the isothermal paths in the single-phase region, the normalized eigenvalue λ^* and local flow velocity u both remain constant as the composition varies along the paths, resulting in a constant velocity for the propagation of the compositions. Physically, when a single-phase fluid is injected to displace another single-phase fluid at identical temperature, it is a single-phase flow with neither transfer of components between phases nor volume change of components resulting from the mass transfer or temperature variation. Therefore, all the compositions travel downstream at identical velocity that is equal to the injection rate.

On the other hand, along the set of solution paths described by the second set of

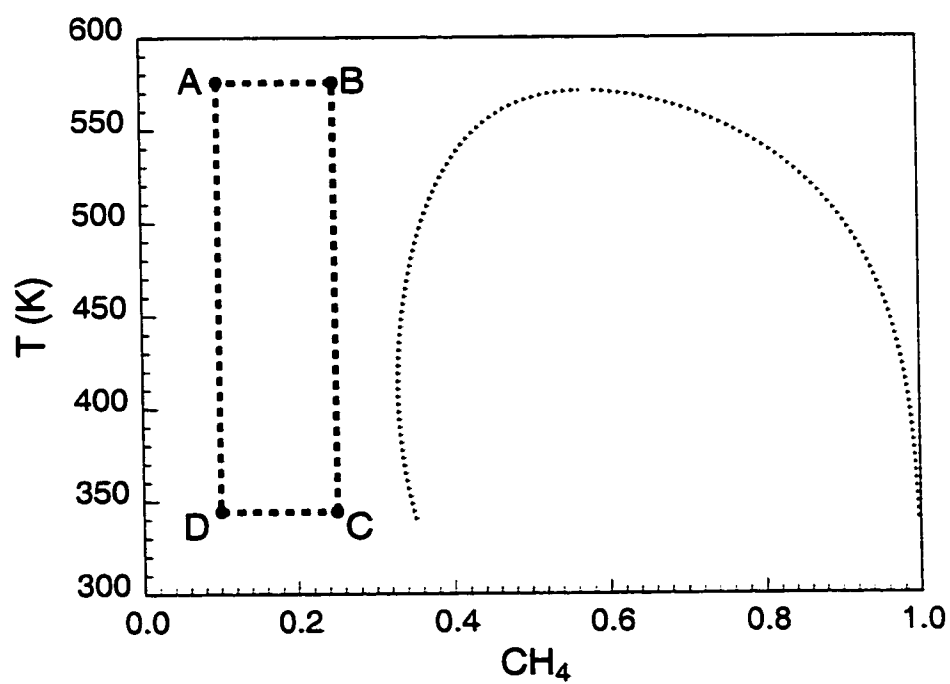


Figure 5.2: Solution paths in the single-phase region of a binary system.

eigenvectors \vec{e}_2 , the local flow velocity is computed from Eq. 2.56 as

$$\frac{1}{\beta} \frac{\partial \beta}{\partial T} \frac{dT}{d\eta} + \frac{1}{u} \frac{du}{d\eta} - \frac{\rho \frac{\partial H}{\partial T}}{\rho \frac{\partial H}{\partial T} + \frac{1-\phi}{\phi} \rho_m C_{pm}} \left(\frac{1}{\beta} \frac{\partial \Gamma}{\partial T} \frac{dT}{d\eta} \right) = 0, \quad (5.11)$$

which yields

$$\frac{1}{u} \frac{du}{d\eta} = \frac{-\frac{1}{\rho} \frac{\partial \rho}{\partial T} \frac{1-\phi}{\phi} \rho_m C_{pm}}{\rho \frac{\partial H}{\partial T} + \frac{1-\phi}{\phi} \rho_m C_{pm}} \frac{dT}{d\eta}. \quad (5.12)$$

Along this set of solution paths, the overall molar composition remains constant but the temperature varies, and hence they are named the temperature paths. Along a temperature path, the eigenvalue and its corresponding eigenvector are named the temperature eigenvalue and temperature eigenvector. The temperature eigenvalue, shown in Eq. 5.4, is significantly lower than that along the isothermal paths, due to its direct dependence on the rock heat capacity. Generally, the rock heat capacity is significantly larger than that of the fluids, at least for gas/oil systems. The rock absorbs or releases large amount of heat when its temperature differs from the reservoir fluids, and hence reduces the propagation velocity of temperature front significantly.

Along the temperature paths, the molar density of the fluids decreases with increasing temperature,

$$\frac{\partial \rho}{\partial T} < 0, \quad (5.13)$$

resulting in increasing local flow velocity with temperature since

$$\frac{du}{dT} > 0. \quad (5.14)$$

The variation of the normalized eigenvalue, local flow velocity, and the product of the two, which is the propagation velocity of composition and temperature, are shown in Fig. 5.3. Along the temperature paths, compositions at lower temperature travel slower than those at higher temperature. When an injection gas at lower temperature is injected to displace a gas with the same composition but at higher temperature, the lower temperature state upstream travels slower than those downstream with higher temperature. Therefore, the continuous solution suffices. On the other hand, if a hotter injection gas is used to displace a colder gas with the same composition, the

higher temperature state at upstream travels faster, resulting in a violation of the velocity rule. Hence, a discontinuous solution is needed.

5.1.2 Discontinuous Solution in the Single-Phase Region

When molar composition and temperature vary discontinuously between two points in the single-phase region of the composition space, conservation of mass and energy must be satisfied by the Rankine-Hugoniot condition,

$$\Lambda_m = \frac{F_i^u - F_i^d}{G_i^u - G_i^d}, \quad i = 1, 2, \quad (5.15)$$

$$\Lambda_h = \frac{\Theta^u - \Theta^d}{\Gamma^u - \Gamma^d}, \quad (5.16)$$

where the superscripts “u” and “d” represent upstream and downstream conditions of the shock.

Across the shock, both molar compositions and temperature change discontinuously, and the shock velocities computed individually from the conservation of mass and energy must be equal.

$$\Lambda_m = \Lambda_h. \quad (5.17)$$

It can be proved that shock solutions in the single-phase region can only occur either as isothermal shocks or as pure temperature shocks without compositional variation, see Appendix A.1.

5.1.3 Examples in the Single-Phase Region

When both the initial and injection mixtures are at the same temperature, all the compositions between the initial and injection mixtures propagate at the same velocity as the injection rate. When the initial and injection mixtures have identical composition but are at different temperatures, only the temperature varies, and it occurs either continuously or discontinuously, depending on the comparison between the temperatures of the initial and injection mixtures.

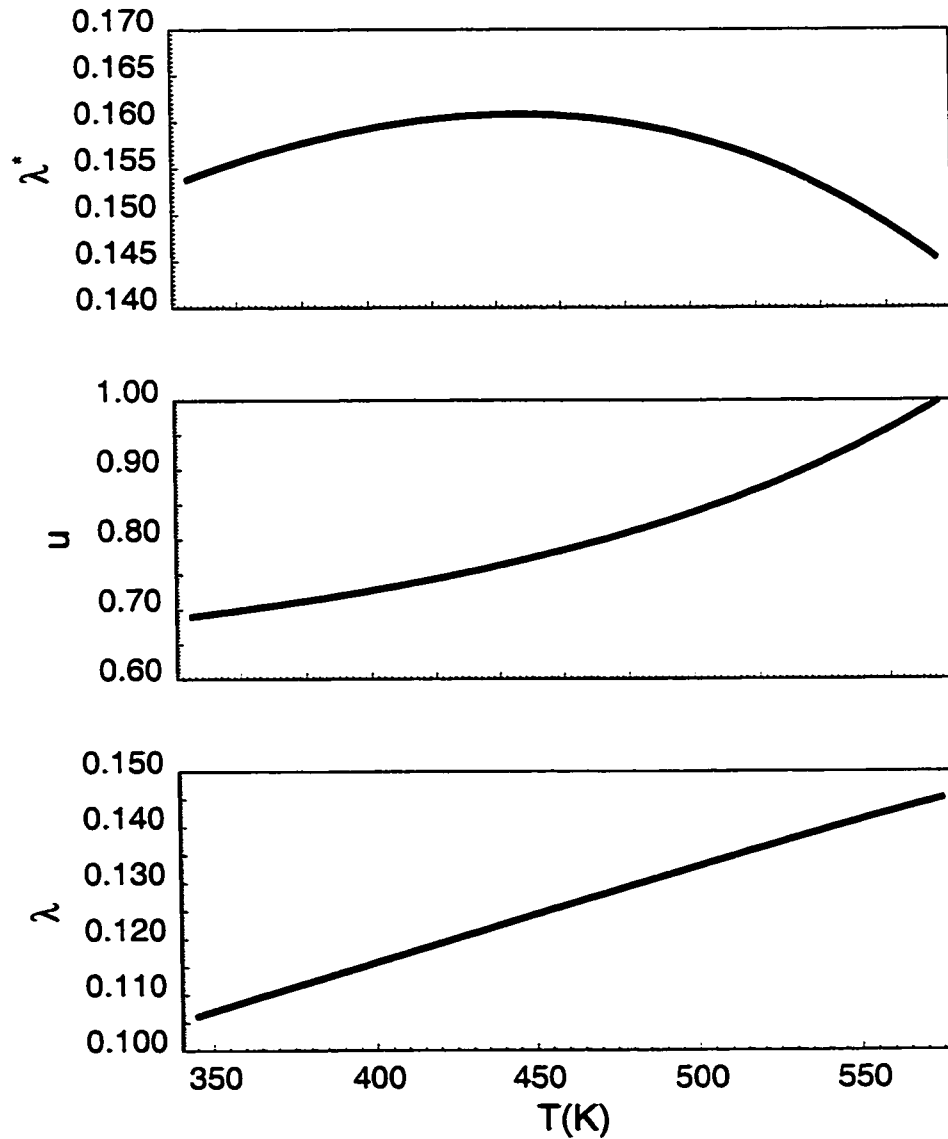


Figure 5.3: Variation of normalized temperature eigenvalue, local flow velocity and propagation velocity along a temperature path in the single-phase region of a binary system.

There are a number of different scenarios to consider when the temperature and composition of the initial and injection mixtures both differ, but still in the single-phase region at the same side of the two-phase envelope (see Fig. 5.2).

In the first of such scenarios, the initial mixture is at a higher temperature than that of the injection mixture. Assume that the initial mixture is located at **A**, and the injection mixture at **C**. In the single-phase region, both continuous and discontinuous variation follow either isothermal or temperature paths. Hence, from the injection mixture **C**, the variation of temperature and composition may either follow path **CD** and **DA** or path **CB** and **BA**. However, the propagation velocity along the solution path **CD** is higher than that along path **DA**, and hence the path switch at **D** violates the velocity rule (see Fig. 5.4). Therefore, the path **CDA** is eliminated, and the correct solution path consists of a slow traveling continuous temperature variation along path **CB**, and a switch at **B** to fast path **BA** where all the compositions propagates downstream at equal velocity, as shown in Fig. 5.5.

Similar analysis can be applied for the example where the initial mixture is at **B** and injection mixture at **D**. The solution consists of a trailing continuous variation along temperature path **DA**, and a switch to the leading continuous variation along the isothermal path **AB**.

For scenarios where the temperature of the initial mixture is lower than that of the injection mixture, consider an example where the initial mixture is at **C** and injection mixture at **A**. By continuous variation along the isothermal path **AB** and then continuous variation along temperature path **BC**, there are two violations of the velocity rule. Firstly, the propagation velocity along the upstream path **AB** is higher than that along the downstream path **BC**. Secondly, along the temperature path **BC**, the propagation velocity decreases monotonically towards the downstream direction (see Fig. 5.6). Replacing the continuous variation along path **BC** with a shock does not satisfy the velocity rule, because the shock velocity is still lower than that along the upstream path **AB** (see Fig. 5.7). On the other hand, if we construct the solution by following the slower temperature path **AD** and a switch to the faster isothermal path **DC** (see Fig. 5.8), and replacing the continuous variation along temperature path **AD** with a shock (see Fig. 5.9), then the velocity rule will be

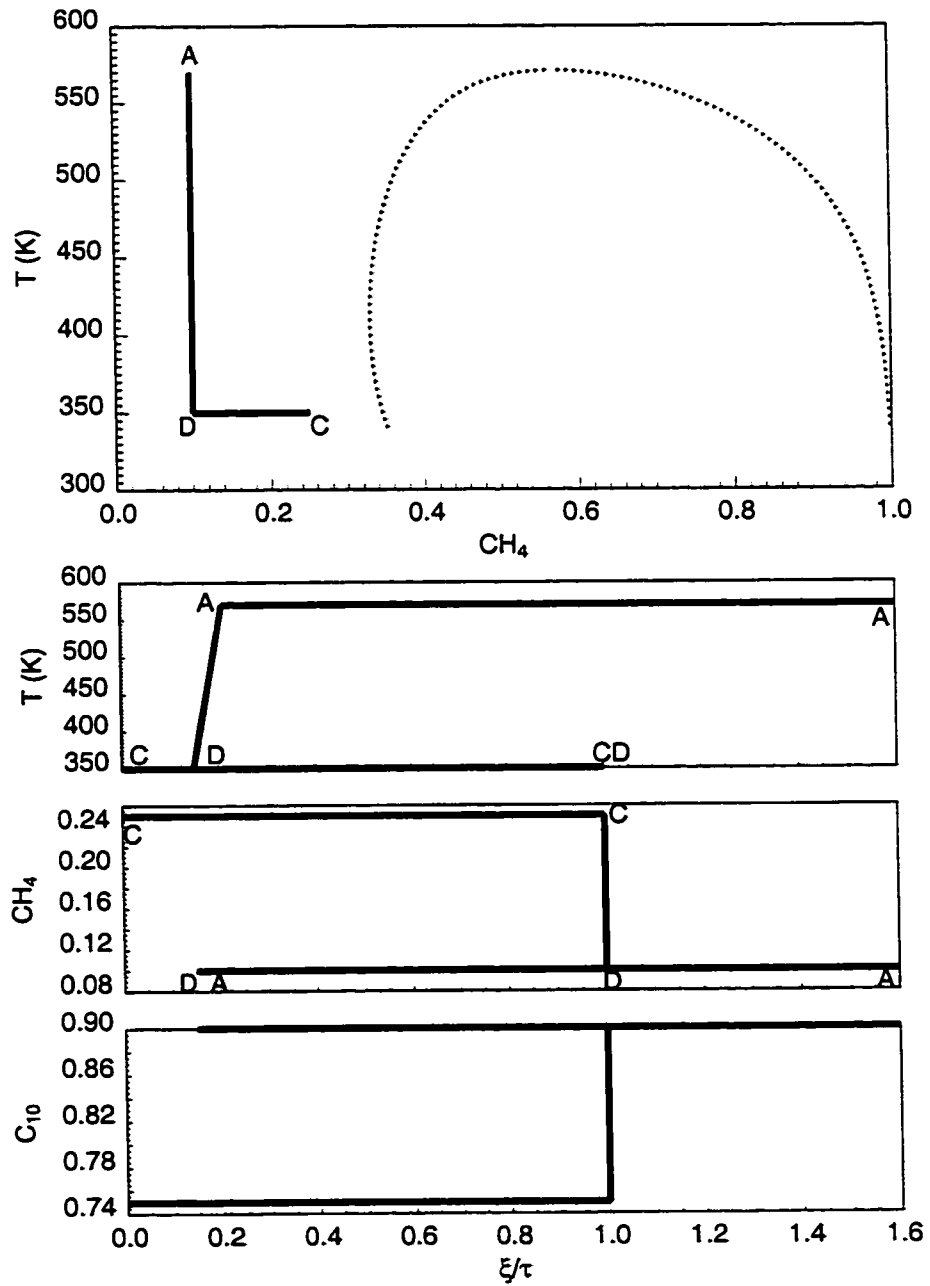


Figure 5.4: Example solution in single-phase region with initial mixture at A and injection mixture at C. The upstream continuous variation along isothermal path CD propagates faster than the downstream continuous variation along temperature path DA, violating the velocity rule.

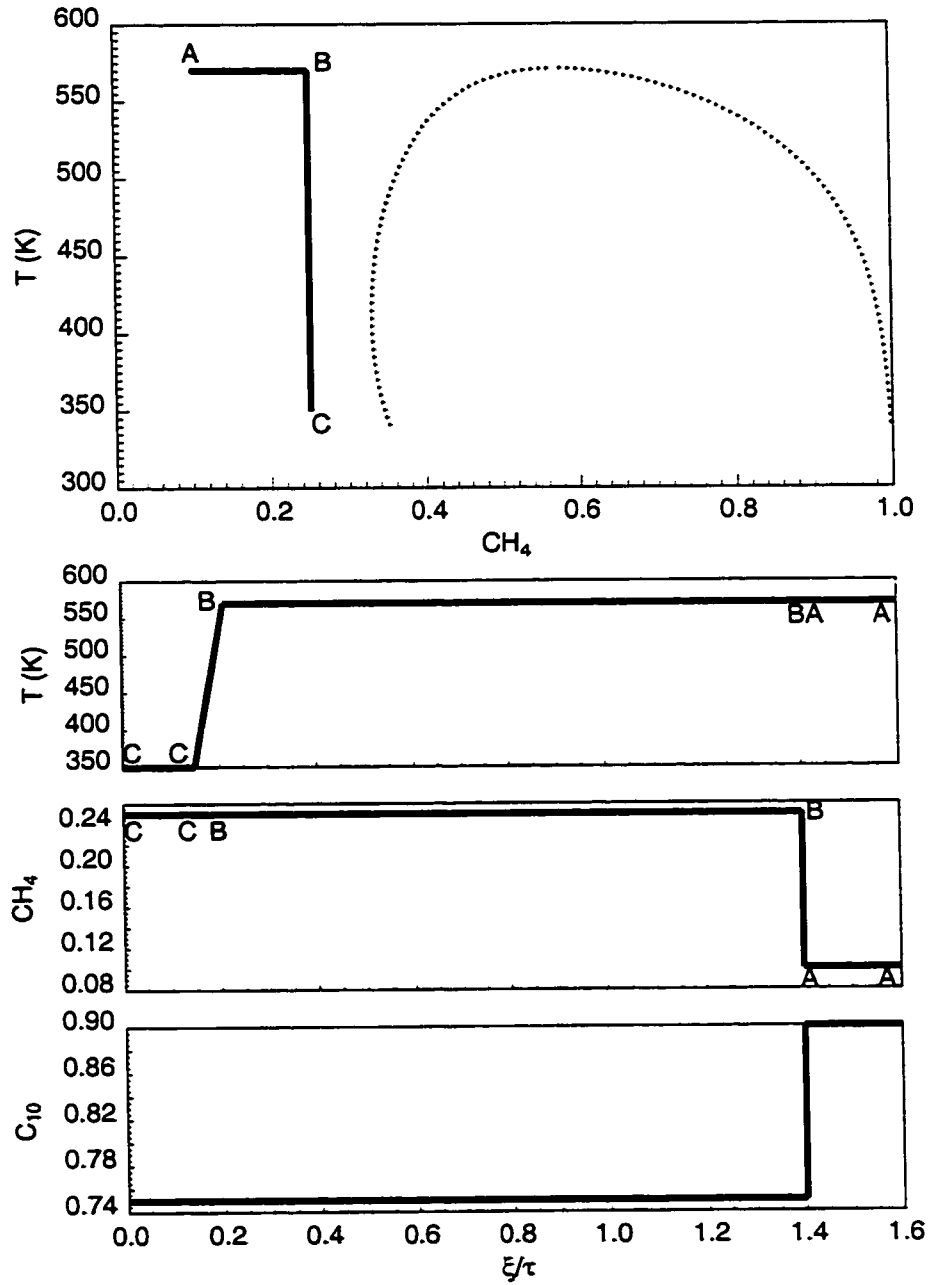


Figure 5.5: Example solution in single-phase region with initial mixture at A and injection mixture at C.

satisfied. Similar analysis can be performed for an example where the initial mixture is at **D** and injection mixture at **B**.

Overall, it can be concluded that the solution consists of separate segments along the isothermal or temperature paths that are arranged according to the propagation velocity along these individual solution segments. Within each solution segment, if continuous variation violates the velocity rule, then it must be replaced with a shock solution segment.

5.2 Solutions in the Two-Phase Region

5.2.1 Continuous Variation in the Two-Phase Region

Consider a gas injection problem where both the initial and injection conditions are located within the two-phase region. The eigenvalue problem for continuous variation of the state variables is established in Appendix A.2, and two sets of eigenvalues and eigenvectors are derived. The first eigenvalue has the form as

$$\lambda_{TL}^* = \frac{df_v}{dS_v}, \quad (5.18)$$

with a corresponding eigenvector

$$\begin{pmatrix} \frac{dZ_1}{d\eta} \\ \frac{dT}{d\eta} \end{pmatrix} = \begin{pmatrix} 1 \\ 0 \end{pmatrix}, \quad (5.19)$$

indicating a continuous variation path direction along which the temperature remains constant. The path is therefore named the isothermal path, the eigenvalue the isothermal eigenvalue, and its corresponding eigenvector the isothermal eigenvector. In the two-phase region of a binary system, the isothermal paths are also tie lines. The isothermal eigenvalue λ_{TL}^* is independent of temperature, and represents the fractional flow behavior, as in all other problems without temperature variation, including the Buckley-Leverett problem. The local flow velocity is constant as has been shown in Appendix A.2. As a product of the eigenvalue λ^* and the local flow

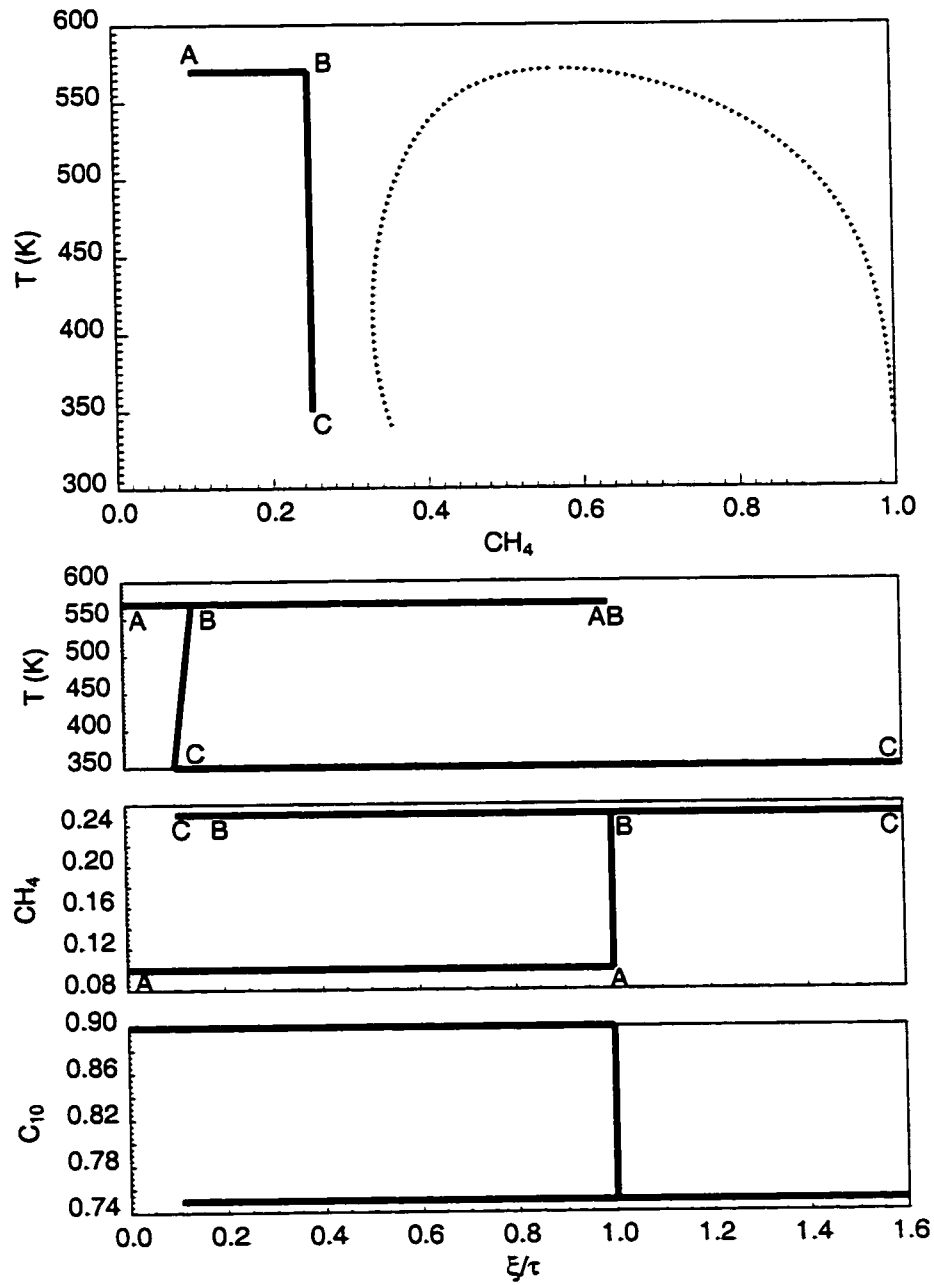


Figure 5.6: Example solution in single-phase region with initial mixture at C and injection mixture at A. The propagation velocity along path AB is higher than that along path BC. Along path BC, the propagation velocity decreases monotonically towards the downstream direction.

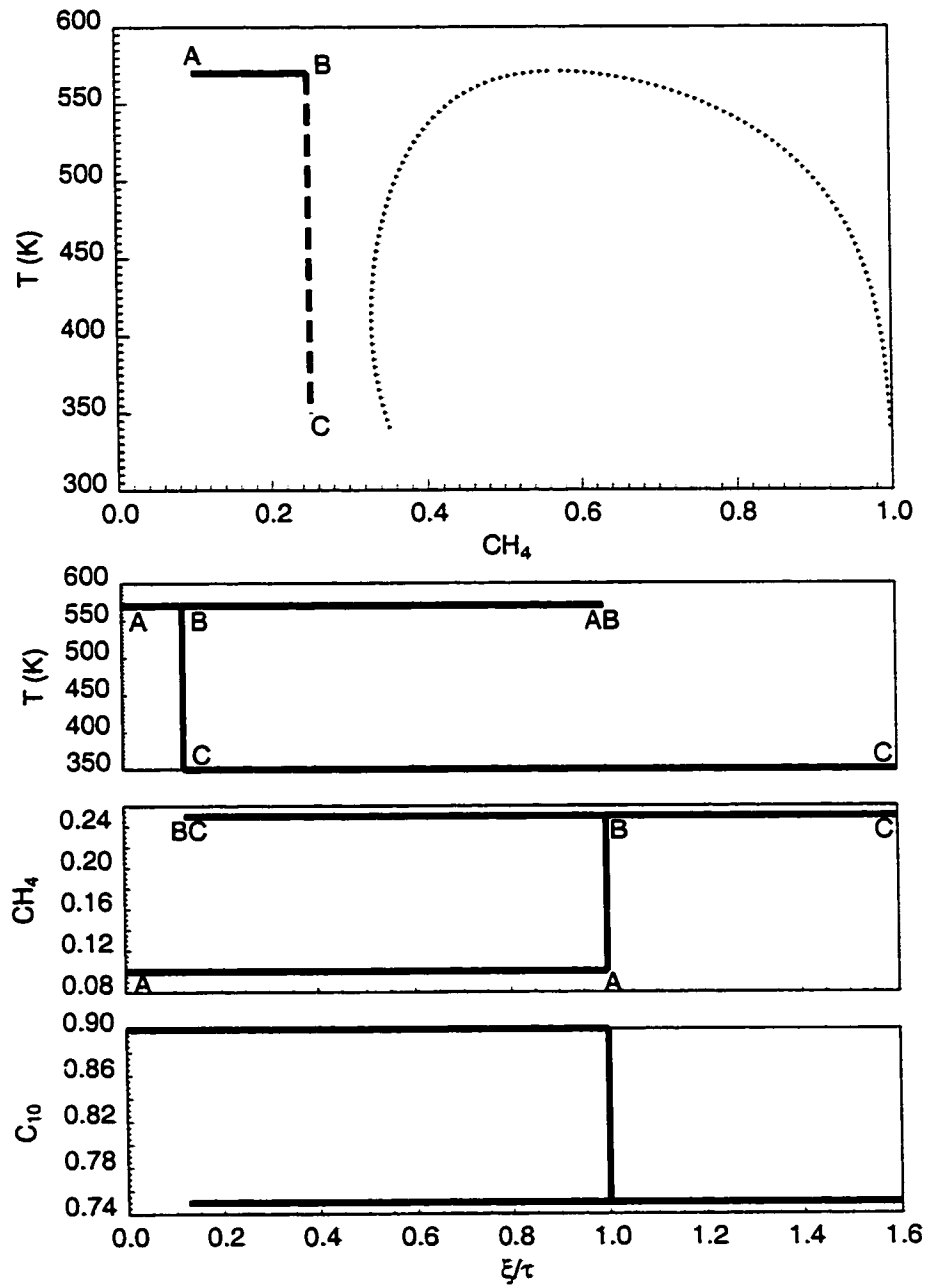


Figure 5.7: Example solution in single-phase region with initial mixture at C and injection mixture at A. The propagation velocity along path AB is higher than that of the shock between B and C.

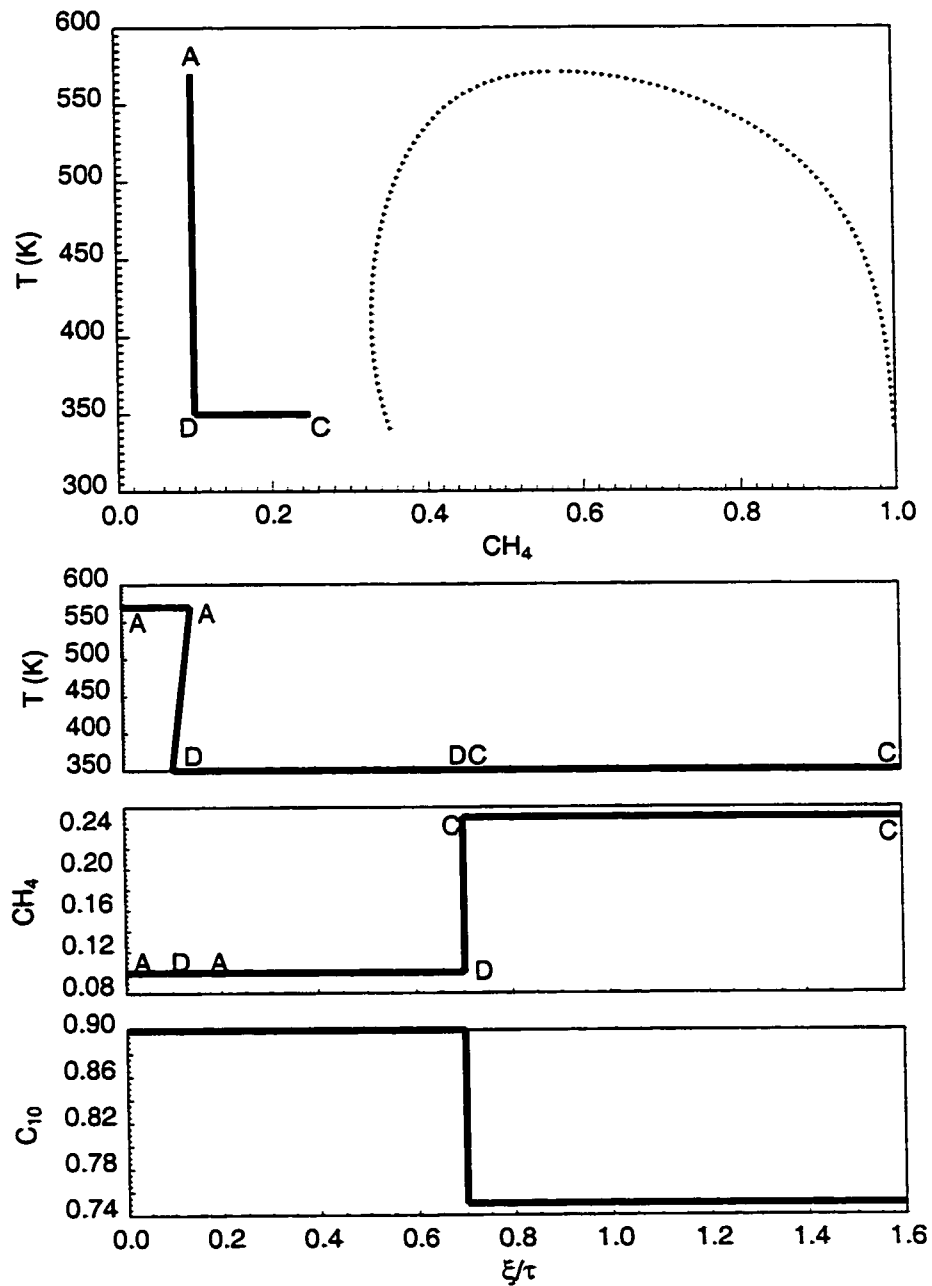


Figure 5.8: Example solution in single-phase region with initial mixture at C and injection mixture at A. For continuous variation along temperature path AD, the propagation velocity decreases monotonically towards the downstream direction.

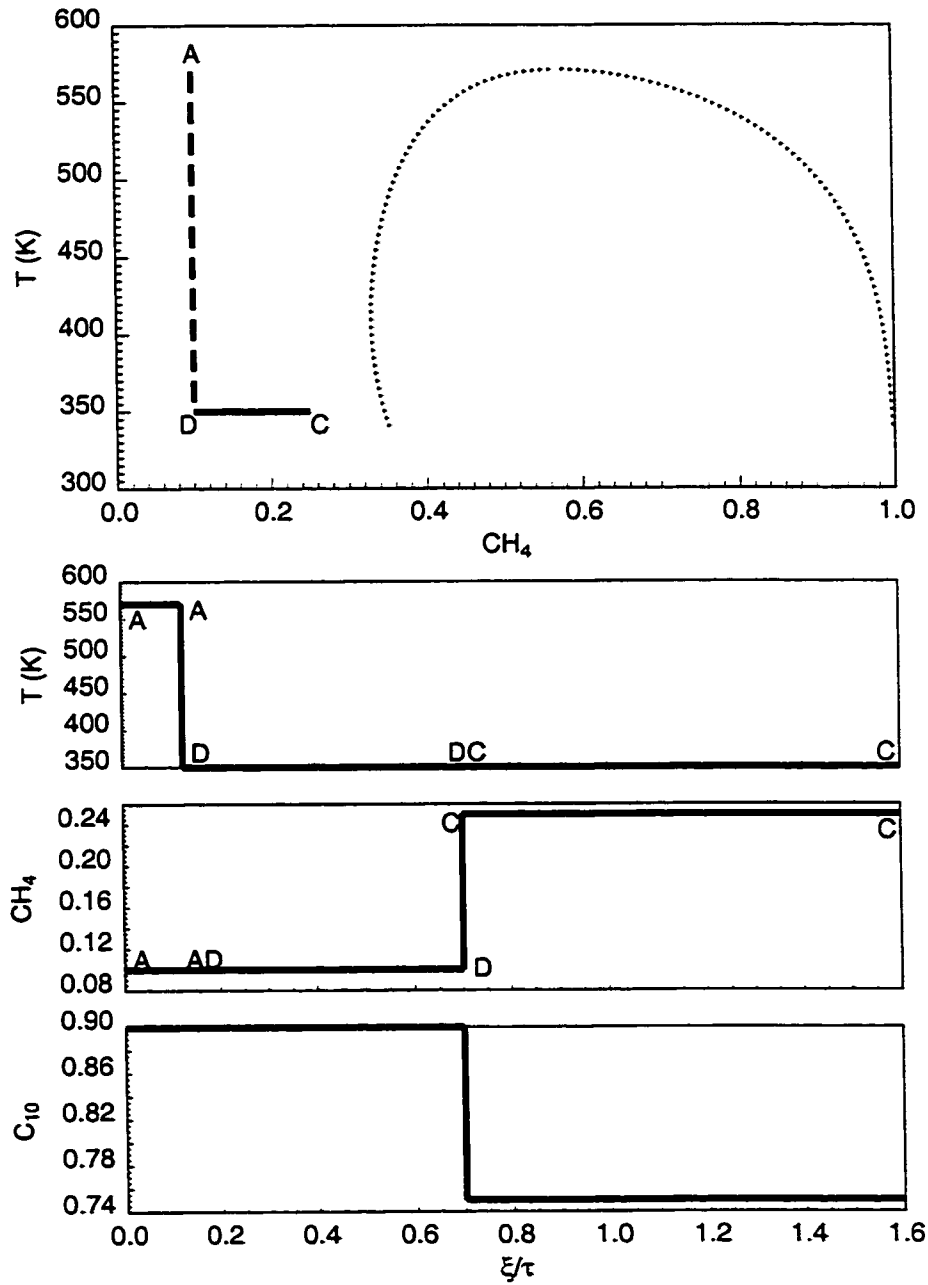


Figure 5.9: Example solution in single-phase region with initial mixture at C and injection mixture at A.

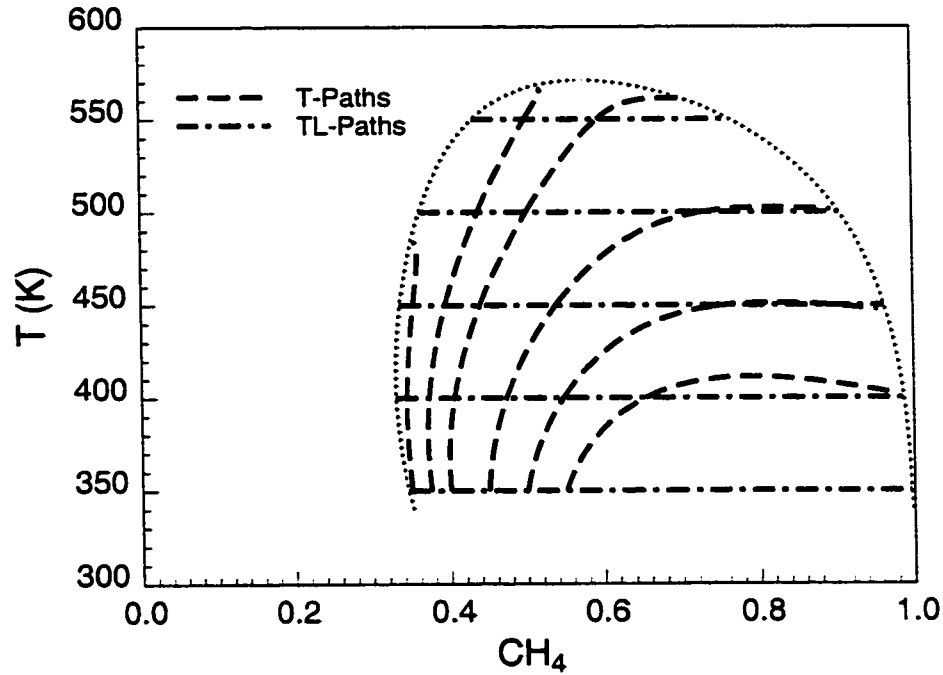


Figure 5.10: Solution paths in the two-phase region of a binary system. The TL paths are isothermal or tie-line paths, and the T-paths are those for which temperature varies.

velocity, the propagation velocity of compositions along the isothermal paths is determined by phase behavior through the fractional flow function, and is independent of temperature effect. The isothermal paths are demonstrated in a sample binary system composed of CH_4 and C_{10} in Fig. 5.10. Along one of the isothermal paths, the variation of the isothermal eigenvalue with vapor phase saturation of the mixture is demonstrated in Fig. 5.11. It can be observed that the isothermal eigenvalue tends to zero as the two-phase mixture's composition approaches the phase envelope.

The second eigenvalue is solved as

$$\lambda_T^* = \frac{f_l G_l + f_v G_v}{S_l G_l S_v G_v - H}, \quad (5.20)$$

where G_l , G_v and H have the complicated definition in Appendix A.2.

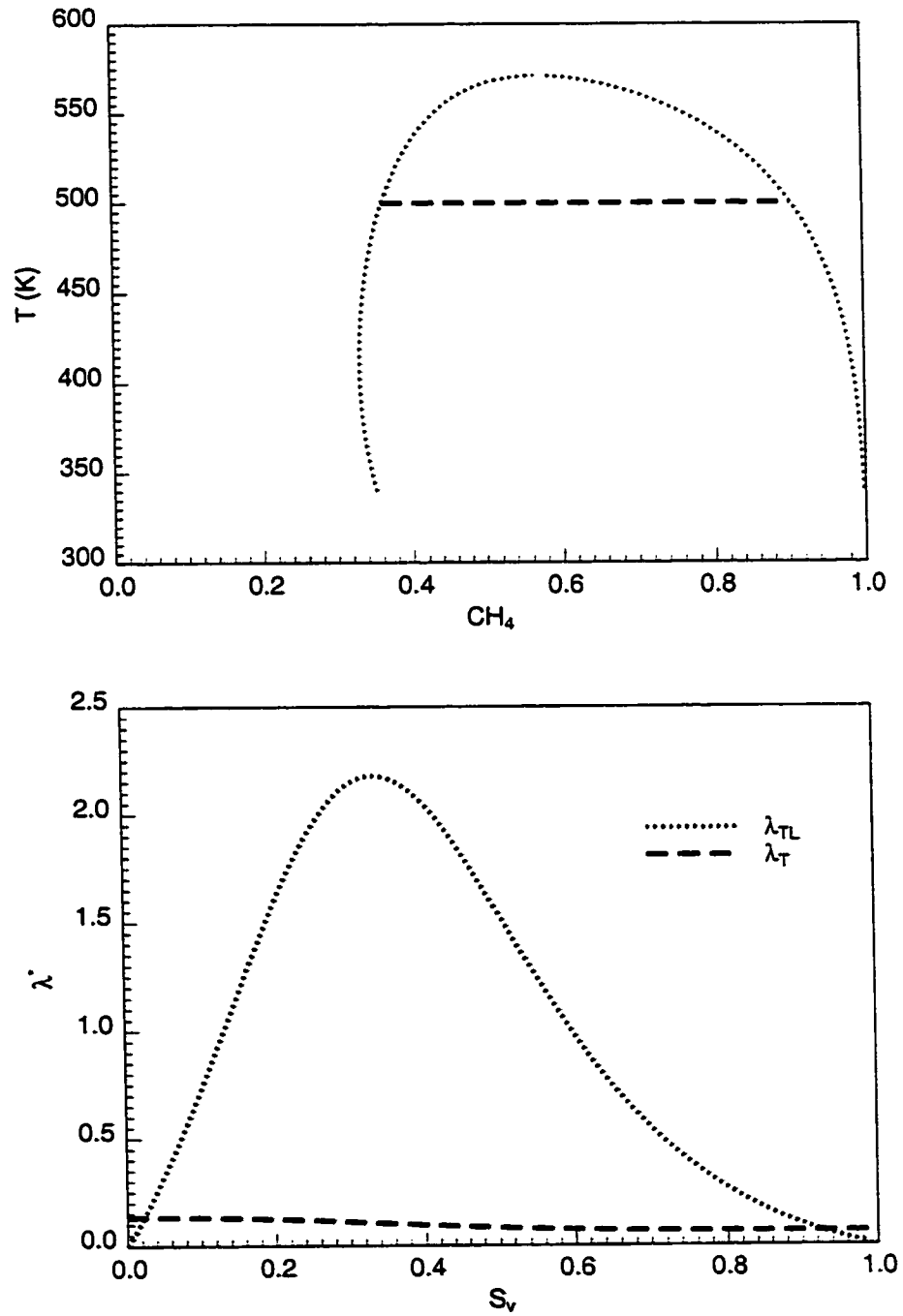


Figure 5.11: Variation of tie-line and temperature eigenvalues along an isothermal path at $500^\circ K$ in the $CH_4 - C_{10}$ system.

Along a solution path indicated by the corresponding eigenvector, the temperature varies. Hence, this set of solution paths is named the temperature path, the eigenvalue the temperature eigenvalue, and its corresponding eigenvector the temperature eigenvector. Temperature paths in the two-phase region of a binary system composed of CH_4 and C_{10} are demonstrated in Fig. 5.10.

The temperature paths are accompanied by variation in both temperature and composition, and do not intersect with each other. When a temperature path is traced, the normalized eigenvalue does not vary monotonically. However, the local flow velocity increases monotonically with temperature, and it is much larger than the normalized temperature eigenvalue. As a product of the normalized eigenvalue and the local flow velocity, the propagation velocity increases monotonically with temperature (see Fig. 5.12).

A maximum in temperature may occur when a temperature is traced to the vicinity of the two-phase envelope, where the temperature eigenvalue is equal to the isothermal eigenvalue, and the temperature eigenvector coincides with the isothermal eigenvector. The variation of temperature eigenvalue along a tie line, shown in Fig. 5.11, also indicates that for most of a tie line path, the isothermal eigenvalue is greater than the temperature eigenvalue, and there exist two equal-eigenvalue points near the two-phase boundary. On the two-phase boundary, the isothermal eigenvalue tends to zero, while the temperature eigenvalue does not change significantly.

When the injected fluid is a two-phase mixture located on the same temperature path as a two-phase initial fluid that is at higher temperature, the states with lower temperature stay upstream of those with higher temperature, and propagate at lower velocity. Therefore, the velocity rule is satisfied and a continuous variation of the state variables suffices. On the other hand, if the injection fluid is on the same temperature path as the initial fluid but at higher temperature, the velocity rule is violated and a discontinuous solution is needed.

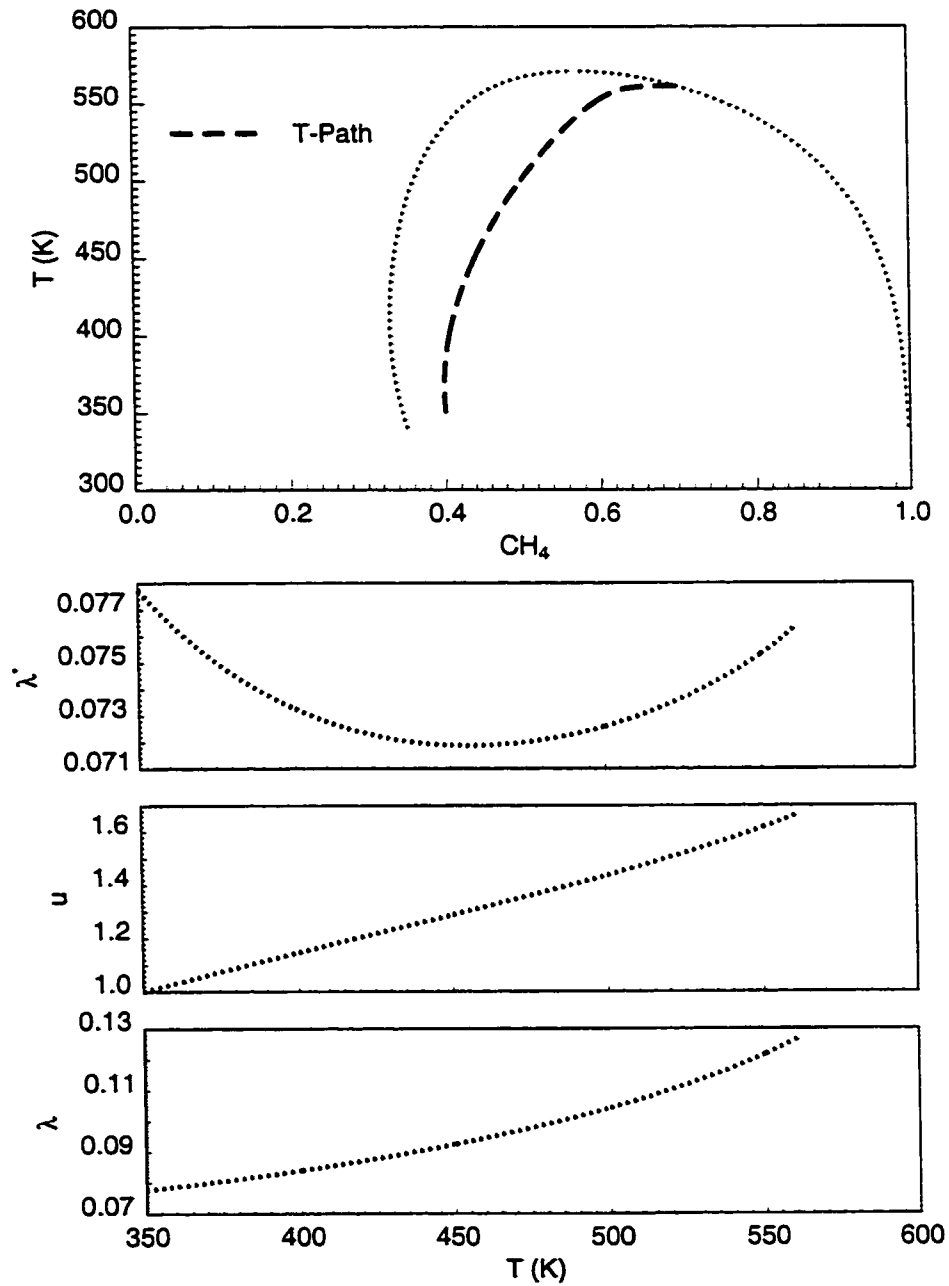


Figure 5.12: Variation of normalized temperature eigenvalue, local flow velocity and propagation velocity along a temperature path in the two-phase region of a binary system.

5.2.2 Discontinuous Solution in the Two-Phase Region

Just as in the single-phase region, the shocks in the two-phase region can be divided into isothermal shocks and temperature shocks. The shock balance equation for the discontinuous solution in the two-phase region is expressed as

$$\Lambda_m = \frac{u^u \alpha_1^u - u^d \alpha_1^d}{G_1^u - G_1^d} = \frac{u^u \alpha_2^u - u^d \alpha_2^d}{G_2^u - G_2^d}, \quad (5.21)$$

and

$$\Lambda_h = \frac{u^u \beta^u - u^d \beta^d}{\Gamma^u - \Gamma^d} = \Lambda_m, \quad (5.22)$$

where we recall the definitions

$$\alpha_i = \rho_l f_l x_i + \rho_v f_v y_i, \quad (5.23)$$

$$G_i = \rho_l S_l x_i + \rho_v S_v y_i, \quad (5.24)$$

$$\beta = \rho_l f_l H_l + \rho_v f_v H_v, \quad (5.25)$$

and

$$\Gamma = \rho_l S_l H_l + \rho_v S_v H_v + \frac{1 - \phi}{\phi} \rho_r H_r. \quad (5.26)$$

When a shock occurs between two compositions on the same tie line in the two-phase region, the contribution to the heat concentration term from the rock is canceled in the shock balance equation, and we construct an isothermal shock as

$$u^d = u^u, \quad (5.27)$$

and

$$\Lambda_m = \Lambda_h = u^u \frac{f_v^u - f_v^d}{S_v^u - S_v^d}. \quad (5.28)$$

Therefore, across an isothermal shock in the two-phase region, the local flow velocity remains unchanged, and the shock velocity is independent of temperature effect. The expression for the isothermal shock velocity is identical to that in problems with no temperature variation effect, including the Buckley-Leverett problem.

Unlike the single-phase region, a temperature shock in the two-phase region must be accompanied by composition variation in order to satisfy the conservation of mass and energy across the shock. The derivation for solving temperature shocks is shown in Appendix A.4.

5.2.3 Examples in the Two-Phase Region

Figure 5.13 shows a loop formed by two isothermal path segments **AB** and **CD**, and two temperature path segments **BC** and **DA** in the binary system composed of component CH_4 and C_{10} , and it is used to illustrate some of the example solutions that are completely within the two-phase region.

If the initial and injection mixtures are both on the same isothermal path **AB** or **CD**, then the gas injection problem is a simple isothermal case and needs no further discussion. If the initial and injection mixtures are located on the same temperature path, then two scenarios need to be considered. Consider temperature path **BC**, if the injection mixture is at lower temperature **C**, while the initial mixture at higher temperature **B**, then as the state variables, including both molar composition and temperature, vary along the temperature path **BC**, the propagation velocity increases monotonically as the solution path is traced towards the downstream direction. A continuous variation solution along the temperature path satisfies the velocity rule; On the other hand, if the injection mixture is at higher temperature **B** and initial mixture at lower temperature **C**, then a continuous variation along the temperature path **BC** violates the velocity rule as the propagation velocity decreases towards the downstream condition. A shock solution is needed to overcome the temperature difference between **B** and **C**, and the shock solution does not follow the solution paths for continuous variation. The solution can be constructed as a temperature shock between **C** and **E** with a switch to an isothermal path solution between **E** and **B**, or a temperature shock between **B** and **F** with a switch to an isothermal path solution between **F** and **C**, as Fig. 5.13 illustrates. The temperature shocks **CE** and **BF** are slower than the isothermal continuous variations along paths **EB** and **FC**. If the state variations follow the path **BE** and then across shock **EC**, the

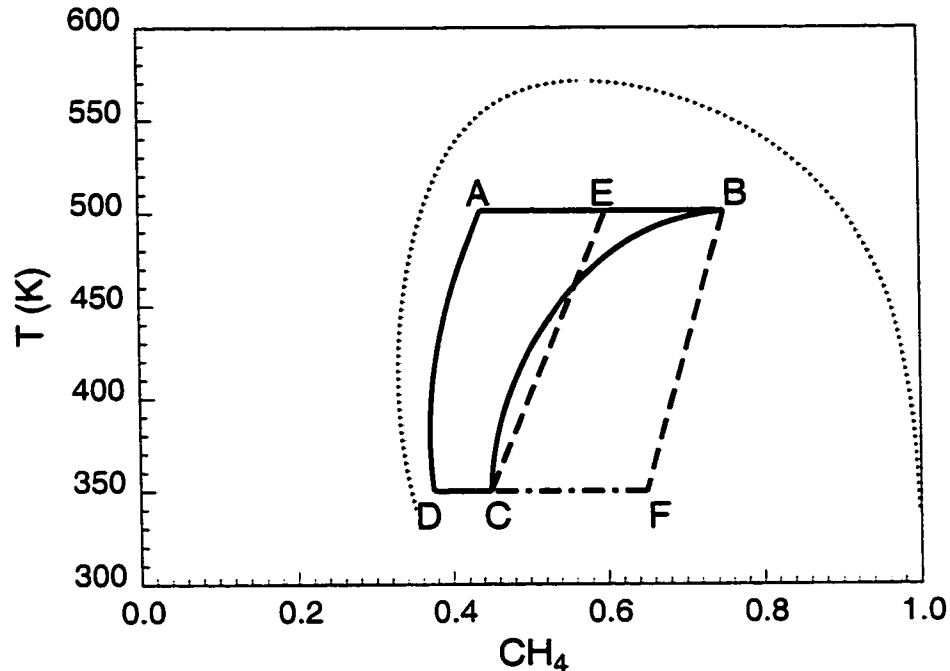


Figure 5.13: Examples with initial and injection mixtures both in the two-phase region.

solution becomes invalid because of a violation of the velocity rule. Therefore, the final solution will consist of an upstream slow moving shock **BF**, and a switch to the isothermal path between **F** and **C**.

Similar analysis can be applied to an example when the initial and injection mixtures are both on the same temperature path **AD**. In the most general configuration, the initial and injection mixtures are neither on the same temperature path nor on the same isothermal path, for example, the initial mixture at **A** and injection mixture at **C**. The analysis is similar to that of the examples where the initial and injection mixtures are on the same temperature path.

Figure 5.14 shows an expanded plot of a temperature path near the equal-eigenvalue point, and an isothermal path that is tangent to the temperature path at the equal-eigenvalue point. Along the temperature paths **CE** and **DE**, the propagation velocity increases monotonically with temperature. Along the isothermal path **AB**,

the propagation velocity decreases monotonically as the composition approaches the two-phase envelope. The eigenvalue along the isothermal path **AB** is equal to that of the temperature path at **E**, and has zero value at the two-phase boundary.

If an initial mixture is at **A**, and an injection gas at **D** on the temperature path, then a continuous variation along temperature path **ED** and a switch at the equal-eigenvalue point **E** to a continuous variation along isothermal path **EA** satisfies the velocity rule. The same solution structure can be obtained if the injection composition is at **C** on the temperature path. If the initial composition is at **B**, then the continuous variation between **E** and **B** violates the velocity rule, and a shock along the isothermal path **EB** is needed.

On the other hand, if the initial mixture is at **C** or **D**, with the injection mixture at **A** or **B**, then continuous variation along the temperature path **EC** or **ED** violates the velocity rule. A shock is needed to cross the temperature difference between the initial and injection mixtures, and it does not follow the temperature path **EC** or **ED**, and hence there is no path switch at the equal-eigenvalue point **E**.

5.3 Solutions across the Two-Phase Boundary

In general EOR practice, single-phase gas mixtures are often used to displace single-phase liquid initial oils. In most settings, a two-phase region occurs for the mixtures of injection gas and the initial oil. The variation of the state variables between single-phase and two-phase regions can be interpreted as solution paths that cross the two-phase boundary in the composition space.

5.3.1 Continuous Variation across the Two-Phase Boundary

Consider all possible switches between the continuous solution paths in the single-phase region and those in the two-phase region. A set of continuous isothermal and temperature paths in the single-phase region and two-phase region that meet at point **E** on the two-phase envelope is shown in Fig. 5.15. Four scenarios need to be considered.

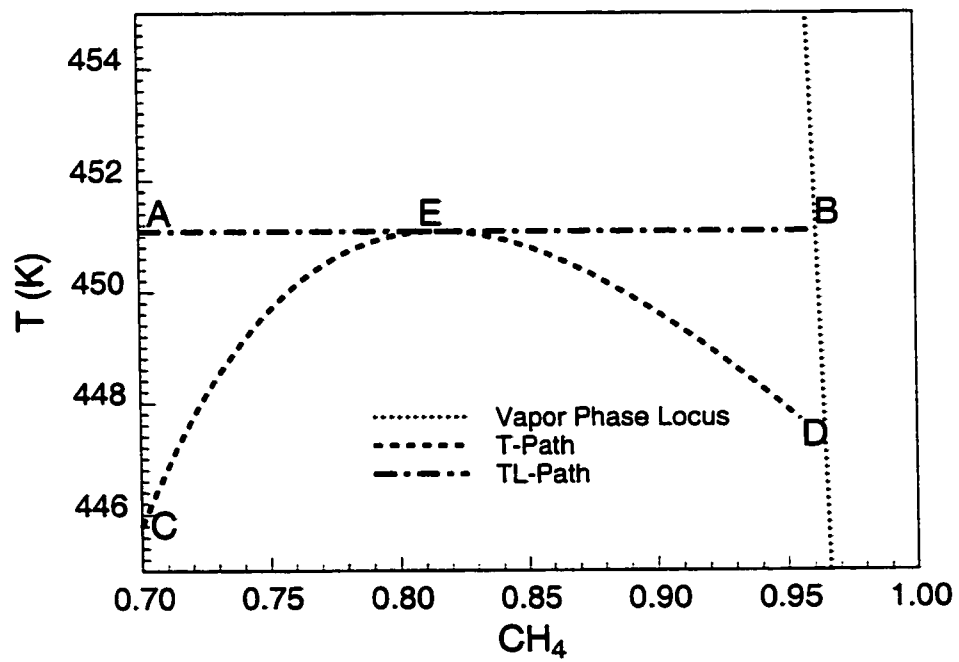


Figure 5.14: Isothermal and temperature path near the equal-eigenvalue point.

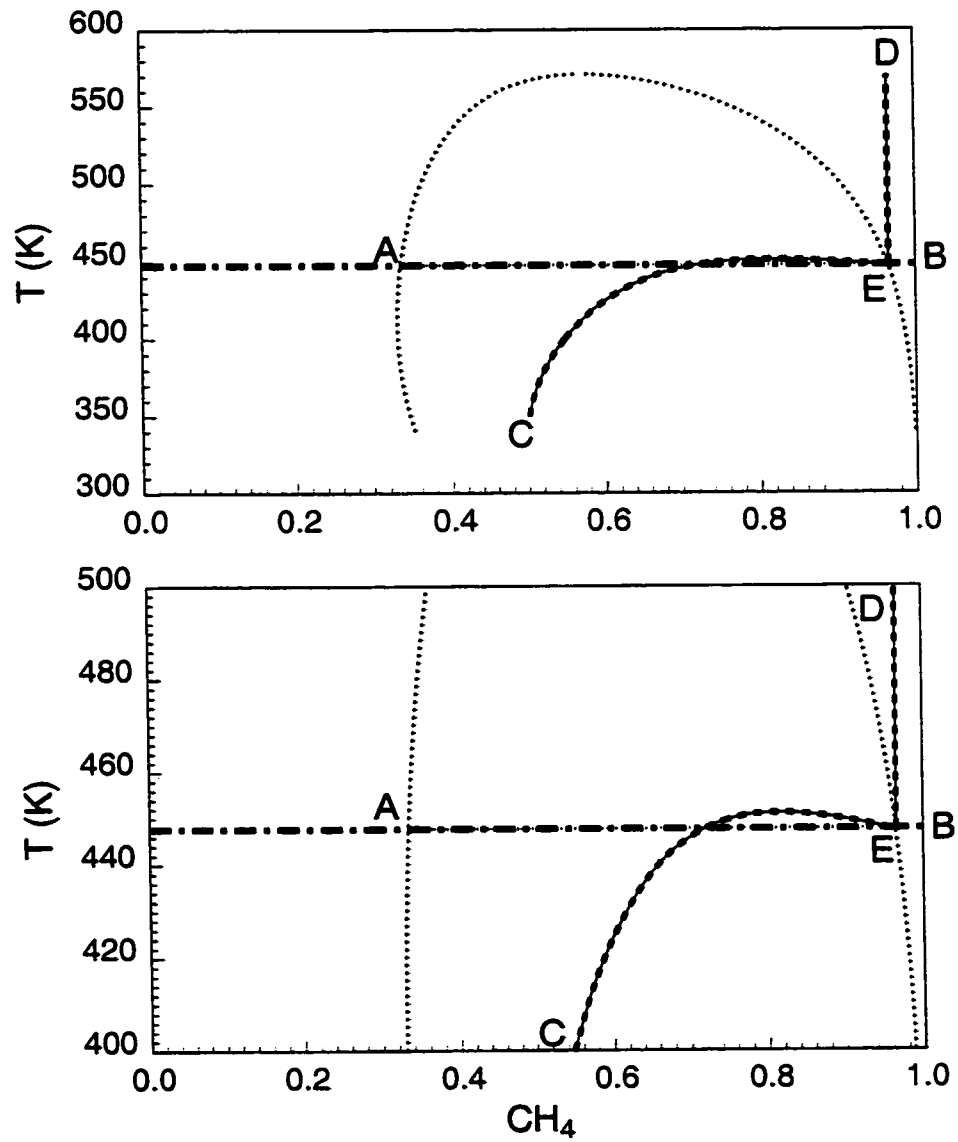


Figure 5.15: Summary of possible switches between the continuous solution paths in the single-phase region and those in the two-phase region. The figure at the bottom is a magnified version of the one on top.

Consider a switch between the continuous isothermal path **AE** in the two-phase region and the isothermal path **EB** in the single-phase region, as shown in Fig. 5.16. Along path **AE**, the isothermal eigenvalue reduces to zero as the molar composition approaches the two-phase boundary at **E** (Fig. 5.16). On the other hand, along path **BE**, the eigenvalue remains constant, as Eq. 5.3 shows. As continuous isothermal paths **AE** and **EB** are traced with a path switch at the two-phase boundary **E**, the composition varies continuously, while the propagation velocity of the compositions is discontinuous with a local minimum of zero velocity occurring at the phase boundary **E**. Depending on the direction that paths **AE** and **EB** are traced, the propagation velocity of the composition must first decrease to zero, either continuously or discontinuously, and then increase again. Therefore, one of the two continuous variation path segments **AE** and **EB** must violate the velocity rule as the two-phase boundary is crossed by a continuous variation of composition along the isothermal paths.

Similar analysis applies to the situation where a path switch is made between the continuous isothermal path **AE** in the two-phase region and the continuous temperature path **ED** in the single-phase region, as Fig. 5.17 illustrates. Within the two-phase region, along the continuous isothermal path **AE**, the propagation velocity decreases to zero as the two-phase boundary is approached. On the other hand, in the single-phase region, the propagation velocity of temperature increases with temperature along the continuous temperature path, starting from the two-phase boundary at **E**. When paths **AE** and **ED** are traced in either direction, the propagation velocity does not vary monotonically and results in violation of the velocity in one of the two continuous variation segments.

When the continuous temperature path **CE** in the two-phase region is connected to the continuous isothermal path **EB** in the single-phase region at **E** on the two-phase envelope (see Fig. 5.18), the propagation velocity of the state variables is discontinuous since the isothermal eigenvalue along path **EB** is significantly larger than the temperature eigenvalue along path **CE**, according to Fig. 5.11 and Eq. 5.3. More importantly, the propagation velocity decreases when path **CE** is traced, and the two-phase boundary at **E** is approached. Therefore, when a path switch is made at **E** either from **CE** to **EB** or from **BE** to **EC**, the propagation velocity does not vary

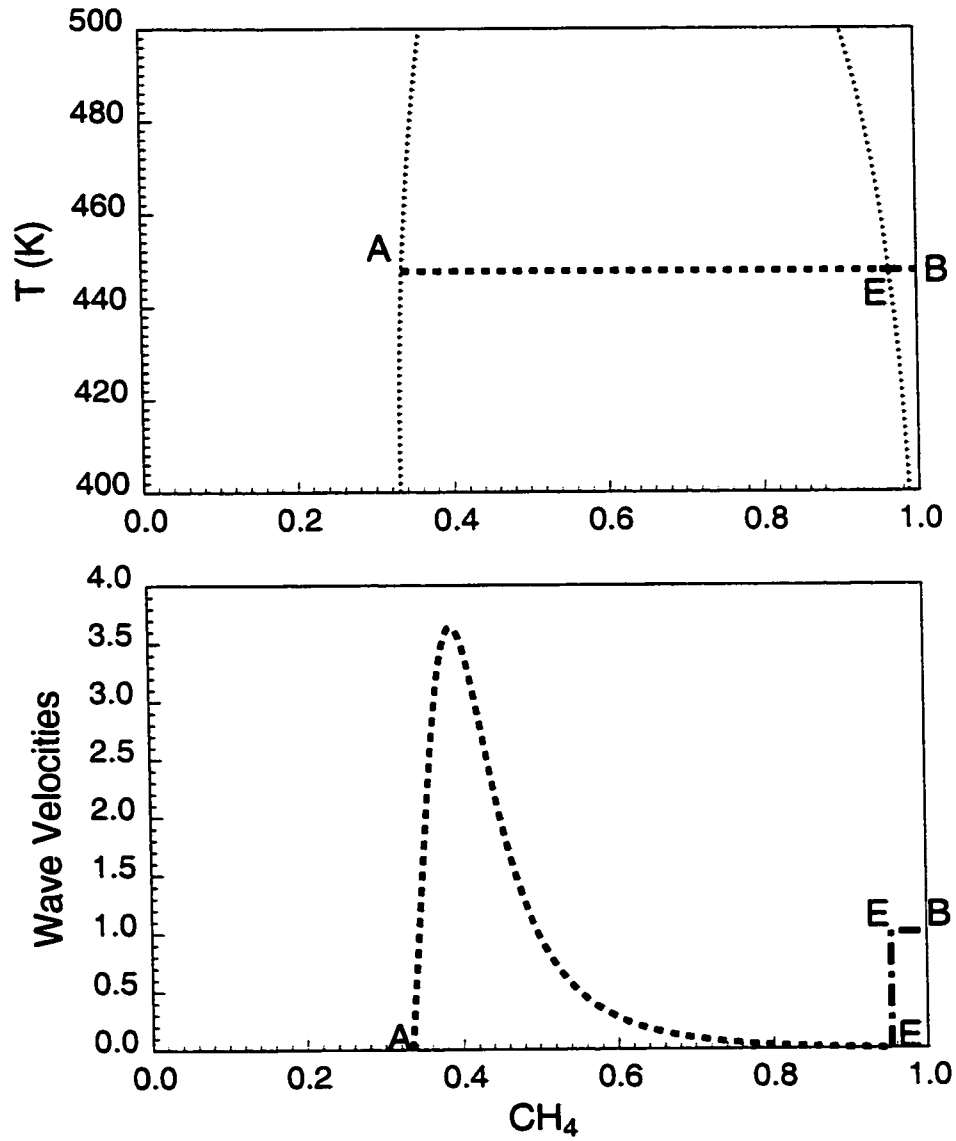


Figure 5.16: Switch between the continuous isothermal paths in the single-phase region and the two-phase region.

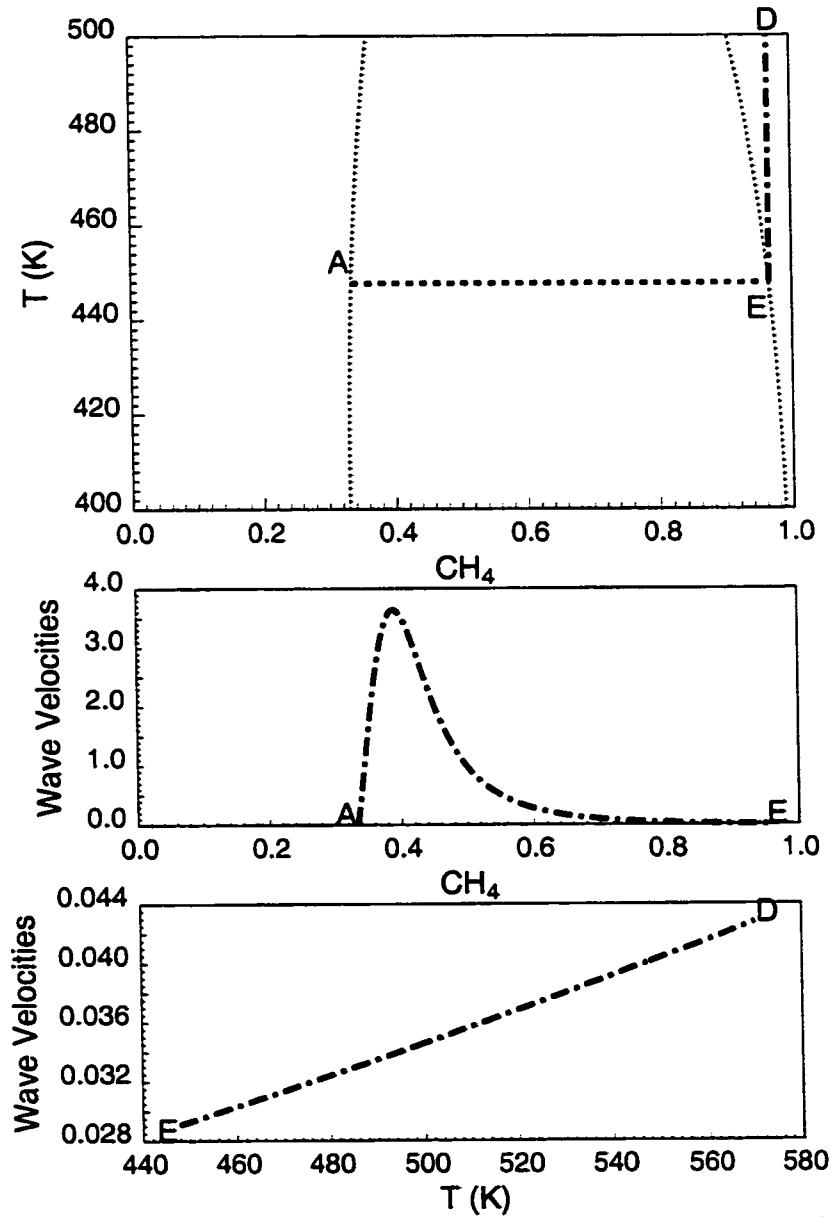


Figure 5.17: Switch between the continuous isothermal path in the two-phase region and continuous temperature path in the single-phase region.

monotonically, and either one of the two continuous variation segments will violate the velocity rule.

In the last case, shown in Fig. 5.19, the continuous temperature path **CE** in the two-phase region is connected to the continuous temperature path **ED** in the single-phase region. The propagation velocity varies continuously as the path switch occurs at **E**. When the temperature path **CE** is traced towards the two-phase boundary at **E**, the propagation velocity for the state variables decreases if the temperature decreases. Similarly, in the single phase region, as the state variables propagate continuously along the temperature path **DE** towards the two-phase boundary, the propagation velocity decreases as temperature decreases. Therefore, a local minimum value for the propagation velocity occurs at **E**. However, when continuous temperature paths **CE** and **ED** are combined, the propagation velocity does not vary monotonically between **C** to **D**, and a violation of velocity rule occurs on one of the two segments when the path is traced by continuous variation.

In summary, all possible switches between the continuous isothermal and temperature paths in the single-phase and two-phase regions are investigated, and proved to be invalid due to violation of velocity rule. Therefore, the two-phase envelope must be crossed by a discontinuous solution, hereby named a phase-change shock.

5.3.2 Phase-Change Shocks

There are two kinds of phase-change shocks that can cross the phase envelope, a nearly isothermal phase-change shock, where only a slight temperature difference occurs across the shock due to latent heat, and a temperature phase-change shock, which spans a significant temperature difference. Figure 5.20 illustrates the two types of shocks.

It is shown in Appendix A.1 that the isothermal discontinuous solutions in the single-phase region occur with constant temperature. Starting from **G** in the single-phase region, isothermal shocks can be constructed with the upstream end fixed at **G**, and all possible downstream ends forming a locus **GA** in the single-phase region.

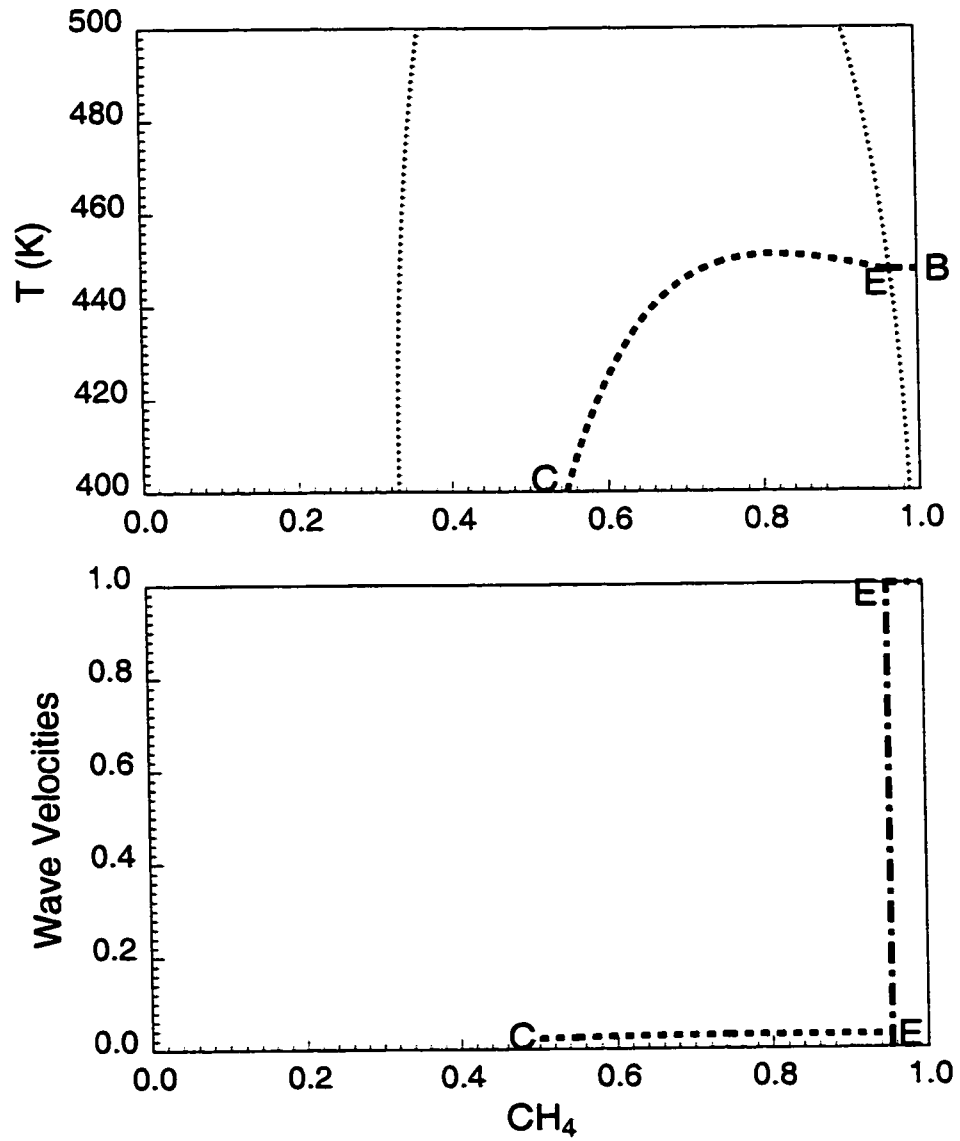


Figure 5.18: Switch between the continuous temperature path in the two-phase region and continuous isothermal path in the single-phase region.

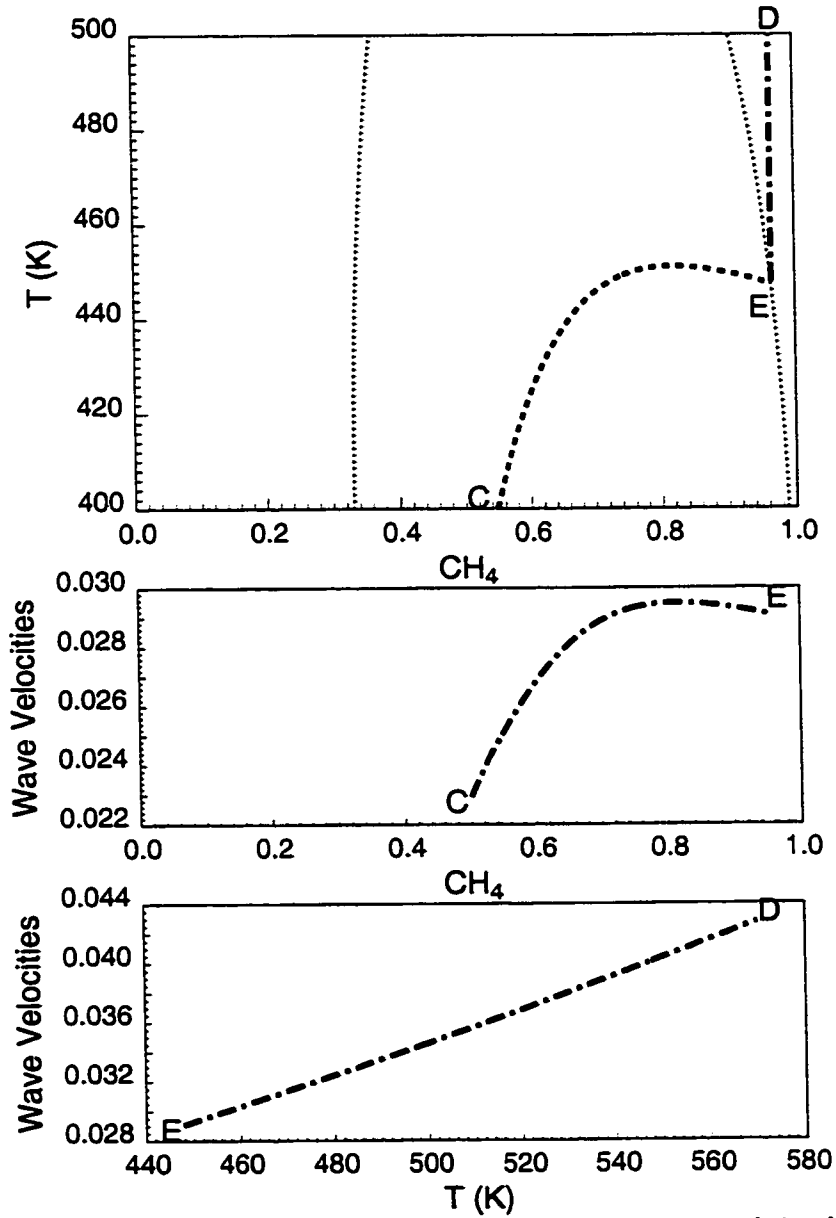


Figure 5.19: Switch between the continuous temperature path in the two-phase region and continuous temperature path in the single-phase region.

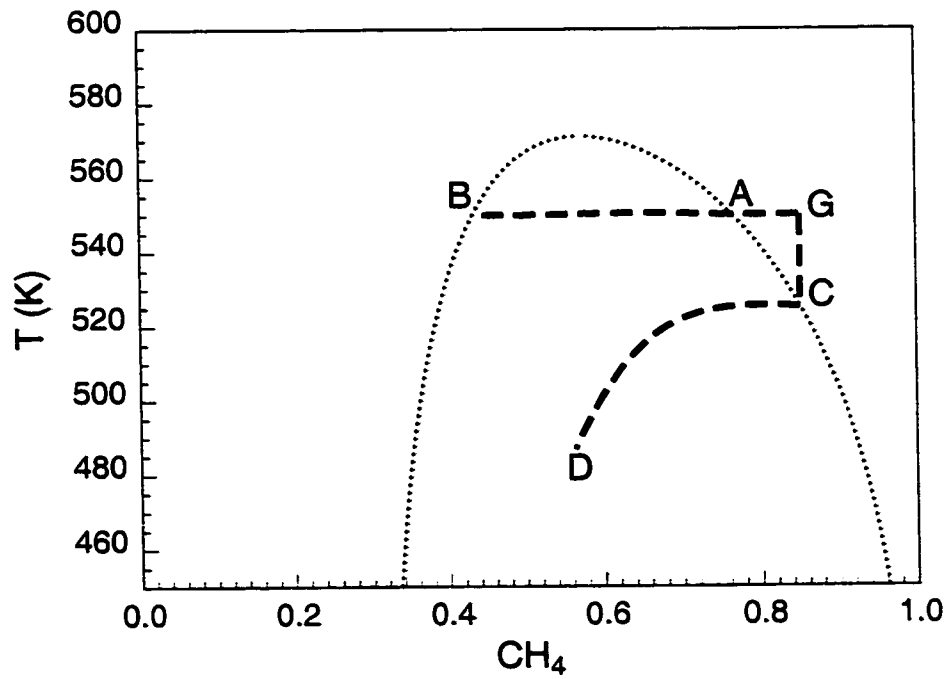


Figure 5.20: All possible landing points of discontinuous variation with one side of the shock at **G** in the single-phase region.

Similar locus can be obtained when the downstream end of the shock enters the two-phase region, shown as locus **BA** in Fig. 5.20. When the downstream end of the shock occurs on the locus **GA** and **AB**, the Rankine-Hugoniot condition is satisfied across the shock, and hence locus **GAB** is also called the Hugoniot locus.

Along locus **BA** the temperature is not constant. Figure 5.21 shows an expanded plot of the temperatures along the locus **BA**. The slight temperature difference across a near-isothermal phase-change shock is caused by the heat of vaporization or condensation. It can be explained with a simple experiment, where pure CH_4 and C_{10} initially at the same temperature are mixed at various ratios. When the mixtures arrive at a thermodynamic equilibrium, a phase equilibrium calculation shows that the combined mixtures are at slightly different temperatures, depending on the overall compositions. The final temperature is determined by the heat content of the individual components and the heat of mixing. Figure 5.22 shows that the temperature of the equilibrium mixture can vary substantially from the temperature of the initial mixtures when the flash calculation is performed holding the enthalpy constant.

The shock velocity remains constant as the downstream end of the shock moves along locus **GA**, and starts declining as it enters the two-phase region. A minimum in the phase-change shock velocity occurs as the downstream end of the phase-change shocks reaches **T** on locus **AB** (see Fig. 5.21).

Appendix A.1 shows that the temperature shocks in the single-phase region occur vertically with no composition variation. A Hugoniot locus in the single-phase region starting from **G** can be easily obtained as **GC** in Fig. 5.23. When the landing point of a temperature shock enters the two-phase region, both temperature and composition vary across the shock (see locus **CD** in Fig. 5.23). The temperature shock velocity decreases as the landing point of a temperature shock from **G** moves down along locus **GC**. Along locus **CD**, the temperature shock velocity first reaches a minimum value at **T**, and then starts increasing again as the locus is traced towards **D**.

The phase-change shock must satisfy the entropy condition. Along the locus for the landing points of all the possible phase-change shocks starting from single-phase mixture **G** (see Fig. 5.21 and Fig. 5.23), the Hugoniot locus, the shock satisfies the

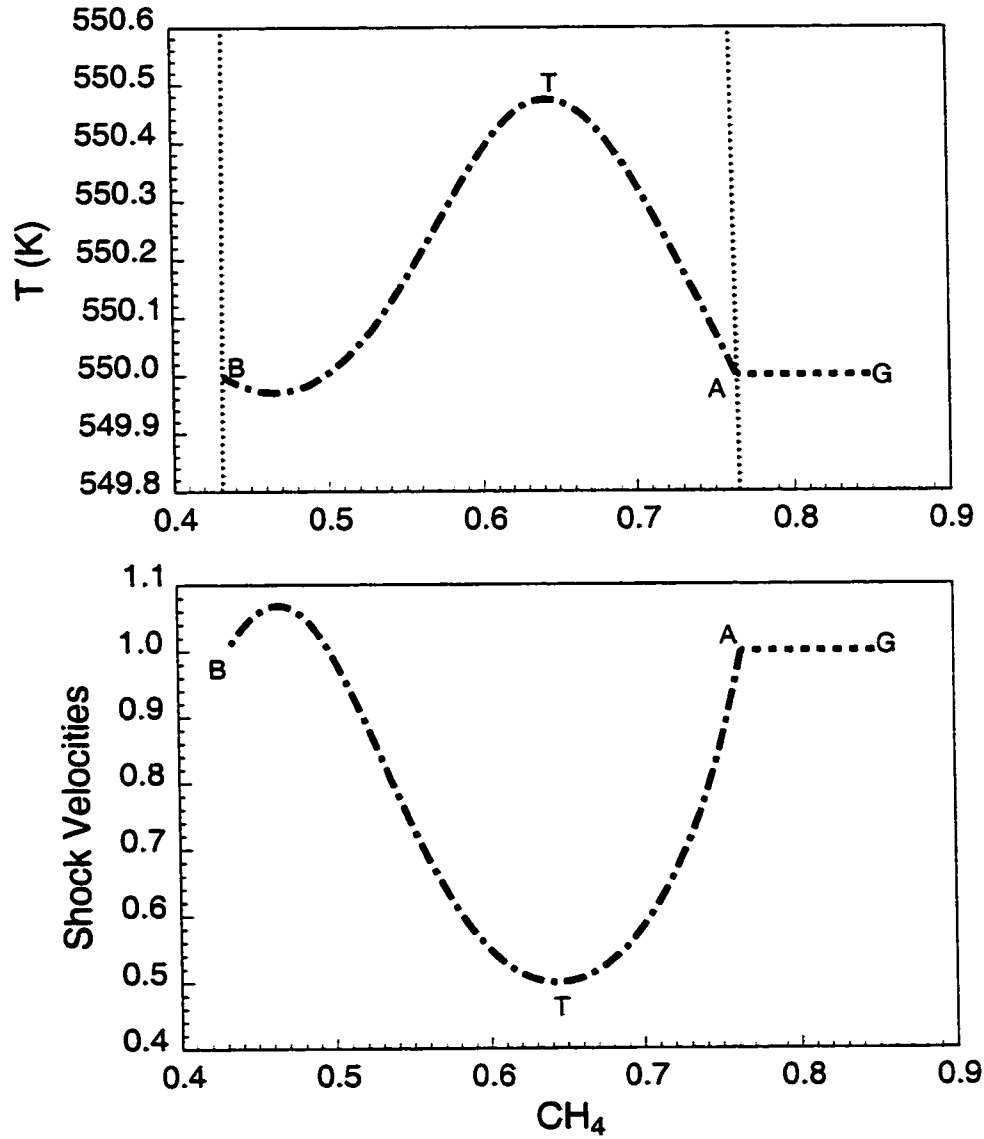


Figure 5.21: All possible landing points of the near isothermal trailing shocks from the injection composition and temperature at G.

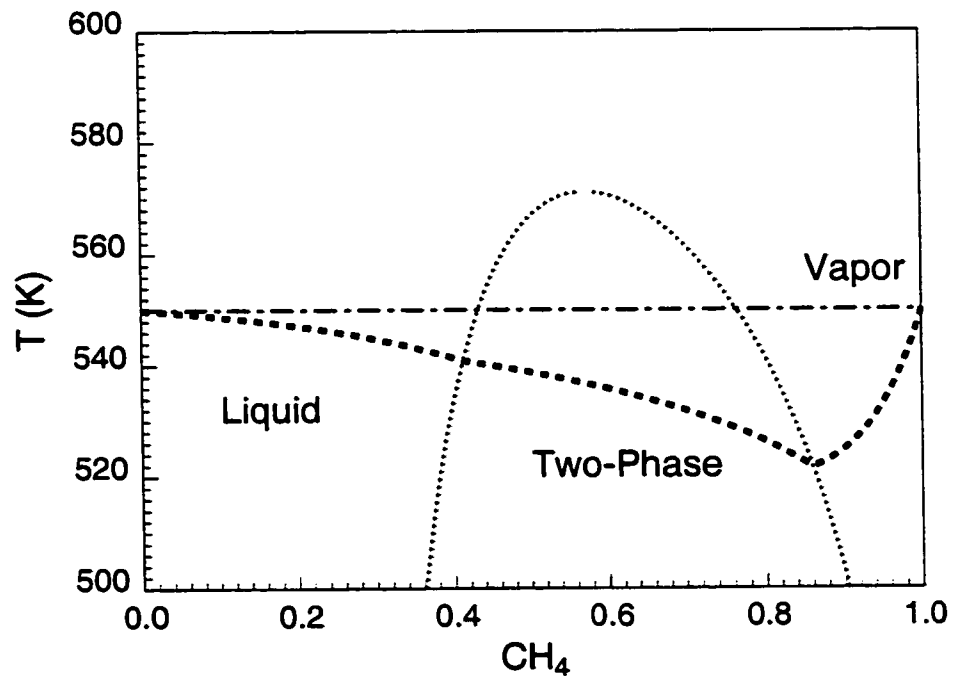


Figure 5.22: Mixing pure CH_4 and C_{10} at identical initial temperature, with no heat added or removed from the mixture, results in two-phase mixtures at slightly different temperature at phase equilibrium.

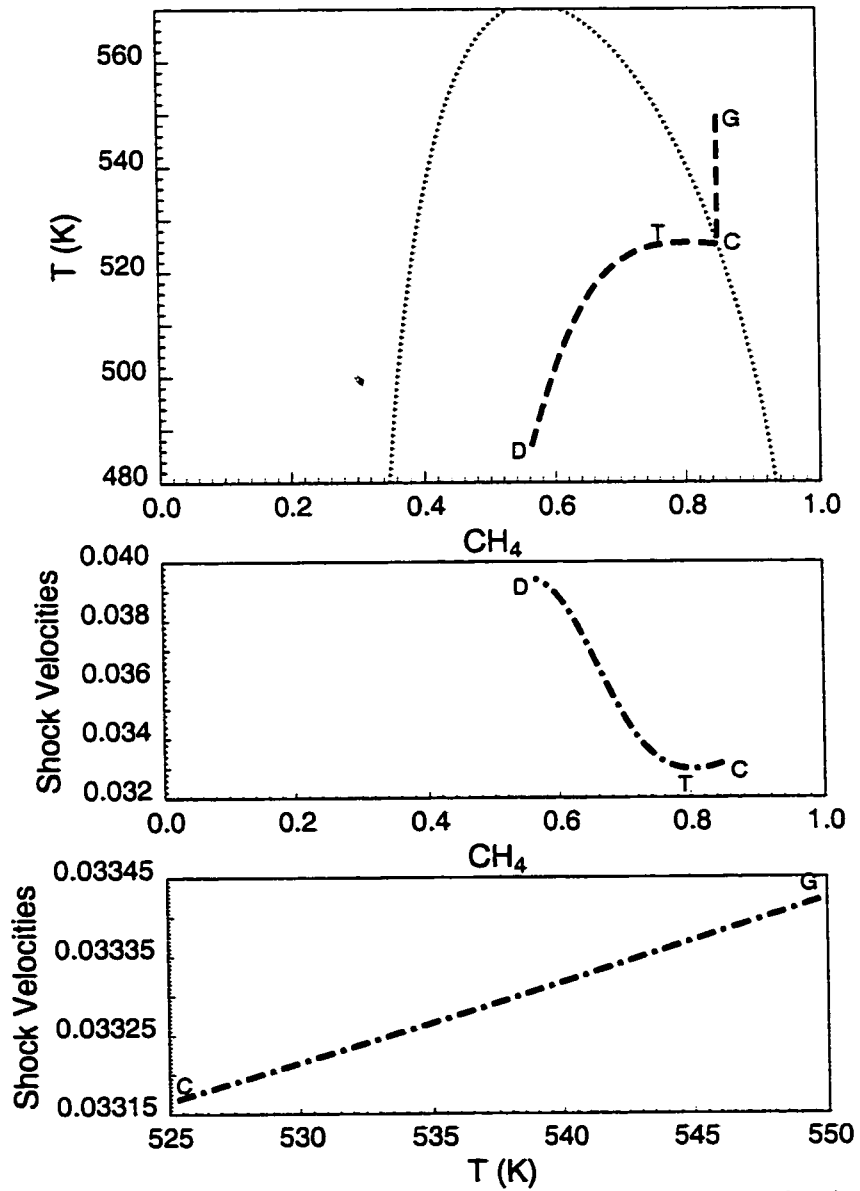


Figure 5.23: All possible landing points of the temperature shocks from the injection composition and temperature at G.

entropy condition if and only if the shock velocity satisfies

$$\Lambda((Z, T)^u, (Z, T)^d) \leq \Lambda((Z, T)^u, (Z, T)^T), \quad (5.29)$$

where the superscripts “ u ” and “ d ” represent upstream and downstream conditions of the shock, superscript “ T ” stands for an intermediate condition on the Hugoniot condition between “ u ” and “ d ”. Figures 5.21 and 5.23 illustrate the variation of shock velocity when the landing points of all phase-change shocks starting from \mathbf{G} trace along the Hugoniot locus. By a similar analysis of the entropy condition for the Buckley-Leverett equation, it is found that the entropy condition for the phase-change shock is satisfied if and only if the phase-change shock is a tangent shock (in which the shock velocity matches the eigenvalue for a continuous variation on one side of the shock), and has the minimum value along the Hugoniot locus as the upstream end of the phase-change shock is fixed in the single-phase region. Similar analysis can be applied to phase-change shocks where the downstream condition is fixed in the single-phase region. In that case, the phase-change shock that satisfies the entropy condition must have the upstream end on the Hugoniot locus and have the maximum shock velocity. The entropy condition is used to help us determine a unique landing point in the two-phase region when constructing a phase-change shock from a single-phase mixture \mathbf{G} (see Fig. 5.21 and Fig. 5.23).

5.4 Example Solutions

The solution paths for continuous variation in the single-phase region and two-phase region can be divided into nearly isothermal ones with only slight temperature effect due to latent heat, and ones with significant temperature variation. Similarly, the shock solutions in the single-phase region, two-phase region, and across the two-phase boundary can be categorized as nearly isothermal shocks and temperature shocks. In general, the continuous variations along temperature paths and temperature shocks travel slower than the continuous variations along isothermal paths and isothermal shocks (see Figs. 5.3, 5.12, 5.21 and 5.23), except when near an equal-eigenvalue point

the continuous variation along an isothermal path may be slower than the one along a temperature path, and an isothermal shock slower than a temperature shock.

In a gas injection problem, the initial oil is often a single-phase liquid and the injection gas a single-phase vapor. In the composition space, a solution path composed of continuous variation solutions and shock solutions in single-phase region, two-phase region, and across the two-phase boundary is needed for the composition and temperature to vary along between the upstream and downstream condition. In order for the velocity rule to be satisfied, the slower traveling solution segments, usually the ones with significant temperature difference, must stay upstream. Therefore, starting from the injection condition, the solution usually takes continuous variation along temperature paths or temperature shocks until the initial temperature is reached, and the rest of the solution path consists of fast moving continuous variation along isothermal paths or isothermal shocks. The solution construction procedure is discussed in more detail in this section.

In the first series of example solutions, we use a binary system of CH_4 and C_{10} , fix the injection mixture composition and temperature in the vapor phase region, and vary the temperature of the initial mixture that is in the liquid phase region. We begin with an example where the initial temperature is only slightly lower than that of the injection gas, and then lower the temperature of the initial mixture for subsequent examples. A variety of solution types is observed.

5.4.1 Solution Type I

In the first example, the temperature difference between the initial and injection mixtures is relatively small. The solution paths and profiles are summarized in Fig. 5.24. The compositions, temperature and propagation velocities at the key points on the profile are summarized in Table. 5.1. The solution consists of a leading tangent near-isothermal phase-change shock oa , where the other end of the shock a is located on an "initial" tie-line at a slightly higher temperature than the initial mixture. A continuous variation occurs along the initial tie-line between a and b . A tangent near-isothermal phase-change shock bc leads the state variables from the two-phase

Table 5.1: Analytical solution for binary displacement with temperature variation in $CH_4 - C_{10}$ system, where the initial oil consists of 100% C_{10} at 530 °K, and the injection gas 85% CH_4 and 15% C_{10} at 550°K.

Composition Label	Composition (Mole Fraction)		Temperature (°K)	Gas Saturation (Volume Fraction)	Wave Velocity (λ)
	CH_4	C_{10}			
<i>g</i>	0.8500	0.1500	550.000	1.0000	0.0000-0.0332
<i>c</i>	0.8500	0.1500	529.345	1.0000	0.0332-0.1424
<i>b</i>	0.7233	0.2767	529.899	0.8200	0.1424
<i>a</i>	0.5760	0.4240	529.899	0.5236	1.0381
<i>o</i>	0.0000	1.0000	530.000	0.0000	1.0381

region to the single-phase region at *c*, where mixture *c* has identical composition with that of the injection gas, and only slightly different temperature from that of the initial tie-line. Between *c* and the injection mixture *g* is a pure temperature shock *cg* in the single-phase region. For this example solution, the near-isothermal segments show small temperature variation and hence have higher propagation velocity for the state variables. The trailing pure temperature shock in the single-phase region, on the other hand, travels more slowly due to the heat absorption by the reservoir rock.

As we gradually lower the temperature of the initial mixture, the solution structure remains the same, except that the temperature of the initial tie-line becomes lower. The ending point of the trailing temperature shock in the single-phase region, *c*, also moves to a lower temperature. A critical case occurs when *c* arrives at the two-phase boundary. The solution paths and profiles for that special case are presented in Fig. 5.25. The compositions, temperatures and propagation velocities at the key points on the solution profile are summarized in Table. 5.2. Since the leading part of the solution remains largely the same as we vary the initial temperature, the difference in solution is primarily at the trailing temperature shock and trailing phase-change shock. In the following presentation of the solution paths and profiles, we concentrate on the upstream segments of the solution.

However, since *c* is on the two-phase boundary, a continuous temperature path *ce*

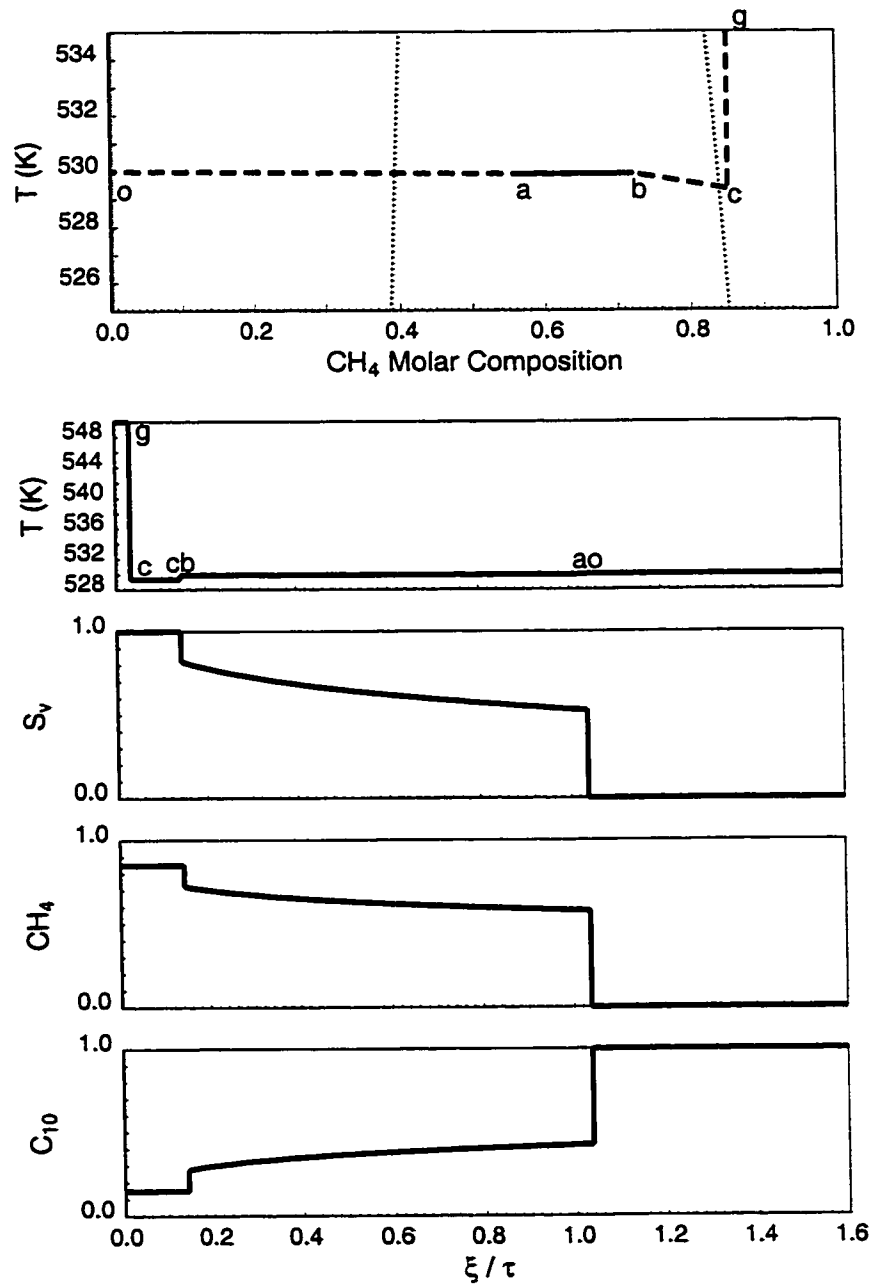


Figure 5.24: Solution paths and profile for Type I example, where the injection mixture is 85% CH_4 and 15% C_{10} at 550 °K, and the initial mixture is pure C_{10} at 530 °K. The trailing temperature shock is separated from the phase-change shock.

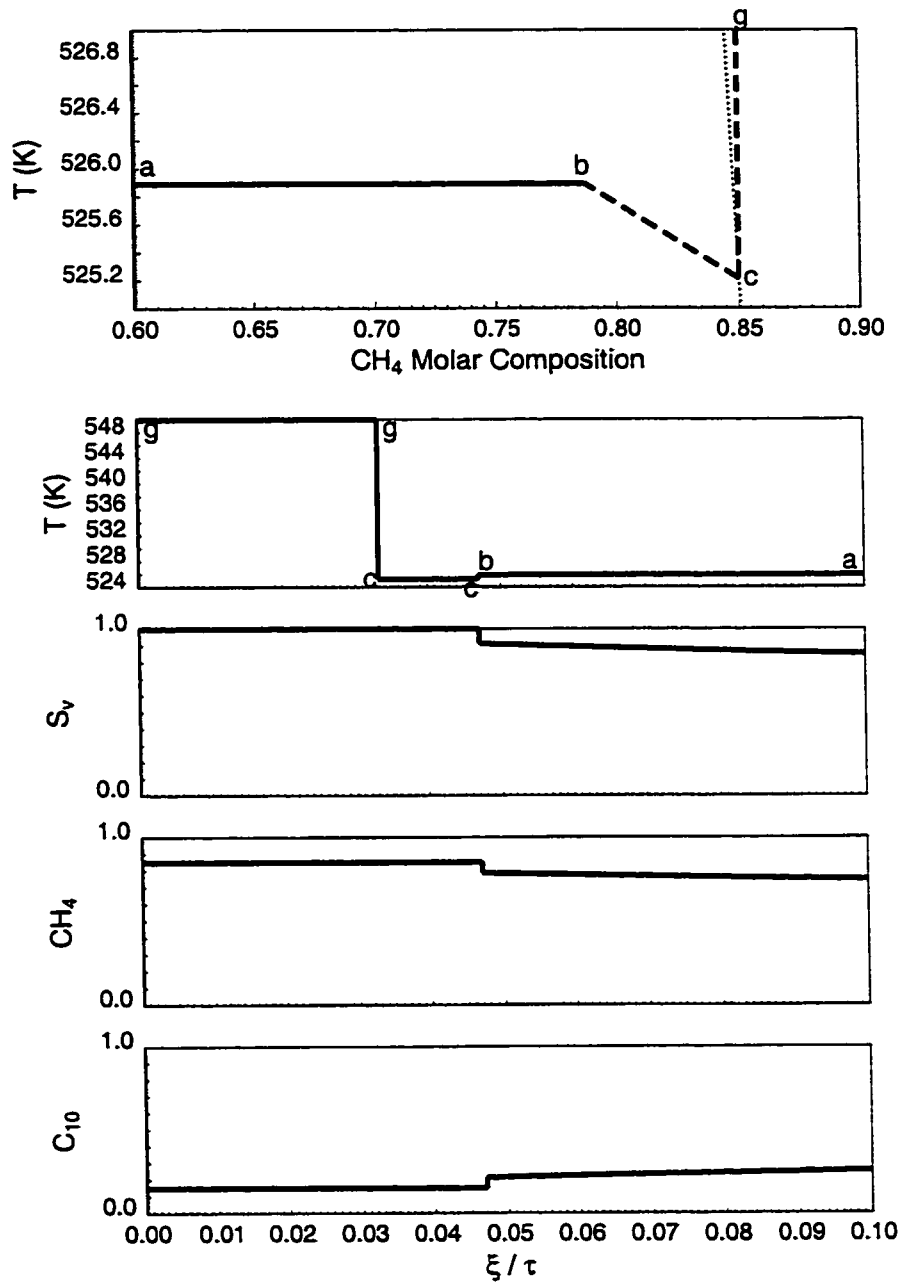


Figure 5.25: Solution paths and profile for the critical case between Type I and II, where the phase envelope is crossed by a phase-change shock that begins on the phase envelope. The injection mixture is 85% CH_4 and 15% C_{10} at 550 °K, and the initial mixture is pure C_{10} at 525.996 °K.

Table 5.2: Analytical solution for binary displacement with temperature variation in $CH_4 - C_{10}$ system, where the initial oil consists of 100% C_{10} at 525.996 °K, and the injection gas 85% CH_4 and 15% C_{10} at 550°K.

Composition Label	Composition (Mole Fraction)		Temperature (°K)	Gas Saturation (Volume Fraction)	Wave Velocity (λ)
	CH_4	C_{10}			
<i>g</i>	0.8500	0.1500	550.000	1.0000	0.0000-0.0332
<i>c</i>	0.8500	0.1500	525.212	1.0000	0.0332-0.0470
<i>b</i>	0.7873	0.2167	525.893	0.9126	0.0470
<i>a</i>	0.5711	0.4289	525.893	0.5127	1.0345
<i>o</i>	0.0000	1.0000	525.996	0.0000	1.0345

in the two-phase region goes through *c*, Fig. 5.26. Along the short temperature path segment *ce*, the propagation velocity for the state variables is rather indifferent to the change in temperature, and is hard to distinguish from that of the phase-change shock *cb*. The continuous variation along temperature path *ce* ends at an equal-eigenvalue point *e* on the initial tie line, which is also the same point *b* that the phase-change shock *cb* ends at.

Therefore, in the critical case, the near-isothermal phase-change shock transfer smoothly into a segment of continuous variation along the temperature path in the two-phase region. The critical case can be determined by constructing a temperature shock in the single phase region that originates from the injection mixture *g* and ends at the two-phase envelope at *C*, a continuous variation along temperature path *CE* to the equal-eigenvalue point *E*, a continuous variation along isothermal path *EA*, and a tangent leading phase-change shock *AO*. When the initial temperature is higher than that of the critical case, the solution is of Type I. Otherwise, the solution may belong to one of the solution types to be discussed in the following sections.

5.4.2 Solution Type II

If the temperature of the initial mixture is further reduced, the segment of continuous variation along temperature path in the two-phase region solution segment *ce* ends at

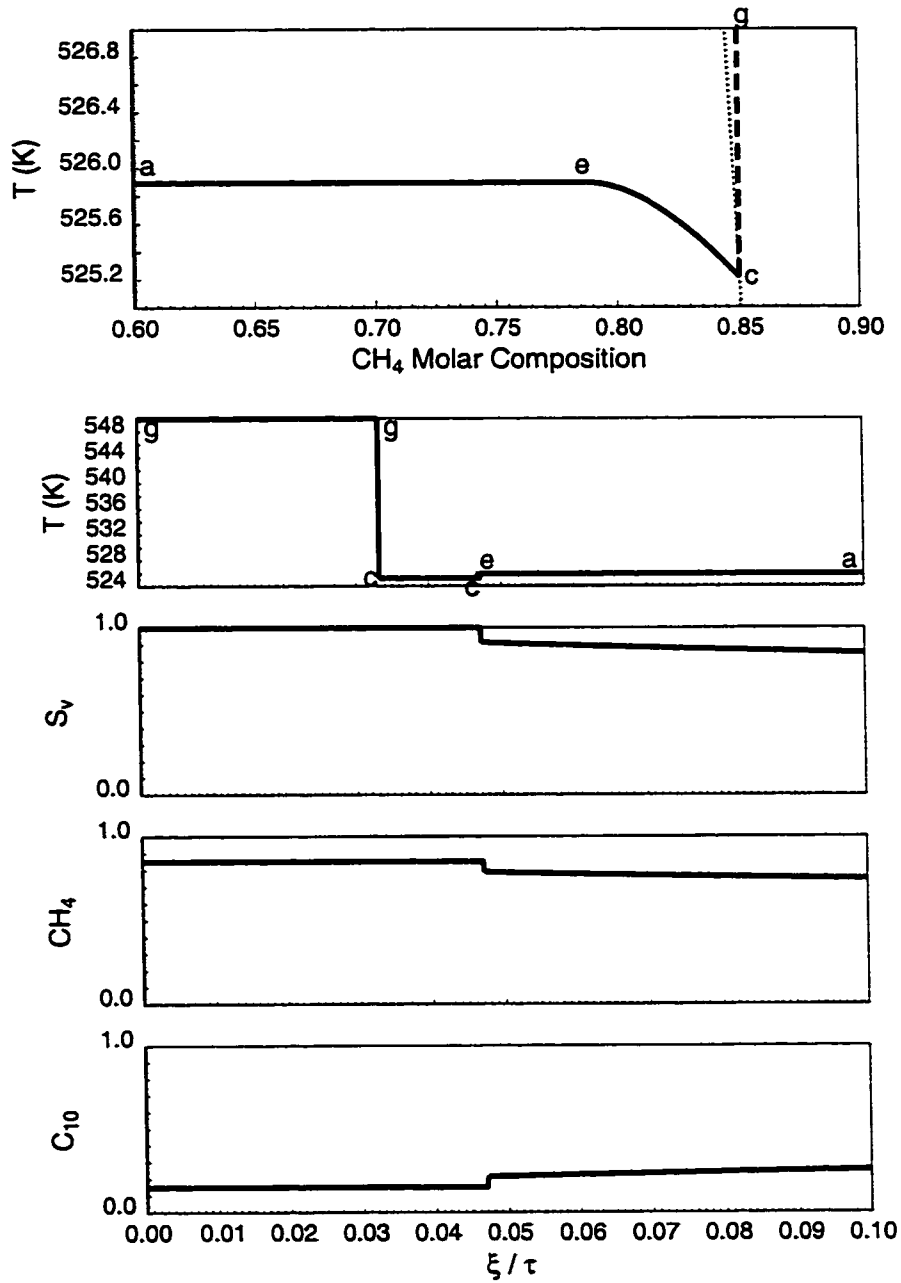


Figure 5.26: Solution paths and profile for the critical case between Type I and II, where the trailing temperature shock ends on the phase envelope and is followed by a continuous variation along temperature path. The injection mixture is 85% CH_4 and 15% C_{10} at 550 °K, and the initial mixture is pure C_{10} at 525.996 °K.

Table 5.3: Analytical solution for binary displacement with temperature variation in $CH_4 - C_{10}$ system, where the initial oil consists of 100% C_{10} at 525.900 °K, and the injection gas 85% CH_4 and 15% C_{10} at 550°K.

Composition Label	Composition (Mole Fraction)		Temperature (°K)	Gas Saturation (Volume Fraction)	Wave Velocity (λ)
	CH_4	C_{10}			
<i>g</i>	0.8500	0.1500	550.000	1.0000	0.0000-0.0331
<i>c</i>	0.8346	0.1654	525.391	0.9795	0.0331-0.0469
<i>e</i>	0.7874	0.2126	525.797	0.9124	0.0470
<i>a</i>	0.5710	0.4290	525.797	0.5124	1.0344
<i>o</i>	0.0000	1.0000	525.900	0.0000	1.0344

a point *c* in the interior of the two-phase region, where the temperature path intersects with the Hugoniot locus that originates from **G** (shown in Fig. 5.23). At *c*, there is a constant state, and a genuine phase-change shock *cg* leading to the injection mixture *g*, shown in Fig. 5.27. The compositions, temperatures and propagation velocities at the key points on the solution profile are summarized in Table. 5.3. The phase-change shock *gc* satisfies the entropy condition, Eq. 5.29, since the velocity of any intermediate shock that occurs between *g* and an intermediate state on the Hugoniot locus between *g* and *c* is higher than that of shock *gc*, as Fig. 5.23 illustrates.

For this type of solution, if we further reduce the temperature of the initial mixture, the solution structure remains the same except that the continuous variation segment *ec* become shorter, and point *c* moves up on the Hugoniot locus. A critical case occurs for an extreme case of Type II solutions when the ending point *c* of the continuous variation along temperature path *ec* arrives at the top of the Hugoniot locus, shown in Fig. 5.28. The compositions, temperatures and propagation velocities at the key points on the solution profile are summarized in Table. 5.4.

5.4.3 Solution Type III

If we further reduce the temperature of the initial mixture, instead of tracing the Hugoniot locus downwards, the ending point *c* remains at the same composition and

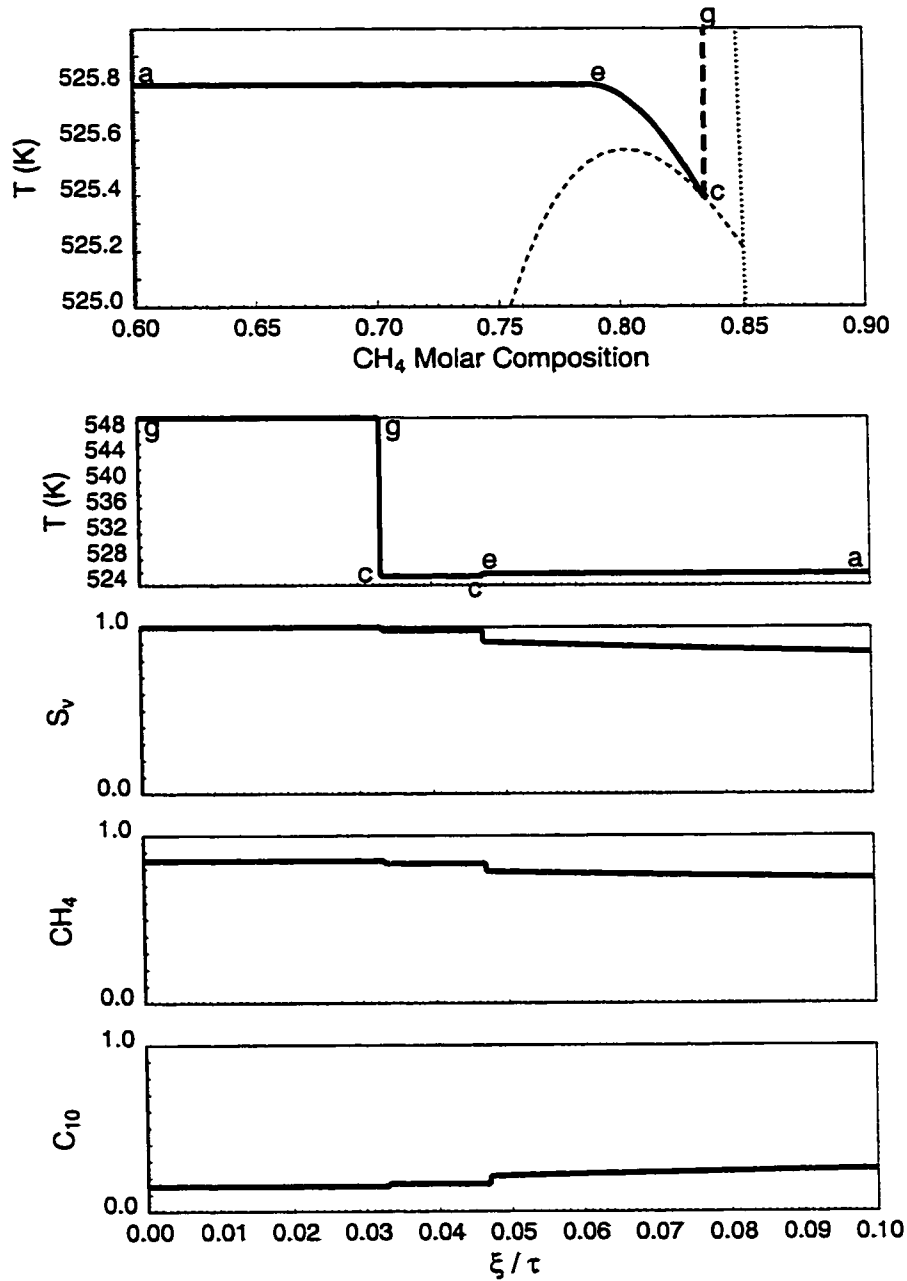


Figure 5.27: Solution paths and profile for a Type II example, where the injection mixture is 85% CH_4 and 15% C_{10} at 550 °K, and the initial mixture is pure C_{10} at 525.900 °K. The trailing temperature shock combines with the genuine trailing phase-change shock, and is followed by a continuous variation along temperature path.

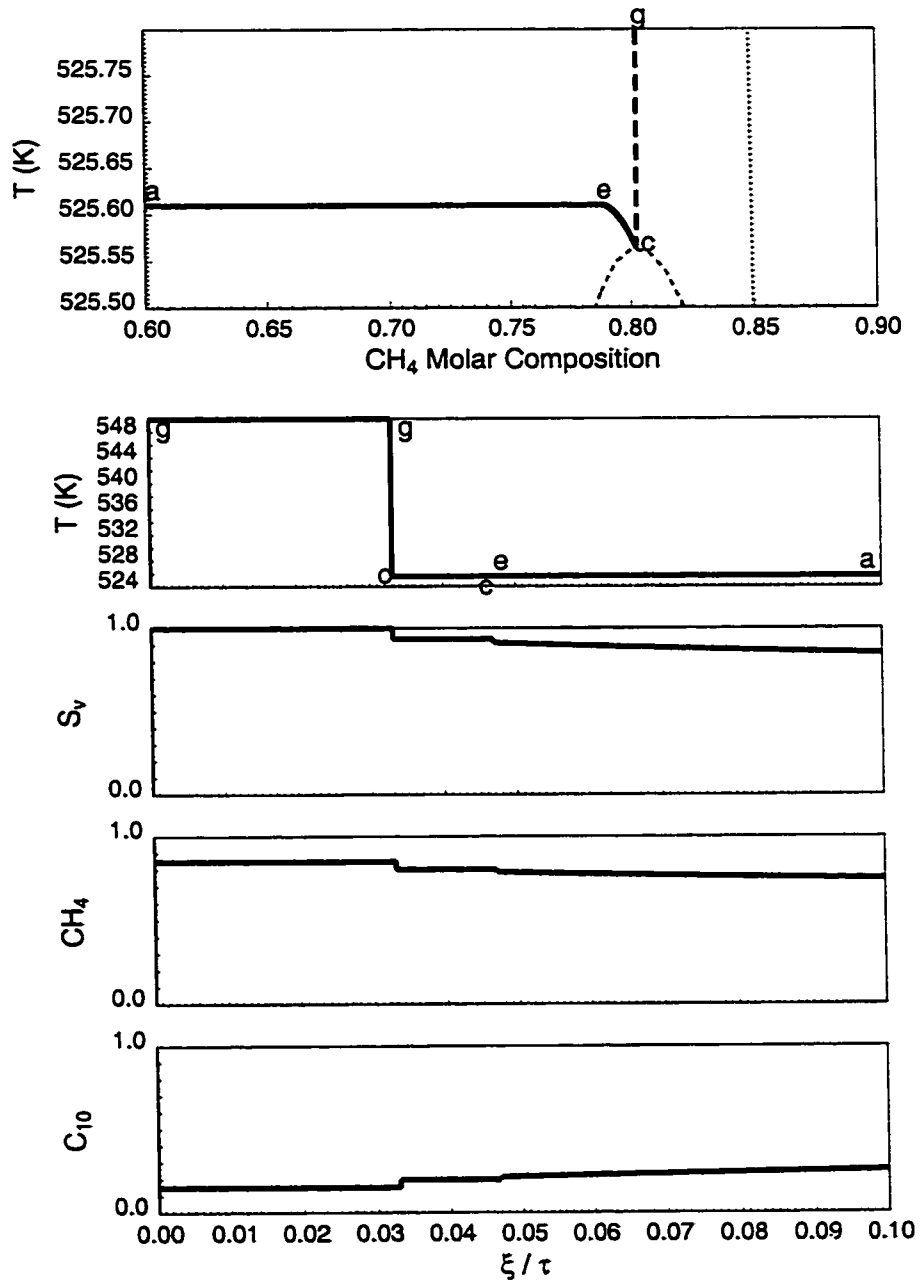


Figure 5.28: Solution paths and profile for the critical case between Type II and III, where the injection mixture is 85% CH_4 and 15% C_{10} at 550 °K, and the initial mixture is pure C_{10} at 525.713 °K. The trailing temperature shock combines with a tangent phase-change shock, and is followed by a continuous variation along temperature path to the “initial” tie line.

Table 5.4: Analytical solution for binary displacement with temperature variation in $CH_4 - C_{10}$ system, where the initial oil consists of 100% C_{10} at 525.713 °K, and the injection gas 85% CH_4 and 15% C_{10} at 550°K.

Composition Label	Composition (Mole Fraction)		Temperature (°K)	Gas Saturation (Volume Fraction)	Wave Velocity (λ)
	CH_4	C_{10}			
<i>g</i>	0.8500	0.1500	550.000	1.0000	0.0000-0.0330
<i>c</i>	0.8024	0.1976	525.563	0.9339	0.0330-0.0469
<i>e</i>	0.7877	0.2123	525.610	0.9123	0.0469
<i>a</i>	0.5708	0.4292	525.610	0.5119	1.0342
<i>o</i>	0.0000	1.0000	525.713	0.0000	1.0342

temperature. If a phase-change shock is constructed between the injection mixture *g* and a point on the Hugoniot locus to the left of the peak, then the inequality in entropy condition Eq. 5.29 is violated since shock between *g* and the peak of the Hugoniot locus *c* (see Fig. 5.23 and Fig. 5.28) is an intermediate shock and has a minimum shock velocity.

The continuous variation along the temperature path in the two-phase region starts from the equal-eigenvalue point *e* on the initial tie-line. However, it ends at a point *d* on an isothermal path that is tangent to the Hugoniot locus at *c*. Between *c* and *b* is a segment of continuous variation along tie-line, (see Fig. 5.29). The compositions, temperatures and propagation velocities at the key points on the solution profile are summarized in Table. 5.5.

When the temperature of the initial mixture is further reduced, the segment of continuous variation along the temperature path *ed* becomes shorter, and it disappears when the initial tie-line temperature arrives at the same temperature as that of *c*. For this critical case, the solution consists of a near-isothermal leading phase-change shock *oa*, a continuous variation along tie line *ac*, and a trailing phase-change shock *cg* (see Fig. 5.30 and Table. 5.6).

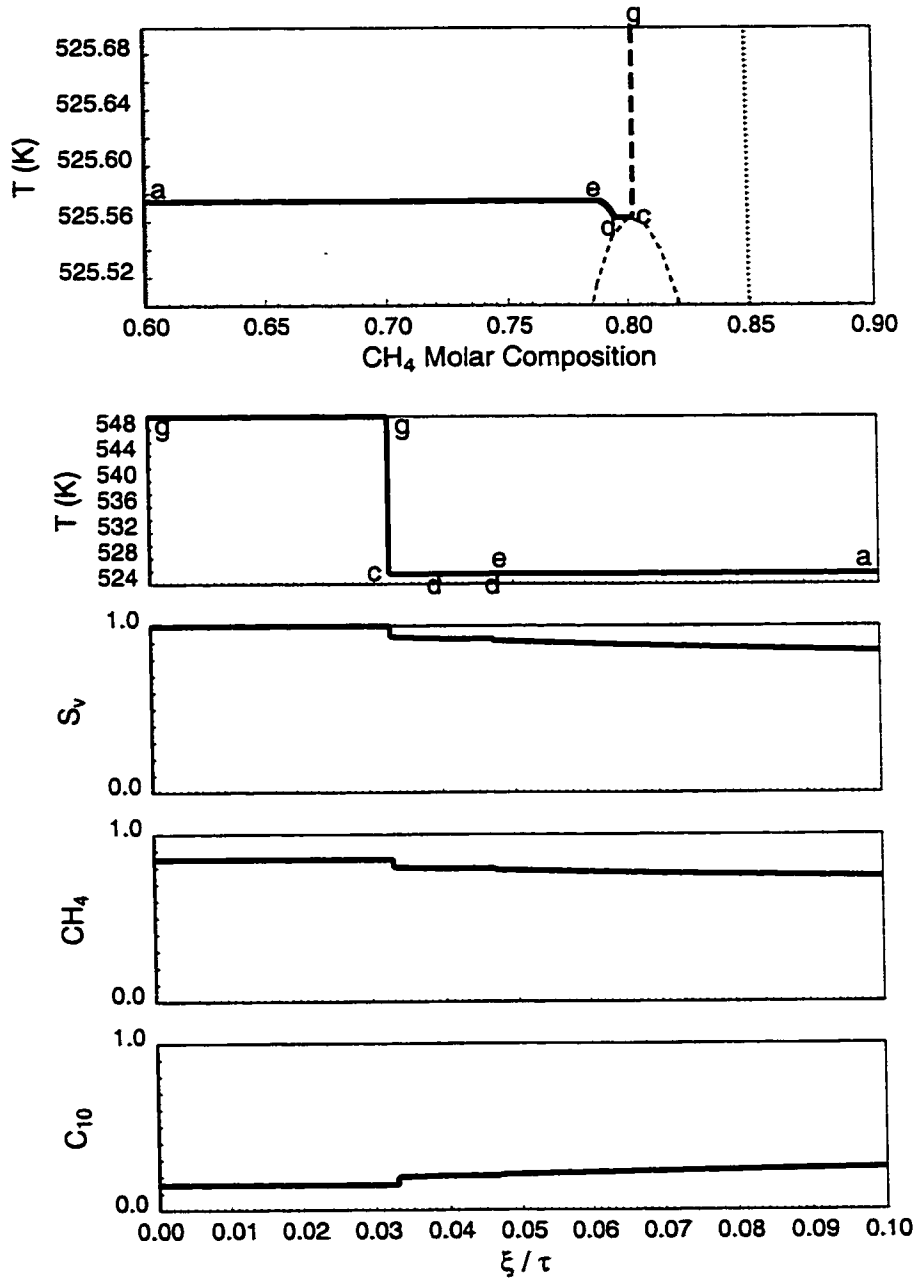


Figure 5.29: Solution paths and profile for a Type III example, where the injection mixture is 85% CH_4 and 15% C_{10} at 550 °K, and the initial mixture is pure C_{10} at 525.678 °K. The trailing temperature shock combines with the tangent trailing phase-change shock, and is followed by a continuous variation along an intermediate tie line, then a switch to temperature path to the “initial” tie line.

Table 5.5: Analytical solution for binary displacement with temperature variation in $CH_4 - C_{10}$ system, where the initial oil consists of 100% C_{10} at 525.678 °K, and the injection gas 85% CH_4 and 15% C_{10} at 550°K.

Composition Label	Composition (Mole Fraction)		Temperature (°K)	Gas Saturation (Volume Fraction)	Wave Velocity (λ)
	CH_4	C_{10}			
<i>g</i>	0.8500	0.1500	550.000	1.0000	0.0000-0.0330
<i>c</i>	0.8024	0.1976	525.563	0.9339	0.0330
<i>d</i>	0.7950	0.2050	525.563	0.9230	0.0398-0.0469
<i>e</i>	0.7877	0.2123	525.575	0.9124	0.0469
<i>a</i>	0.5708	0.4292	525.575	0.5118	1.0342
<i>o</i>	0.0000	1.0000	525.678	0.0000	1.0342

Table 5.6: Analytical solution for binary displacement with temperature variation in $CH_4 - C_{10}$ system, where the initial oil consists of 100% C_{10} at 525.666 °K, and the injection gas 85% CH_4 and 15% C_{10} at 550°K.

Composition Label	Composition (Mole Fraction)		Temperature (°K)	Gas Saturation (Volume Fraction)	Wave Velocity (λ)
	CH_4	C_{10}			
<i>g</i>	0.8500	0.1500	550.000	1.0000	0.0000-0.0330
<i>c</i>	0.8024	0.1976	525.563	0.9339	0.0330
<i>a</i>	0.5707	0.4293	525.563	0.5118	1.0342
<i>o</i>	0.0000	1.0000	525.666	0.0000	1.0342

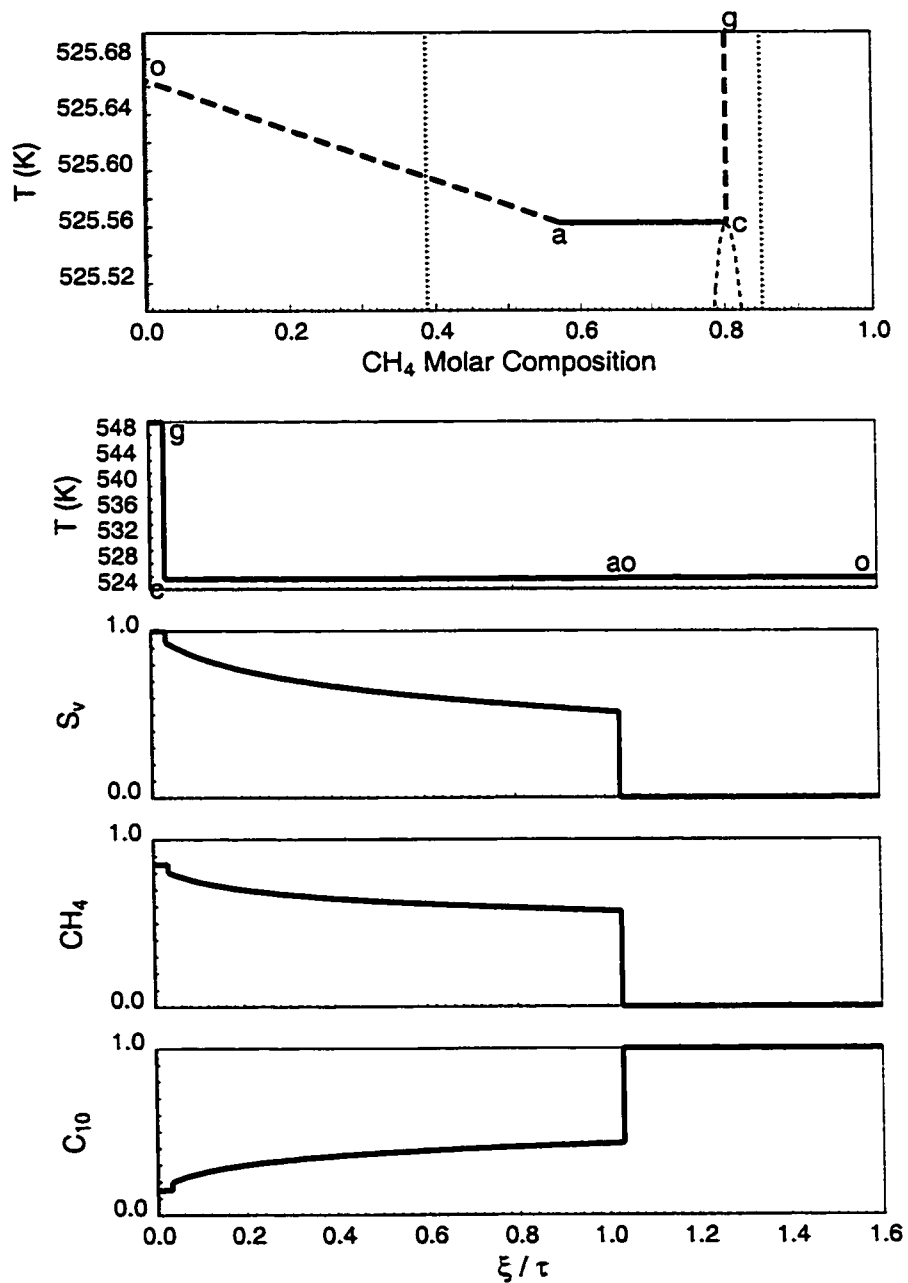


Figure 5.30: Solution paths and profile for the critical case between Type III and IV, where the injection mixture is 85% CH_4 and 15% C_{10} at 550 °K, and the initial mixture is pure C_{10} at 525.666 °K. The trailing temperature shock combines with a tangent phase-change shock, and is followed by a continuous variation along the “initial” tie line.

Table 5.7: Analytical solution for binary displacement with temperature variation in $CH_4 - C_{10}$ system, where the initial oil consists of 100% C_{10} at 500.000 °K, and the injection gas 85% CH_4 and 15% C_{10} at 550°K.

Composition Label	Composition (Mole Fraction)		Temperature (°K)	Gas Saturation (Volume Fraction)	Wave Velocity (λ)
	CH_4	C_{10}			
<i>g</i>	0.8500	0.1500	550.000	1.0000	0.0000-0.0330
<i>c</i>	0.8024	0.1976	525.563	0.9339	0.0330
<i>u</i>	0.7902	0.2098	525.563	0.9158	0.0444
<i>d</i>	0.5933	0.4067	499.902	0.5551	0.0444-0.5290
<i>a</i>	0.5385	0.4615	499.902	0.4476	1.0151
<i>o</i>	0.0000	1.0000	500.000	0.0000	1.0151

5.4.4 Solution Type IV

When the initial tie-line temperature is lower than that of *c* in the last critical case, the temperature difference between the two must be taken by a shock between the two tie lines in order for the velocity rule to be satisfied, as Fig. 5.31 and Table. 5.7 show. Therefore, the temperature difference between the initial and injection mixtures is broken into two primary sections, one that occurs across the trailing phase-change shock, and the other across the temperature shock between two tie lines in the two-phase region. These two temperature shocks are connected by a continuous variation along an isothermal path *cu* in the two-phase region.

5.4.5 Finite-Difference Simulation

A single-point upstream-weighted finite-difference simulator was developed to solve the gas injection problems with temperature variation in an one-dimensional model. Results were obtained with 5000 grid blocks in the model. For the Type I example, the finite-difference simulation results are in good agreement with the solution paths and profiles obtained from the analytical method. Figure 5.32 shows the comparison. With this grid resolution, there is very little difference between the solutions.

For the Type IV example, the finite-difference solution shows significant effects of

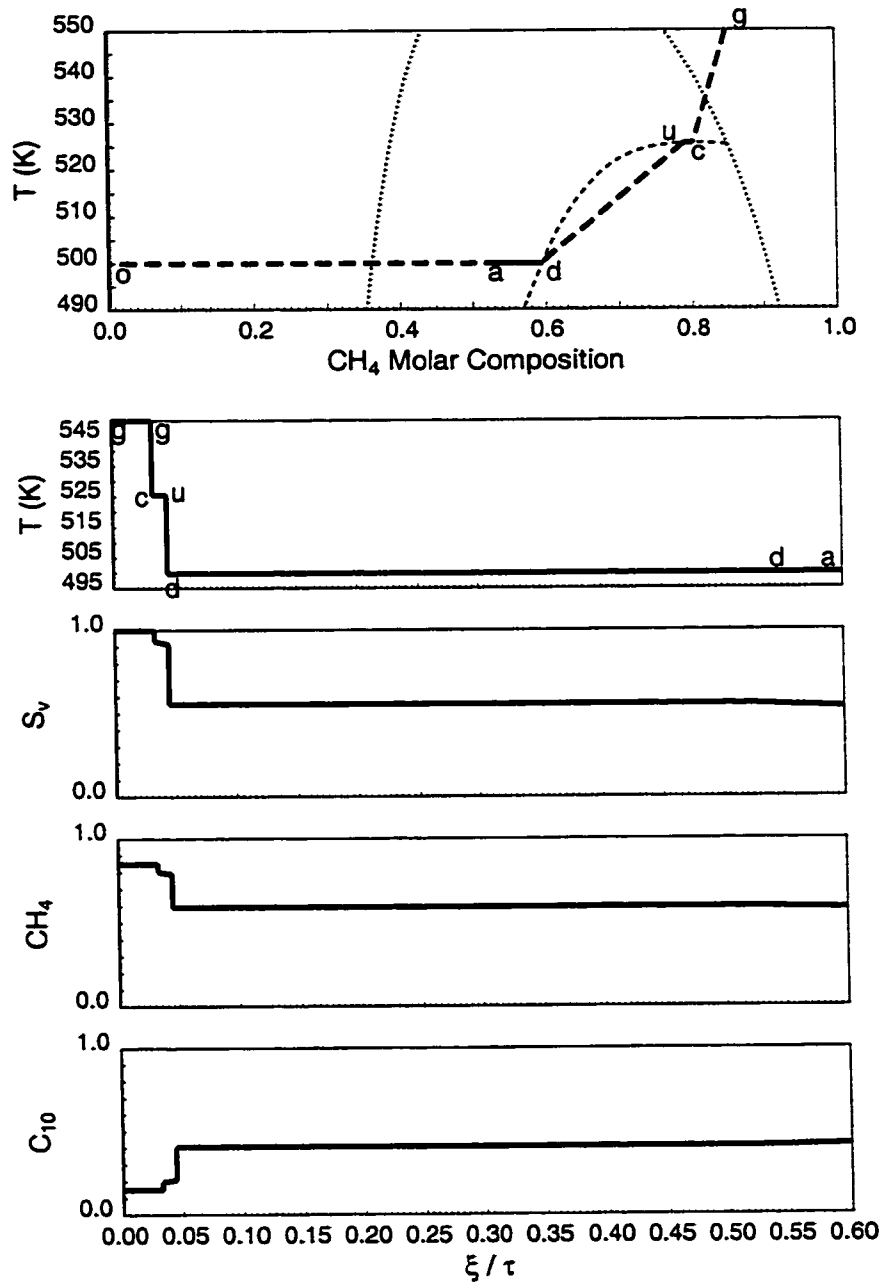


Figure 5.31: Solution paths and profile for a Type IV example, where the injection mixture is 85% CH_4 and 15% C_{10} at 550 °K, and the initial mixture is pure C_{10} at 500.000 °K. The trailing temperature shock combines with the tangent trailing phase-change shock, and is followed by a continuous variation along an intermediate tie line, then a nontie-line shock to the “initial” tie line.

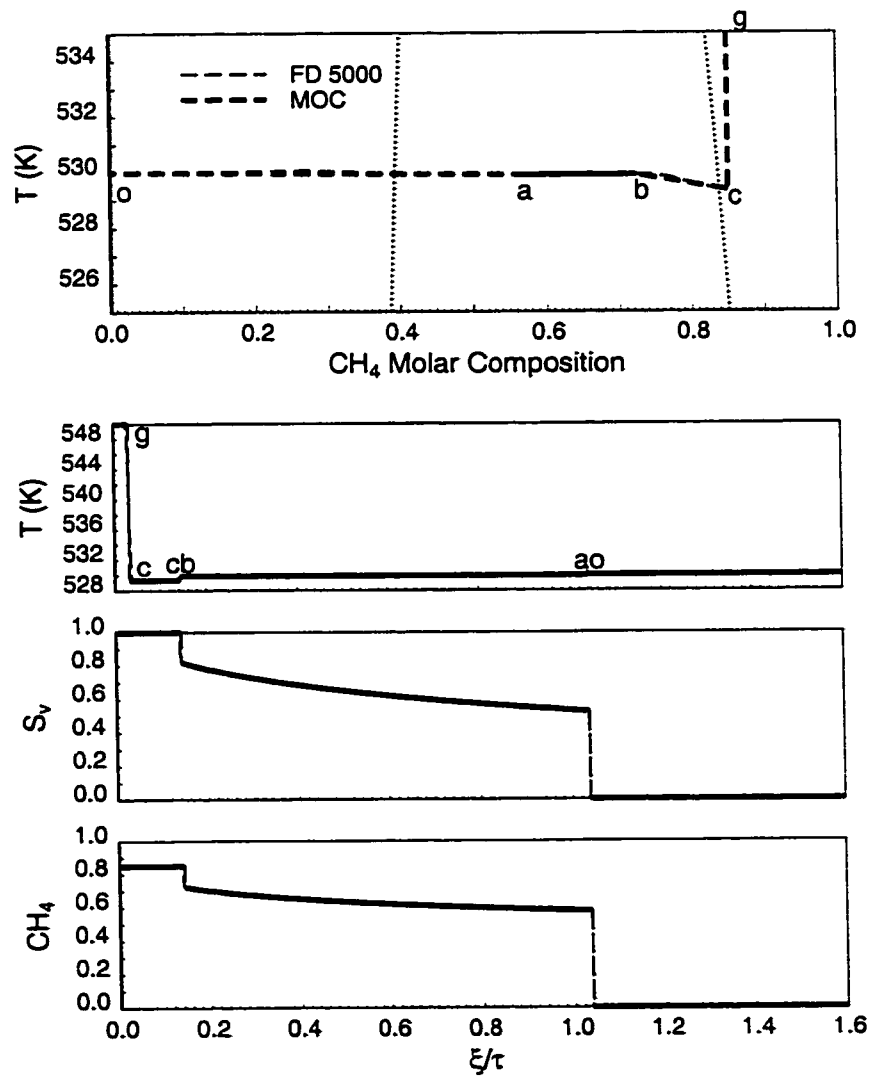


Figure 5.32: Comparison of finite-difference solution and analytical solution for Type I example.

numerical dispersion (Fig. 5.33). Especially, the trailing temperature phase-change shock gc and the nontie-line shock ud in the two-phase region are affected significantly. Instead of discontinuous change in temperature and composition across these two shocks, the variation becomes continuous and follows the continuous temperature paths. However, in the solution profiles, the shock fronts are well preserved, since along the continuous temperature paths, the propagation velocities are rather indifferent to the changes in temperature and compositions.

For the other examples with intermediate initial temperatures between the Type I and Type IV examples, the subtle differences in the analytical solutions due to the change in initial condition are inundated by the numerical dispersion effect and hard to observe in output of the finite-difference simulation. The effect of numerical dispersion is more significant when fewer grid blocks are used in the simulation. For a finite-difference simulation with 5000 grid blocks, the CPU time needed for each simulation run is in the order of hours, while the analytical approach takes a fraction of a second using an identical computer set-up.

5.4.6 Effect of Rock Heat Capacity

Rock heat capacity determines the amount of heat absorbed or released to the surrounding fluids, given a temperature difference between the reservoir rock and the reservoir fluids. Especially along the temperature paths, the propagation velocity of the composition and temperature is affected significantly by the rock heat capacity through the expression of temperature eigenvalues, as shown in Eqs. 4.8, 5.4 and A.34, and through the expression for the velocity of temperature shocks, shown in Eqs. 4.14 and 5.16, as the rock heat capacity participates in the heat concentration terms.

The effect of rock heat capacity is illustrated through a series of examples where the initial and injection mixtures are fixed and identical as the Type I example presented above. The variation of the rock heat capacity has a more significant effect on the temperature solution segments, such as the trailing temperature shock in the single-phase region, temperature phase-change shock and continuous variation along

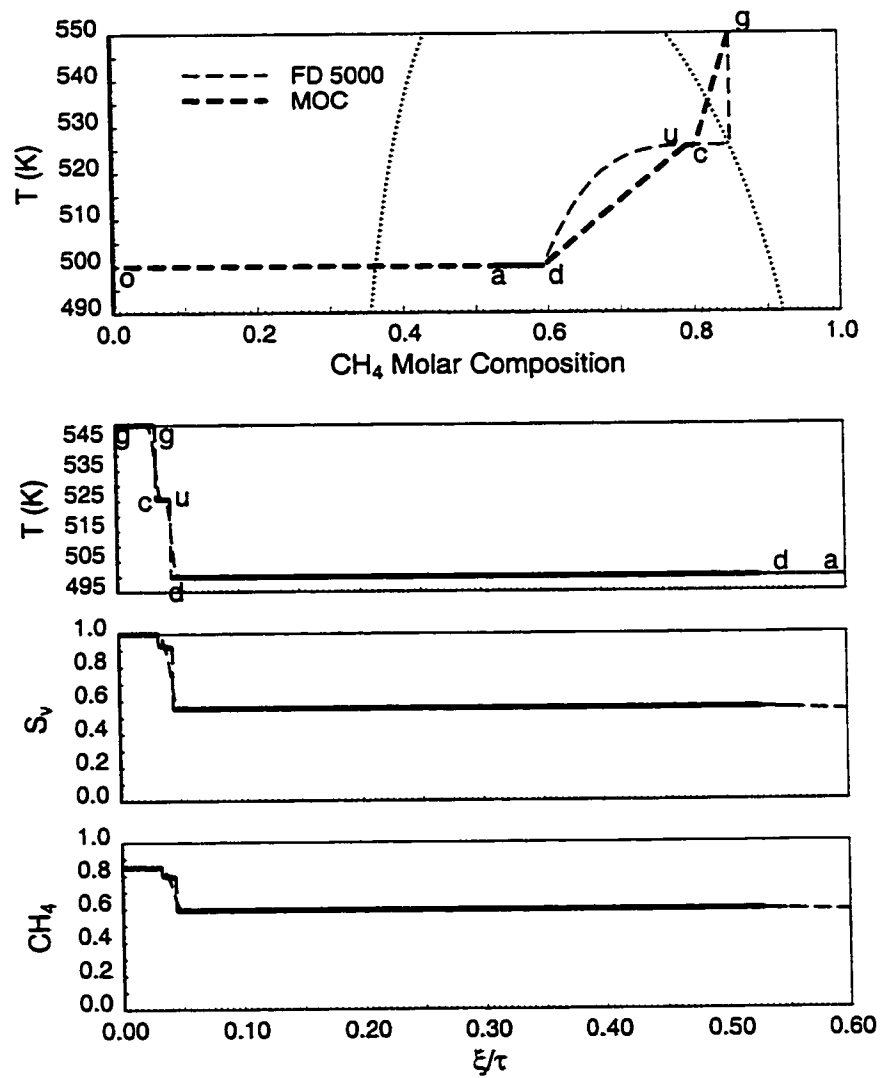


Figure 5.33: Comparison of finite-difference solution and analytical solution for Type IV example.

temperature paths in the two-phase region, than on the isothermal solution segments, such as the isothermal phase-change shock and continuous variation along tie line in the two-phase region. When the rock heat capacity is reduced gradually, very little change in the leading and trailing isothermal phase-change shocks is observed, when the shock velocities are normalized by the local flow velocity. The trailing temperature shock in the single-phase region, however, travels much faster at lower rock heat capacity. Figure 5.34 shows that when the rock heat capacity is reduced to the 1/10 of its original value, the trailing temperature shock *gc* has a higher velocity than the trailing isothermal phase-change shock *cb*. That would be a violation of the velocity rule that results in a multi-valued solution, as the profiles of Fig. 5.34 show.

To resolve the violation of the velocity rule, instead of constructing a trailing temperature shock that ends near the initial tie-line temperature, we end the trailing temperature shock *gc* at a higher intermediate temperature, and from this intermediate state *c* construct an isothermal phase-change shock into the two-phase region, landing at an intermediate tie line. Now that, state *c* is further away from the two-phase boundary, resulting in higher velocity of the trailing isothermal phase-change shock. State *c* is completely determined when shocks *gc* and *cb* have the same velocity and merge as one single shock, as shown in Fig. 5.35 and Table. 5.8. From *b*, there is a segment of continuous variation *bu* along tie line, followed by a nontie-line shock *ud* leading to the initial tie line, a tie line rarefaction *da* and a leading isothermal phase-change shock *ao*. As a result, due to the decreased rock heat capacity, the Type I example demonstrated a Type IV example solution.

5.4.7 Effect of Injection Gas Solubility

Through the example solutions in the CH_4-C_{10} binary system, it can be observed that varying the temperature of the initial mixture causes very little change to the solution structure for the downstream section, which remains to be composed of a leading tangent phase-change shock between the interior of the two-phase region and the initial mixture, and a continuous variation along the “initial” tie line. But the relative position of the injection mixture to the “initial” tie line in the composition

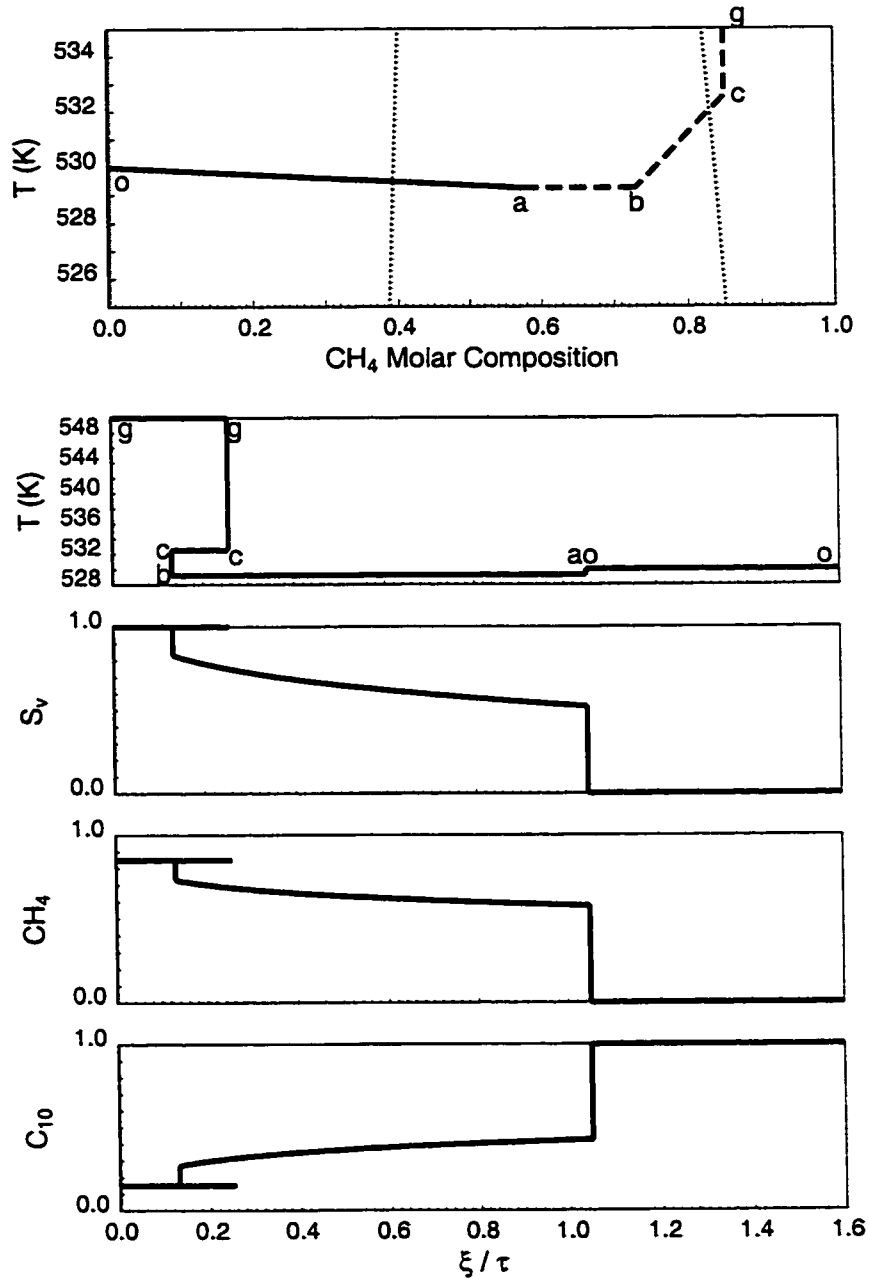


Figure 5.34: Type I example with rock heat capacity reduced to 1/10 of its original value. The temperature shock gc travels faster than the phase-change shock cb downstream, and hence violates the velocity rule.

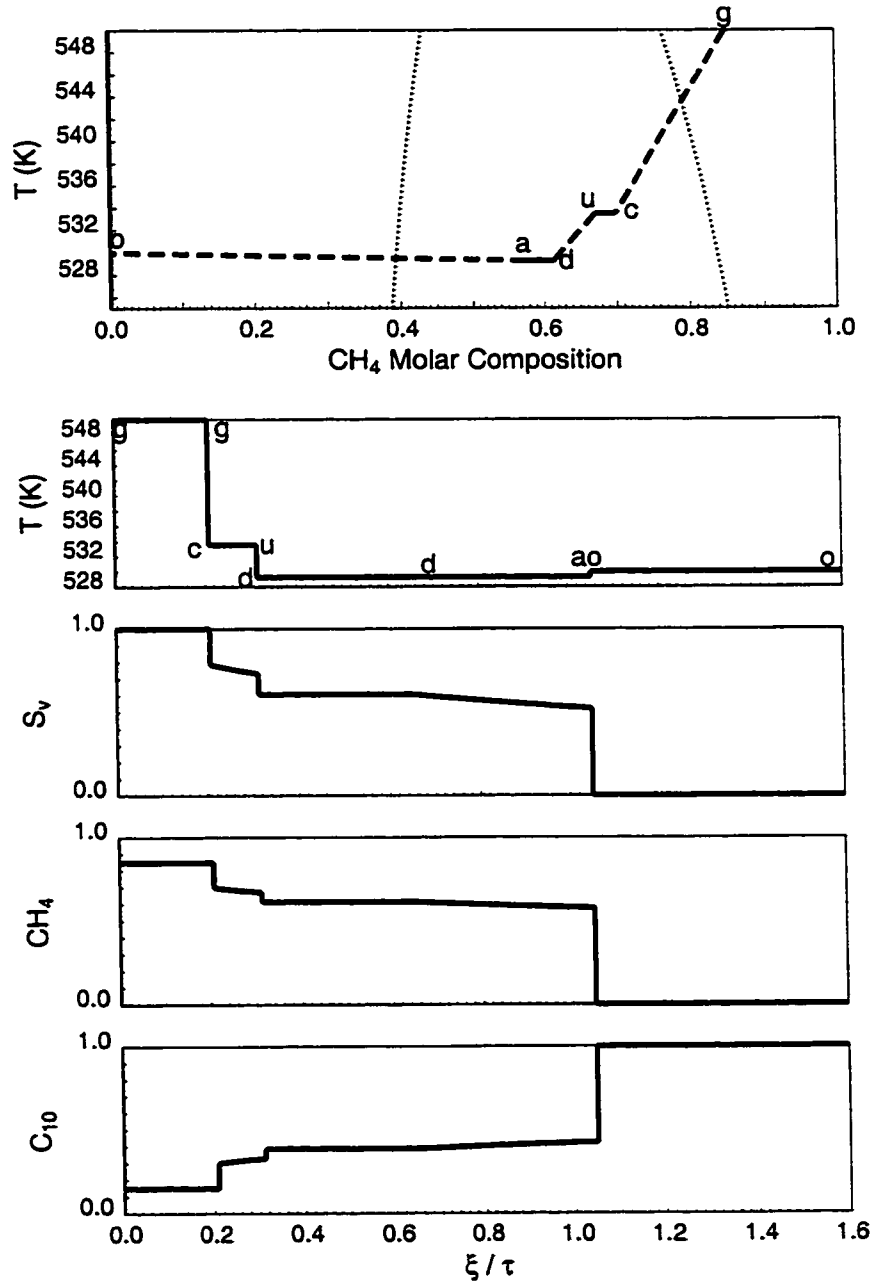


Figure 5.35: Correct solution construction for the Type I example with rock heat capacity reduced to 1/10 of its original value.

Table 5.8: Analytical solution for Type I example with rock heat capacity reduced to 1/10 of its original value.

Composition Label	Composition (Mole Fraction)		Temperature ($^{\circ}K$)	Gas Saturation (Volume Fraction)	Wave Velocity (λ)
	CH_4	C_{10}			
<i>g</i>	0.8500	0.1500	550.000	1.0000	0.0000-0.2083
<i>c</i>	0.6987	0.3013	533.491	0.7850	0.2083
<i>u</i>	0.6707	0.3293	533.491	0.9158	0.3139
<i>d</i>	0.6134	0.3866	529.250	0.6068	0.3139-6506
<i>a</i>	0.5752	0.4248	529.250	0.5218	1.0493
<i>o</i>	0.0000	1.0000	530.000	0.0000	1.0493

space is altered significantly, which determines the solution segments upstream that connect the injection mixture with the interior of the two-phase region. When the injection mixture is cooled to a temperature around the “initial” tie line due to heat loss to the reservoir rock, the distance between this point and the two-phase boundary measures the solubility of the injection gas, and determines the solution structure for upstream segments. This idea can be better illustrated through the following examples, where we fix the initial composition and temperature and the injection temperature. By varying the injection composition only, we have more direct control of the solubility of the injection gas.

Example solutions are reported for a binary system of CO_2 and C_{16} . The pressure remains at 11.03 MPa. The initial oil is pure C_{16} at 600 $^{\circ}K$. The injection gas is a single-phase mixture of CO_2 and C_{16} at 650 $^{\circ}K$. The temperatures are relatively high so that in the example solutions a good range of solubility of the injection gas is available. For each of the following examples, we change the injection gas composition such that it moves towards the two-phase boundary in the composition space.

Figure 5.36 shows an example of a Type I solution. For this type of solution, if the injection gas composition is slightly more enriched with the heavy component while retaining the same temperature, the intermediate mixture represented by *c* will move closer to the two-phase boundary, resulting in a slightly faster “near” isothermal

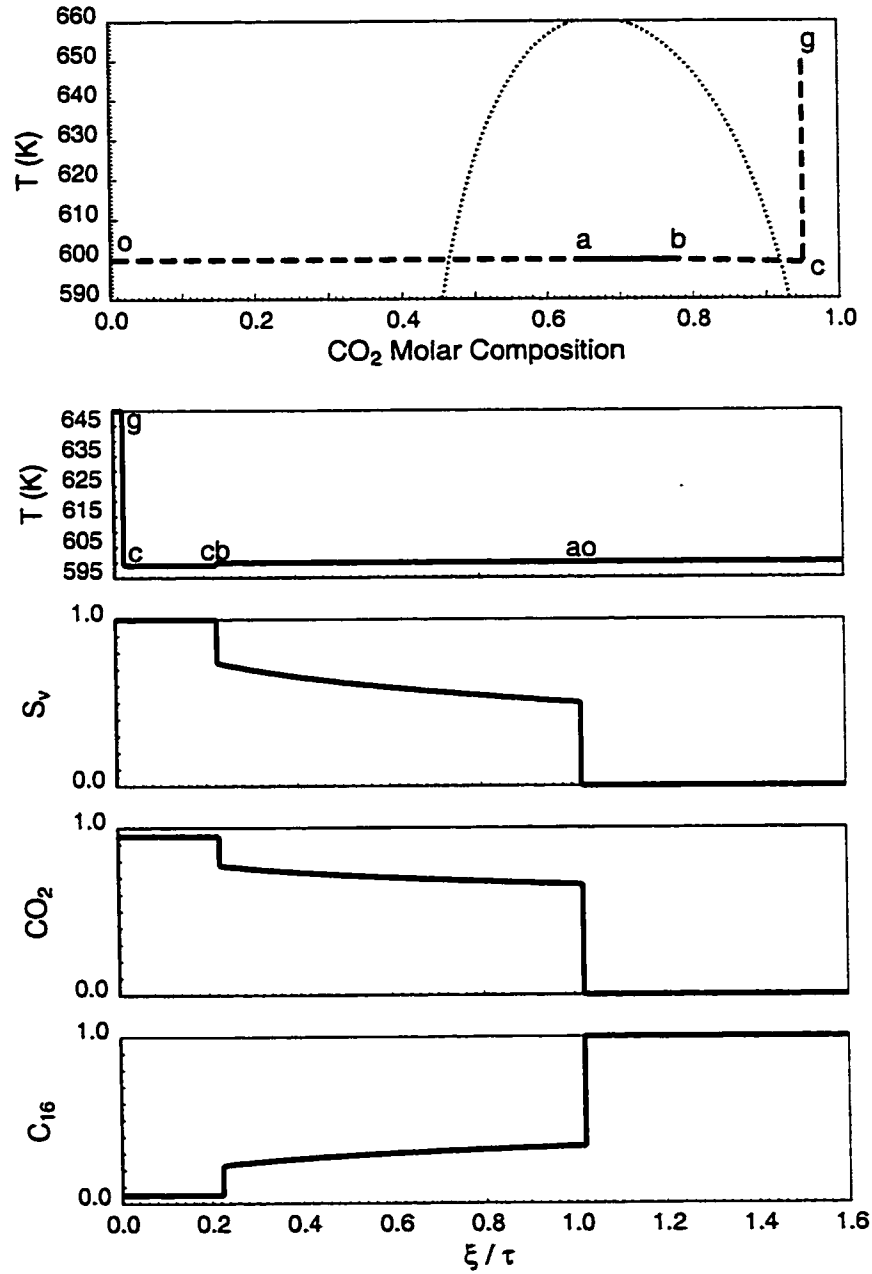


Figure 5.36: A Type I example in the CO_2 - C_{16} system, where the initial oil is pure C_{16} at $600^\circ K$. The injection gas consists of 95% CO_2 and 5% C_{16} at $650^\circ K$.

trailing tangent phase-change shock **cb**.

An extreme case occurs when **c** arrives at the two-phase boundary, as shown in Fig. 5.37. However, since the intermediate mixture **c** is already on the two-phase boundary, a continuous temperature path in the two-phase region may go through this composition and temperature, and lead to the equal-eigenvalue point on the "initial" tie line, as shown in Fig. 5.38. The propagation velocity along the continuous temperature path **ce** in the two-phase region is rather indifferent to the variation of temperature, and remains the same as that of the phase-change shock **cb**. Therefore, the two solutions are effectively identical, as has occurred in Fig. 5.25 and Fig. 5.26.

Type II and Type III solutions take place when the injection gas is further enriched slightly with the heavy component. However, for the CO_2-C_{16} system, the range of values for varying injection composition to have Type II and Type III solutions is so narrow that the difference in solutions is hard to distinguish from computer's round off error during the solution construction process. An extreme case of Type III solution occurs when the continuous variation along two-phase temperature path **ce** is shortened to zero so that the trailing tangent phase-change shock **gb** ends at the "initial" tie line (see Fig. 5.39). Beyond this point, if the injection gas is further enriched, a Type IV solution occurs, as shown in Fig. 5.40. The molar composition of CO_2 in the injection mixtures is 0.9184 for examples in Fig. 5.37 and Fig. 5.38, 0.9180 for example in Fig. 5.39.

5.5 Summary

In this chapter, a detailed study of solutions in single-phase region, two-phase region and solutions across the two-phase boundary is presented. Isothermal paths and temperature paths are found for continuous variations in these regions. When velocity rule is violated, isothermal and temperature shock solutions can be constructed. In general, due to the relatively large rock heat capacity, the continuous variations along isothermal paths and the isothermal shocks propagate faster than the continuous variations along temperature paths and temperature shocks, except when near the equal-eigenvalue points in the two-phase region. The two-phase boundary can be

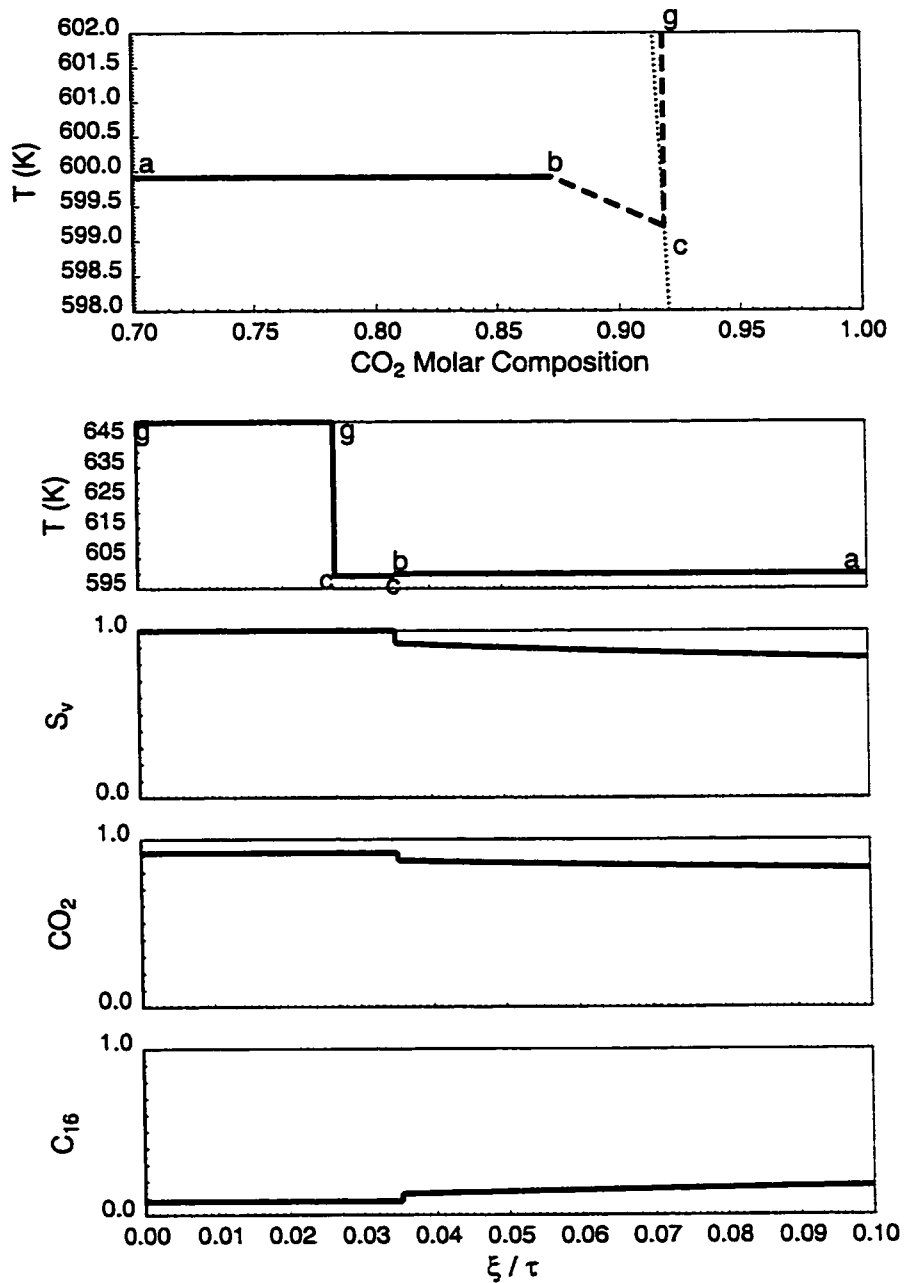


Figure 5.37: A critical case between Type I and Type II in the CO_2 - C_{16} system, where the phase envelope is crossed by a phase-change shock that begins on the phase boundary. The initial gas is pure C_{16} at 600°K . The injection gas is composed of 91.8373% CO_2 and 8.1627% C_{16} at 650°K .

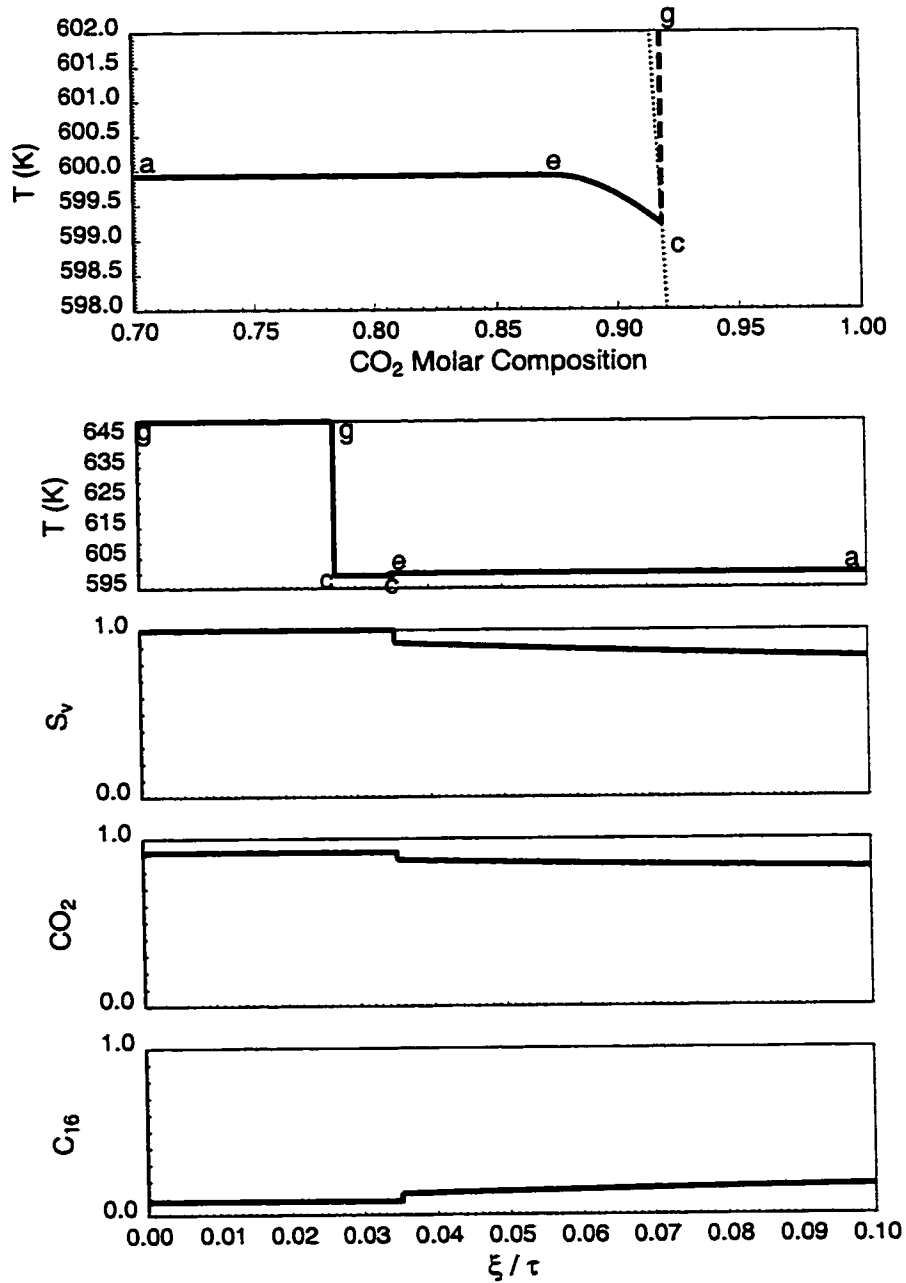


Figure 5.38: A critical case between Type I and Type II in the CO_2-C_{16} system, where the two-phase region is entered by a continuous variation along a temperature path that begins from the two-phase envelope. The initial gas is pure C_{16} at $600^\circ K$. The injection gas is composed of 91.8373% CO_2 and 8.1627% C_{16} at $650^\circ K$.

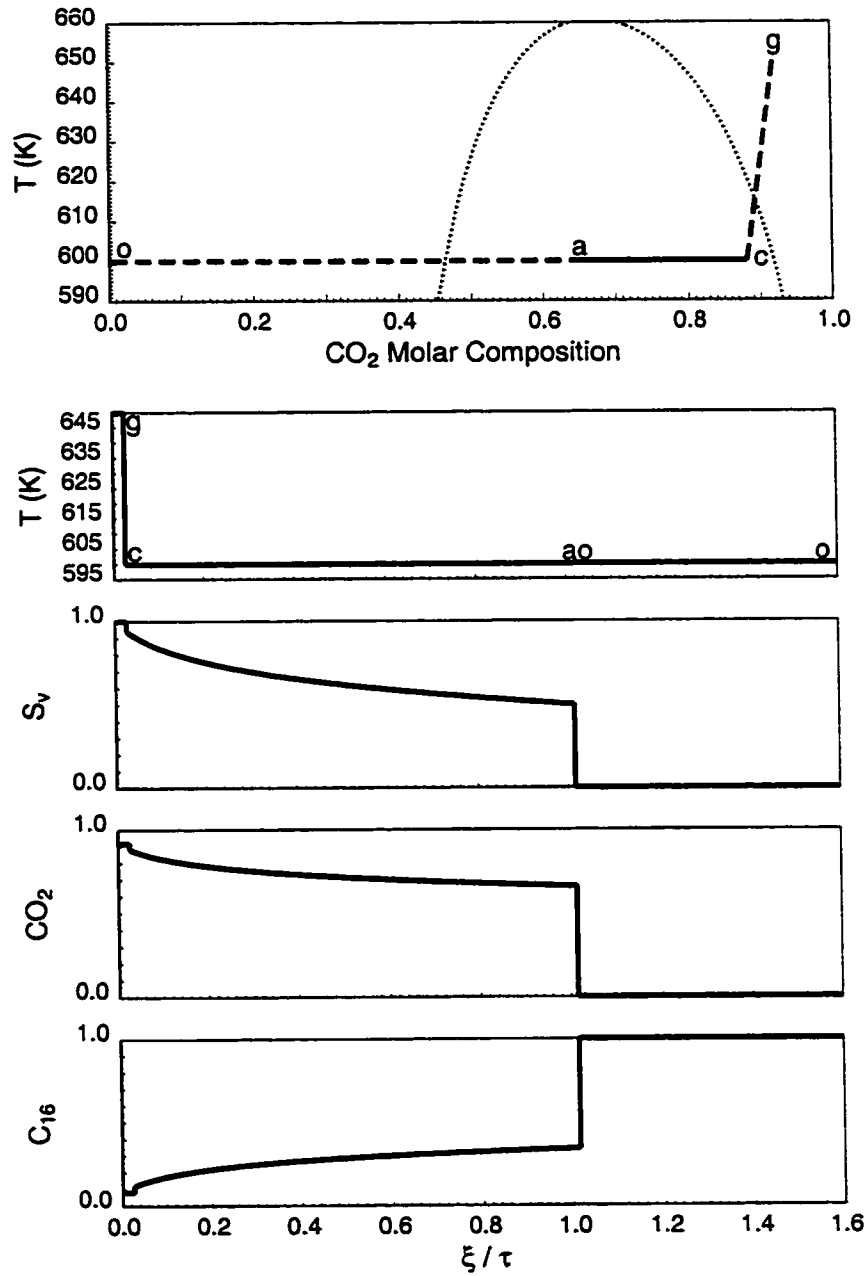


Figure 5.39: A critical case between Type III and Type IV in the CO_2-C_{16} system, where the trailing tangent phase-change shock lands on the “initial” tie line directly. The initial gas is pure C_{16} at $600\text{ }^\circ K$. The injection gas is composed of 91.7981% CO_2 and 8.2029% C_{16} at $650\text{ }^\circ K$.

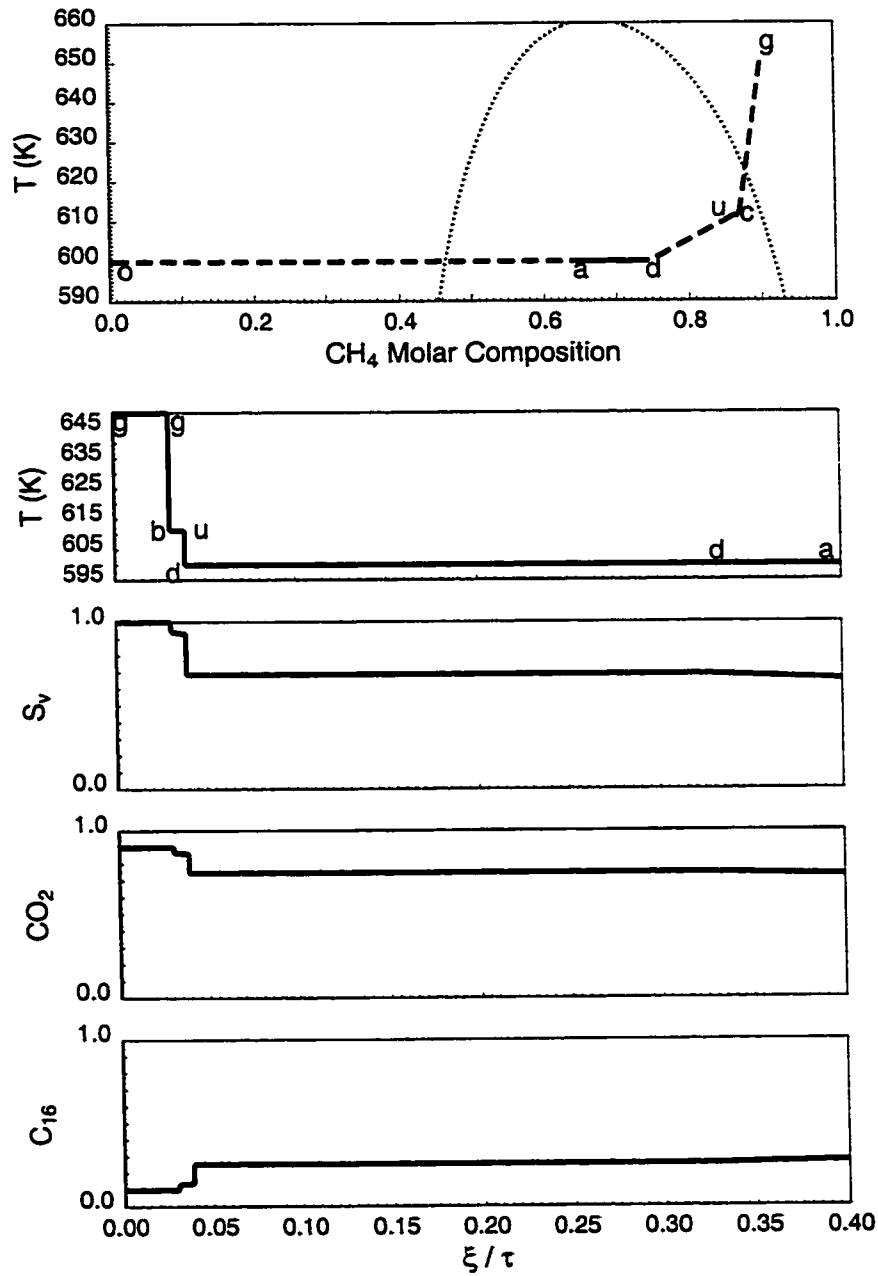


Figure 5.40: A Type IV example in the CO_2 - C_{16} system, where the trailing tangent phase-change shock lands on an intermediate tie line, then to the “initial” tie line via a nontie-line shock within the two-phase region. The initial gas is pure C_{16} at $600^\circ K$. The injection gas is composed of 90% CO_2 and 10% C_{16} at $650^\circ K$.

crossed by phase-change shocks only, and isothermal phase-change shocks travel faster than the temperature ones.

The continuous and discontinuous solutions in the single-phase region, two-phase region, and across the two-phase boundary serve as building blocks for common gas injection problems where the initial mixture is a single-phase liquid, and the injection mixture a single-phase vapor. Dependence of the solution structure on the temperature of the initial mixture and composition of the injection gas was examined exhaustively, which demonstrated a series of four common solution types. The upstream solution segments are affected by the changes in initial and injection conditions most significantly since the changes alter the relative position of the injection mixture to the two-phase boundary, and the upstream waves propagate the slowest. Reducing the rock heat capacity will speed up the continuous variations along the temperature paths and the temperature shocks, and may change the sequence of the upstream solution segments that are affected by temperature variation most significantly.

The analytical solutions reported here are similar to the ternary solutions without temperature variation in a few ways. The tangent phase-change shocks appear in both problems, as do the path switch between temperature path and isothermal path at the equal-eigenvalue point, and the shock solutions between two tie lines. The solutions differ significantly, however, in the effect of heat transport. Heat is different from a third component in that it can be transported by any component in either phase, and absorbed or released from the reservoir rocks. The most significant variation in temperature usually propagates slowly and stay upstream, with the rest of the problem being a nearly isothermal solution along the initial tie line. Thus, there is not always a tie line that corresponds to the injection mixture in problems with temperature variation.

Separation of different gas species can be observed from the analytical solutions. Hence, the coal bed may serve as a chromatograph. When green house gas that primarily consists of CO_2 and N_2 is injected to enhanced the recovery of coal-bed methane, the CO_2 component will be sequestered by the coal bed due to the strong affinity of CO_2 to the coal-bed surface.

Chapter 6

Conclusions and Discussion

This chapter consists of two parts. In the first section, general conclusions are drawn from the work performed on analytical solutions for enhanced coal-bed methane recovery and enhanced oil recovery by gas injection method with temperature variation. In the second section, we discuss possible improvements of the current work and extension of current solution methods to more complicated problems.

6.1 General Conclusions

A general mathematical model was established to describe problems of one-dimensional flow of multicomponent and multiphase mixtures through porous media, including the effects of adsorption and desorption of fluid components at the surface of the solid matrix and temperature variation. Analytical solutions were presented for enhanced recovery of coal-bed methane and oil recovery by gas injection. More specific conclusions are summarized in the following sections.

These analytical solutions can help us better understand the interaction of phase behavior with multiphase flow through porous media. Compared with solutions obtained with finite-difference simulations, the analytical solutions are fast and free of numerical dispersion. The analytical solutions provide us with an opportunity to isolate and investigate certain aspects of the driving mechanism in gas injection processes, and potentially can be used in streamline methods to solve gas injection

problems in three-dimensional models.

6.1.1 Enhanced Recovery of Coal-Bed Methane

A more specific mathematical model for the enhanced recovery of coal-bed methane was derived for the study of adsorption and desorption of gas species at coal bed surfaces. The temperature effect from the general model was not included. An extended Langmuir isotherm was used to describe the adsorption/desorption behavior. The exchange of gas components between the flowing phase and stationary coal bed surfaces resembles that between multiple phases but with phase behavior that is specific to the adsorption problem.

Solutions were constructed for binary systems and ternary systems. Analysis of the structure of the solutions and the results for specific injection gas compositions leads to the following conclusions:

1. A solution may consist of continuous variation and discontinuous solution segments. Along solution path for a continuous variation segment, the propagation velocity of the state variables increases monotonically towards the downstream direction. The discontinuous solution segments must satisfy an entropy condition. All the continuous and discontinuous solution segments are arranged such that the faster moving solution segments stay upstream of slower moving ones.
2. A continuous variation solution segment occurs when a mixture richer with more strongly adsorbing components is downstream and on the solution path for continuous variation that goes through an upstream mixture with less such components.
3. When a gas that is rich in strongly adsorbing components is upstream of a weakly adsorbing gas, a discontinuous, or shock, solution occurs.
4. In ternary system, when an injection gas mainly composed of CO_2 and N_2 displaces an initial gas rich in CH_4 , the total amount of time needed to recover all the CH_4 originally in place is relatively indifferent to the injection gas composition. However, the gas composition at the producing end and the breakthrough

time of the injected gas are affected by the injection composition significantly. An injection gas rich in N_2 leads to a higher initial recovery rate of CH_4 and earlier breakthrough of N_2 .

5. When mixtures of CO_2 and N_2 are used as injection gas for the enhanced coal-bed methane recovery, the separation of CO_2 and N_2 can be observed during the gas injection processes. Effectively, the coal bed can also serve as a chromatograph, and sequester the CO_2 component in the injection gas.

6.1.2 Enhanced Oil Recovery with Temperature Variation

For the enhanced oil recovery problem, temperature is allowed to vary, and the effect of adsorption and desorption is removed from the general mathematical model. Continuous and discontinuous solution segments were sought for single-component system, and single-phase region, two-phase region and across the phase boundary in binary systems respectively. A detailed study of solution patterns is performed in binary systems. It is concluded that

1. For continuous variation along isothermal solution paths and isothermal shocks, the effect of temperature variation is only caused by heat of vaporization and condensation and is small.
2. For continuous variation along temperature paths and temperature shocks, the propagation velocity for the composition and temperature is reduced significantly due to the heat adsorption and desorption by the reservoir rock, which has relatively large heat capacity compared to the reservoir fluids.
3. In the single-phase region and for most of the two-phase region, continuous variations along temperature paths and temperature shocks travel slower than continuous variations along isothermal paths and isothermal shocks. However, near the equal-eigenvalue points in the two-phase region, especially when the two-phase mixture is close to the two-phase boundary, the temperature solution segments, continuous or discontinuous, may have higher propagation velocity than their isothermal counterpart.

4. The two-phase envelope must be crossed by discontinuous solutions, or phase-change shocks. In order to satisfy the entropy condition, the phase-change shocks must be tangent shocks. Two kinds of phase-change shocks can be constructed from a single-phase mixture, the isothermal and temperature phase-change shocks. If the single-phase mixture is a distance away from the two-phase boundary, then the isothermal phase-change shock originated from this single-phase mixture is faster than the temperature phase-change shock. However, when the single-phase mixture gets close to the two-phase boundary, the isothermal phase-change shock becomes slower, while the temperature phase-change shock velocity does not change significantly.
5. Continuous variation along temperature path and temperature shocks may occur in the two-phase region. Similar to isothermal gas injection problems in ternary systems, a nontie-line path (temperature path) may be connected to a tie-line path (isothermal path) at the equal-eigenvalue point. A nontie-line shock (temperature shock) may occur between two tie lines at different temperatures.
6. For binary system with temperature variation, four types of solutions are found. The transitions between different types of solutions can be driven by changes in initial injection compositions, initial temperature, and heat capacity, and ultimately are determined by the relative position of the initial and injection mixtures in the composition space with respect to the two-phase region.
7. For many problems where a single-phase injection gas is chosen with temperature higher than that of the initial reservoir, most of the variation in temperature occurs near the inlet, and propagates very slowly downstream, while most of the displacement is nearly isothermal and travels much faster. When the single-phase injection gas is cooled down to a point in the composition space that is sufficiently close to the two-phase envelope, the trailing near-isothermal phase-change shock may become comparably slow with the trailing temperature shock in the single-phase region, and the variation in temperature may occur across the two-phase envelope.

6.2 Possible Improvements and Future Work

The mathematical models we present here are far from accurately describing the real world, as a number of assumptions and simplifications have been made so an attempt to solve these problem using the analytical approach is possible.

Other than the intrinsic restrictions for the method of characteristics approach to apply, such as limitation of one-dimensional model, constant pressure, homogeneous reservoir rock properties, and constant initial and injection conditions, improvements can still be made to the rest of the assumptions and restrictions, and will be discussed for the coal-bed methane and temperature variation problems respectively.

6.2.1 Enhanced Recovery of Coal-Bed Methane

In this study, only a single gaseous phase is considered. An immediate improvement would be to include an aqueous phase that describe the real reservoir flow more accurately. The difficulties may come from the complexity at describing the the adsorption behavior of a multicomponent multiphase mixture at the coal-bed surfaces, and phase equilibrium calculation when multiphase adsorption is included.

If not adding an additional phase, another improvement that is possible to make is to increase the number of components in the system. Beyond ternary system, the solution paths will be significantly more complicated. However, the solution method remains the same, that is, to seek all the possible continuous and discontinuous solution solution segments, arrange them according to the requirement of velocity rule, and eliminate the non-physical combinations that violates velocity rule, the entropy condition or the continuity condition.

6.2.2 Enhanced Oil Recovery with Temperature Variation

As the solutions with temperature variation have been studied in great detail in binary systems, a natural move is to increase the complexity by attacking gas problems in ternary systems with temperature variation. If the gas injection problems with temperature variation in binary systems are somewhat parallel to isothermal gas

injection problems in ternary systems, regarding flow of heat as a special component, then with ternary systems and temperature variation, it is equivalent to isothermal gas injection problems in quaternary systems. The solution segments can still be divided into continuous and discontinuous, near-isothermal and temperature solution categories. The composition space now becomes three-dimensional, with isothermal ternary diagrams stacked up along a temperature axis.

When there exists a temperature difference between the initial and injection mixtures, the temperature difference will be taken by either a continuous or discontinuous variation across two ternary diagrams at different temperatures, with the downstream solution segments in a ternary diagram near the initial temperature.

The difficulties for this attempt to improve the model mainly focus on solving the phase-change shock, where convergence is more difficult to achieve as the two-phase side may be located at a different plane of unknown temperature and with many tie lines. Analysis of continuous and discontinuous temperature variation within the two-phase region can be also very challenging as the temperature eigenvalues and eigenvectors have an extremely complicated form. While this problem is certainly challenging, it should be possible to perform the analysis using procedures and tools similar to those developed here.

Once the phase-change shocks in a ternary system with temperature variation can be solved with confidence, complete solutions can be constructed with relative ease for Type I solution at least, as most of the temperature difference occurs as temperature variation within the single-phase region, and the propagation of this temperature variation is separated from the downstream near-isothermal solution patterns. Hence, the Type I solution can be constructed as a trailing single-phase temperature shock that varies from the injection composition and temperature to a temperature value near the initial temperature, from where a phase-change shock brings the state variables into the interior of the two-phase region to a ternary plane of slightly different temperature. Isothermal tie line paths solution and nontie-line paths solutions may occur in this ternary diagram that takes the state variables to the "initial" tie line, from where a leading phase-change shock leads to the initial condition with slightly different temperature.

Bibliography

- [1] Arri, L. E., Yee, D., Morgan, W. D., and Jeansonne, WM. W.: "Modeling Coalbed Methane Production with Binary Gas Adsorption," paper SPE 24363 in proceedings of the 1992 SPE Rocky Mountain Regional Meeting, Casper, Wyoming, May 18-21.
- [2] Bell, G. J. and Rakop, K. C.: "Hysteresis of Methane/Coal Sorption Isotherms," paper SPE 15454 in proceedings of the 1986 Annual SPE Technical Conference and Exhibition, New Orleans, LA, October 5-8.
- [3] Chaback, J. J., Morgan, W. D., and Yee, D.: "Sorptions Irreversibilities and Mixture Compositional Behavior during Enhanced Coalbed Methane Recovery Processes," paper SPE 35622 in proceedings of the 1996 Gas Technology Conference, Calgary, Alberta, Canada, April 28 - May 1.
- [4] Dindoruk, B.: *Analytical Theory of Multiphase, Multicomponent Displacement in Porous Media*, PhD dissertation, Stanford University, Stanford, CA (1992).
- [5] Dindoruk, B., Johns, R.T. and Orr, F.M., Jr.: "Analytical Solution for Four Component Gas Displacements with Volume Change on Mixing," (June 1992) Third European Conference on the Mathematics of Oil Recovery, Delft, The Netherlands.
- [6] Dumoré, J.M. Hagoort, J. and Risseuw, A.S.: "An Analytical Model for One-Dimensional, Three-Component Condensing and Vaporizing Gas Drives," *Soc. Pet. Eng. J.* (April 1984) **24**, 169-179.

- [7] Ermakov, P.: "Analytical Solutions for 1D Oil Displacement by Gases," Master's thesis, Stanford University, Stanford, CA (June 2000).
- [8] Fayers, F.J.: "Some Theoretical Results Concerning the Displacement of a Viscous Oil by Hot Fluid in a Porous Medium," *J. Fluid Mechanics* (1962) **13**, 65-76.
- [9] Greaves, K. H., Owen, L. B., McLennan, J. D., and Olszewski, A.: "Multi-Component Gas Adsorption-Desorption Behavior of Coal," Proceedings (May 17-21 1993) International Coalbed Methane Symposium, Birmingham, Alabama.
- [10] Helfferich, F.G.: "Theory of Multicomponent, Multiphase Displacement in Porous Media," *Soc. Pet. Eng. J.* (February 1981) **271**, 51-62.
- [11] Hirasaki, G.J.: "Applications of the Theory of Multicomponent, Multiphase Displacement to Three-Component, Two-Phase Surfactant Flooding," *Soc. Eng. Pet. Eng. J.* (April 1981) 191-204.
- [12] Jessen, K.: *Effective Algorithms for the Study of Miscible Gas Injection Processes*, PhD dissertation, Technical University of Denmark (March 2000).
- [13] Jessen, K. and Orr, F. M., Jr.: "Compositional Streamline Simulation," paper SPE 77379 in proceedings of the 2002 SPE Annual Technical Conference and Exhibition, San Antonio, TX, September 29 - October 2.
- [14] Jessen, K.R., Wang, Y., Ermakov, P., Zhu, J., and Orr, F.M., Jr.: "Fast, Approximate Solutions for 1D Multicomponent Gas Injection Problems," *SPE 56608 SPE Annual Technical Conference and Exhibition, Houston, TX* (October 1999).
- [15] Johansen, T., and Winther, R.: "The Solution of the Riemann Problem for a Hyperbolic System of Conservation Laws Modeling Polymer Flooding," *SIAM J. Math. Anal.* (May 1988) **19**, 541-566.
- [16] Johansen, T., and Winther, R.: "The Riemann Problem for Multicomponent Polymer Flooding," *SIAM J. Math. Anal.* (1989) **20**, 909-929.

- [17] Johns, R.T.: *Analytical Theory of Multicomponent Gas Drives With Two-Phase Mass Transfer*, PhD dissertation, Stanford University, Stanford, CA (1992).
- [18] Johns, R.T., B. Dindoruk, and Orr, F.M., Jr.: "Analytical Theory of Combined Condensing/Vaporizing Gas Drives," *SPE Advanced Technology Series* (May 1993) **1**, No. 2, 7-16.
- [19] Johns, R.T., Fayers, F.J. and Orr, F.M., Jr.: "Effect of Gas Enrichment and Dispersion on Nearly Miscible Displacements in Condensing/Vaporizing Drives," *SPE Advanced Technology Series* (1993) **2**, No. 2, 26-34.
- [20] Lake, L.W.: *Enhanced Oil Recovery*, Prentice Hall, Englewood Cliffs, NJ (1989) 461-467.
- [21] Lake, W.L.: *Enhanced Oil Recovery*, first edition, Prentice Hall, Englewood Cliffs, NJ (1989).
- [22] Larson, R.G.: "The Influence of Phase Behavior on Surfactant Flooding," *Soc. Eng. Pet. Eng. J.* (December 1979) 411-422.
- [23] Larson, R.G., and Hirasaki, G.J.: "Analysis of the Physical Mechanisms in Surfactant Flooding," *Soc. Eng. Pet. Eng. J.* (February 1978) 42-58.
- [24] Lax, P.D.: "Hyperbolic Conservation Laws II," *Comm. Pure and Applied Math.* (1957) **10**, 537-566.
- [25] Lax, P.D.: "Hyperbolic Systems of Conservation Laws and the Mathematical Theory of Shock Waves," paper SPE 11, SIAM in proceedings of the 1973 Regional Conference Series in Applied Mathematics, Philadelphia, PA.
- [26] Markham, E. C. and Benton, A. F.: "The Adsorption of Gas Mixtures by Silica," *Journal of American Chemistry Society* (1931) **53**, 497-507.
- [27] Monroe, W.W., Silva, M.K., Larsen, L.L. and Orr, F.M., Jr.: "Composition Paths in Four-Component Systems: Effect of Dissolved Methane on 1D CO_2 Flood Performance," *SPE Reservoir Engineering* (1990) **5**, 423-432.

- [28] Orr, F.M., Jr., Johns, R.T. and Dindoruk, B.: "Development of Miscibility in Four-Component CO_2 Floods," *SPE Reservoir Engineering* (1993) **8**, No. 28, 135-142.
- [29] Passut, C.A. and Danner, R.P.: "Correlation of Ideal Gas Enthalpy, Heat Capacity, and Entropy," *Ind. Eng. Chem. Process Des. Develop.* (1972) **11**, No. 4, 543-546.
- [30] Peng, D.Y. and Robinson, D.B.: "A New Two-Constant Equation of State," *Ind. Eng. Chem. Fund.* (1976) **15**, 59-64.
- [31] Prats, M.: *Thermal Recovery*, Henry L. Doherty Memorial Fund of AIME, Society of Petroleum Engineers of AIME (1982) 226-232.
- [32] Ruppel, T. C., Grein, C. T., and Bienstock, D.: "Adsorption of Methane on Dry Coal at Elevated Pressure," *Fuel* (July 1974) **53**, 152-162.
- [33] Saunders, J. T., Benjamin, M. C., and Yang, R.: "Adsorption of Gases on Coals and Heat-Treated Coals at Elevated Temperature and Pressure: Adsorption from Hydrogen-Methane Mixture," *Fuel* (July 1985) **64**, 621-626.
- [34] Shutler, N.D., and Boberg, T.C.: "A One-Dimensional Analytical Technique for Predicting Oil Recovery by Steamflooding," *Soc. Pet. Eng. J.* (December 1972) 489-498.
- [35] Stevens, S. H., Spector, D., and Riemer, P.: "Enhanced Coalbed Methane Recovery Using CO_2 Injection: Worldwide Resource and CO_2 Sequestration Potential," paper SPE 48881 in proceedings of the 1998 SPE International Conference and Exhibition, Beijing, China, November 2-6.
- [36] Wachmann, C: "The Mathematical Theory for the Displacement of Oil and Water by Alcohol," *Soc. Pet. Eng. J.* (September 1964) **231**, 250-266.
- [37] Wang, Y. and Orr, F.M., Jr.: "Analytical Calculation of Minimum Miscibility Pressure," *Fluid Phase Equilibrium* (1997) **139**, 101-124.

- [38] Wang, Y. and Orr, F.M., Jr.: "Calculation of Minimum Miscibility Pressure," *SPE 39683 presented at the 1998 SPE/DOE Symposium on Improved Oil Recovery, Tulsa, OK* (April 1998) 19–22.
- [39] Welge, H.J., Johnson, E.F., Ewing, S.P., Jr., and Brinkman, F.H.: "The Linear Displacement of Oil from Porous Media by Enriched Gas," *J. Pet. Tech.* (1961) **13**, 787–796.
- [40] Wingard, J.S.: *Multicomponent, Multiphase Flow in Porous Media with Temperature Variation*, PhD dissertation, Stanford University, Stanford, CA (November 1988).
- [41] Wingard, J.S. and Orr, F.M., Jr.: "An Analytical Solution for Steam/Oil/Water Displacement," *SPE Advanced Technology Series* (1994) **2**, No. 2, 167–176.

Appendix A

Miscellaneous Proofs and Derivations

A.1 Shock Solution in the Single-Phase Region of Binary Systems

Shock solutions in the single-phase region can only occur either as an isothermal shock or as a pure temperature shock without compositional variation. To prove this, we first assume that across a shock that is completely within the single-phase region, both temperature and composition are different, *i.e.*,

$$z_i^u \neq z_i^d, \quad (\text{A.1})$$

$$T^u \neq T^d. \quad (\text{A.2})$$

The Rankine-Hugoniot condition states a mass balance across the shock as

$$\Lambda_m = \frac{u^u \rho^u z_1^u - u^d \rho^d z_1^d}{\rho^u z_1^u - \rho^d z_1^d} = \frac{u^u \rho^u z_2^u - u^d \rho^d z_2^d}{\rho^u z_2^u - \rho^d z_2^d}. \quad (\text{A.3})$$

In a binary system, we have

$$z_2^u = 1 - z_1^u, \quad (\text{A.4})$$

$$z_2^d = 1 - z_1^d. \quad (\text{A.5})$$

Therefore,

$$\Lambda_m = \frac{u^u \rho^u z_1^u - u^d \rho^d z_1^d}{\rho^u z_1^u - \rho^d z_1^d} = \frac{(u^u \rho^u - u^d \rho^d) - (u^u \rho^u z_1^u - u^d \rho^d z_1^d)}{(\rho^u - \rho^d) - (\rho^u z_1^u - \rho^d z_1^d)}, \quad (\text{A.6})$$

which can be simplified to

$$\begin{aligned} \Lambda_m &= \frac{u^u \rho^u - u^d \rho^d}{\rho^u - \rho^d} \\ &= \frac{u^u \rho^u z_1^u - u^d \rho^d z_1^d}{\rho^u z_1^u - \rho^d z_1^d}. \end{aligned} \quad (\text{A.7})$$

By further simplification, we have

$$z_1^u (u^u - u^d) = z_1^d (u^u - u^d). \quad (\text{A.8})$$

Since $z_1^u \neq z_1^d$ by our assumption, we have

$$u^u = u^d. \quad (\text{A.9})$$

Substitution of u^d in the expression for mass shock velocity gives

$$\Lambda_m = u^u = u^d. \quad (\text{A.10})$$

On the other hand, the Rankine-Hugoniot condition also states conservation of energy as

$$\Lambda_m = \Lambda_h = u^u = u^d = \frac{u^u \rho^u h^u - u^d \rho^d h^d}{\rho^u h^u - \rho^d h^d + \rho_r C_{pr} (T^u - T^d)}, \quad (\text{A.11})$$

which yields

$$T^u = T^d. \quad (\text{A.12})$$

This conclusion contradicts with the assumption $T^u \neq T^d$. Therefore, it is invalid to assume that across a single-phase shock, both temperature and composition are

different. A single-phase shock must occur either along a constant temperature direction, which will be called an isothermal shock, or along a constant composition direction, a temperature shock.

A.2 Continuous Variation in the Two-Phase Region of Binary Systems

The eigenvalue problem represented by Eq. 2.55 becomes

$$[F - \lambda^* G] = 0 = \left[\begin{array}{l} \left(\frac{df^v}{dS^v} - \lambda^* \right) \frac{\partial S^v}{\partial Z_1} \\ \left[\begin{array}{l} (y_1 \rho^v - x_1 \rho^l) - \\ \frac{\alpha_1}{\beta} (\rho^v H^v - \rho^l H^l) \end{array} \right] \\ \\ \left(\frac{df^v}{dS^v} - \lambda^* \right) \frac{\partial S^v}{\partial Z_1} \\ \left[\begin{array}{l} (y_2 \rho^v - x_2 \rho^l) - \\ \frac{\alpha_2}{\beta} (\rho^v H^v - \rho^l H^l) \end{array} \right] \end{array} \right] \left[\begin{array}{l} (f^l - \lambda^* S^l) \left[\begin{array}{l} \frac{\partial(x_1 \rho^l)}{\partial T} - \\ \frac{\alpha_1}{\beta} \frac{\partial(\rho^l H^l)}{\partial T} \end{array} \right] + \\ (f^v - \lambda^* S^v) \left[\begin{array}{l} \frac{\partial(y_1 \rho^v)}{\partial T} - \\ \frac{\alpha_1}{\beta} \frac{\partial(\rho^v H^v)}{\partial T} \end{array} \right] + \\ \lambda^* \frac{\alpha_1}{\beta} \frac{1-\phi}{\phi} \rho_m C_{pm} \\ \\ (f^l - \lambda^* S^l) \left[\begin{array}{l} \frac{\partial(x_2 \rho^l)}{\partial T} - \\ \frac{\alpha_2}{\beta} \frac{\partial(\rho^l H^l)}{\partial T} \end{array} \right] + \\ (f^v - \lambda^* S^v) \left[\begin{array}{l} \frac{\partial(y_2 \rho^v)}{\partial T} - \\ \frac{\alpha_2}{\beta} \frac{\partial(\rho^v H^v)}{\partial T} \end{array} \right] + \\ \lambda^* \frac{\alpha_2}{\beta} \frac{1-\phi}{\phi} \rho_m C_{pm} \end{array} \right] \quad (A.13)$$

One of the eigenvalues is

$$\lambda_t^* = \frac{df^v}{dS^v}, \quad (A.14)$$

with a corresponding eigenvector

$$\left[\begin{array}{l} \frac{dZ_1}{d\eta} \\ \frac{dT}{d\eta} \end{array} \right] = \left[\begin{array}{l} 1 \\ 0 \end{array} \right], \quad (A.15)$$

which indicates a direction where the temperature remains constant, a tie-line in the binary system. We call this eigenvalue the isothermal eigenvalue and its corresponding

eigenvector the isothermal eigenvector.

The other eigenvalue λ_T , which we call temperature eigenvalue, can be solved from

$$\left| \begin{array}{l} \left[\begin{array}{l} (y_1 \rho^v - x_1 \rho^l) - \\ \frac{\alpha_1}{\beta} (\rho^v H^v - \rho^l H^l) \end{array} \right] \begin{array}{l} (f^l - \lambda^* S^l) \left[\begin{array}{l} \frac{\partial(x_1 \rho^l)}{\partial T} - \\ \frac{\alpha_1}{\beta} \frac{\partial(\rho^l H^l)}{\partial T} \end{array} \right] + \\ (f^v - \lambda^* S^v) \left[\begin{array}{l} \frac{\partial(y_1 \rho^v)}{\partial T} - \\ \frac{\alpha_1}{\beta} \frac{\partial(\rho^v H^v)}{\partial T} \end{array} \right] + \\ \lambda^* \frac{\alpha_1}{\beta} \frac{1-\phi}{\phi} \rho_m C_{pm} \end{array} \right. \\ \left. \left[\begin{array}{l} (y_2 \rho^v - x_2 \rho^l) - \\ \frac{\alpha_2}{\beta} (\rho^v H^v - \rho^l H^l) \end{array} \right] \begin{array}{l} (f^l - \lambda^* S^l) \left[\begin{array}{l} \frac{\partial(x_2 \rho^l)}{\partial T} - \\ \frac{\alpha_2}{\beta} \frac{\partial(\rho^l H^l)}{\partial T} \end{array} \right] + \\ (f^v - \lambda^* S^v) \left[\begin{array}{l} \frac{\partial(y_2 \rho^v)}{\partial T} - \\ \frac{\alpha_2}{\beta} \frac{\partial(\rho^v H^v)}{\partial T} \end{array} \right] + \\ \lambda^* \frac{\alpha_2}{\beta} \frac{1-\phi}{\phi} \rho_m C_{pm} \end{array} \right. \end{array} \right| = 0 \quad (\text{A.16})$$

Define the following variables pertinent to a given tie-line:

$$A_1 = y_1 \rho^v - x_1 \rho^l, \quad (\text{A.17})$$

$$A_2 = y_2 \rho^v - x_2 \rho^l, \quad (\text{A.18})$$

$$B = \rho^v H^v - \rho^l H^l, \quad (\text{A.19})$$

$$C_1^l = \frac{\partial(x_1 \rho^l)}{\partial T}, \quad (\text{A.20})$$

$$C_1^v = \frac{\partial(y_1 \rho^v)}{\partial T}, \quad (\text{A.21})$$

$$C_2^l = \frac{\partial(x_2 \rho^l)}{\partial T}, \quad (\text{A.22})$$

$$C_2^v = \frac{\partial(y_2 \rho^v)}{\partial T}, \quad (\text{A.23})$$

$$D^l = \frac{\partial(\rho^l H^l)}{\partial T}, \quad (\text{A.24})$$

$$D^v = \frac{\partial(\rho^v H^v)}{\partial T}, \quad (\text{A.25})$$

$$E = \frac{1-\phi}{\phi} \rho_m C_{pm}, \quad (\text{A.26})$$

and the variables pertinent to a given composition on the given tie-line:

$$F_1 = \frac{\alpha_1}{\beta}, \quad (\text{A.27})$$

$$F_2 = \frac{\alpha_2}{\beta}, \quad (\text{A.28})$$

Then we have

$$\begin{vmatrix} A_1 - F_1 B & (f^l - \lambda^* S^l)(C_1^l - F_1 D^l) + \\ & (f^v - \lambda^* S^v)(C_1^v - F_1 D^v) + \\ & \lambda^* F_1 E \\ A_2 - F_2 B & (f^l - \lambda^* S^l)(C_2^l - F_2 D^l) + \\ & (f^v - \lambda^* S^v)(C_2^v - F_2 D^v) + \\ & \lambda^* F_2 E \end{vmatrix} = 0. \quad (\text{A.29})$$

Expansion of the determinant gives

$$\begin{aligned} & (f^l - \lambda^* S^l) [(C_2^l A_1 - C_1^l A_2) + F_1(D^l A_2 - C_2^l B) - F_2(D^l A_1 - C_1^l B)] \\ & + (f^v - \lambda^* S^v) [(C_2^v A_1 - C_1^v A_2) + F_1(D^v A_2 - C_2^v B) - F_2(D^v A_1 - C_1^v B)] \\ & + \lambda^* E(F_2 A_1 - F_1 A_2) = 0. \end{aligned} \quad (\text{A.30})$$

Define

$$G^l = (C_2^l A_1 - C_1^l A_2) + F_1(D^l A_2 - C_2^l B) - F_2(D^l A_1 - C_1^l B), \quad (\text{A.31})$$

$$G^v = (C_2^v A_1 - C_1^v A_2) + F_1(D^v A_2 - C_2^v B) - F_2(D^v A_1 - C_1^v B), \quad (\text{A.32})$$

$$H = E(F_2 A_1 - F_1 A_2). \quad (\text{A.33})$$

Then

$$\lambda^* = \frac{f^l G^l + f^v G^v}{S^l G^l + S^v G^v - H}. \quad (\text{A.34})$$

A.3 Isothermal Shock in the Two-Phase Region of Binary Systems

Consider an isothermal shock in the two-phase region of a binary system. The shock occurs along a tie line. It satisfies conservation of mass and energy in an integral form, *i.e.*, a Rankine-Hugoniot condition,

$$\Lambda_M = \frac{F_i^u - F_i^d}{G_i^u - G_i^d}, \quad i = 1, 2 \quad (\text{A.35})$$

$$\Lambda_H = \frac{\Theta^u - \Theta^d}{\Gamma^u - \Gamma^d}, \quad (\text{A.36})$$

where the superscripts “u” and “d” stand for upstream and downstream conditions of the shock.

Substitution of the definition for the flux and concentration terms for mass and energy,

$$F_i = u(\rho_l x_i f_l + \rho_v y_i f_v), \quad (\text{A.37})$$

$$G_i = \rho_l x_i S_l + \rho_v y_i S_v, \quad (\text{A.38})$$

$$\Theta = u(\rho_l h_l f_l + \rho_v h_v f_v), \quad (\text{A.39})$$

$$\Gamma = \rho_l h_l S_l + \rho_v h_v S_v, \quad (\text{A.40})$$

yields

$$\Gamma_M = \frac{u^u f_l^u - u^d f_l^d}{S_l^u - S_l^d} + \frac{y_i}{\rho_l x_i - \rho_v y_i} \frac{\rho_v (u^u - u^d)}{S_l^u - S_l^d}. \quad (\text{A.41})$$

If the local flow velocity varies across the isothermal shock, *i.e.*,

$$u^u \neq u^d, \quad (\text{A.42})$$

then for component 1 and 2 in the binary system, we have

$$\frac{y_1}{\rho_l x_1 - \rho_v y_1} = \frac{y_2}{\rho_l x_2 - \rho_v y_2} = \frac{1 - y_1}{(\rho_l - \rho_v) - (\rho_l x_1 - \rho_v y_1)} = \frac{1}{\rho_l - \rho_v}, \quad (\text{A.43})$$

which leads to

$$x_l = y_l. \quad (\text{A.44})$$

This is a conclusion that requires a zero-length tie line. Therefore, it is invalid to assume that across an isothermal shock in the two-phase region, the local flow velocity varies. Thus the shock velocity according to conservation of mass across the shock is

$$\Lambda_M = u \frac{f_l^u - f_l^d}{S_l^u - S_l^d} = \Lambda_H. \quad (\text{A.45})$$

A.4 Solving Temperature Shocks

Recall the definition for molar concentration for the components and enthalpy as

$$G_i = \rho_l x_i S_l + \rho_v y_i S_v, \quad (\text{A.46})$$

$$F_i = u \alpha_i, \quad (\text{A.47})$$

$$\Gamma = \rho_l H_l S_l + \rho_v H_v S_v + \frac{1 - \phi}{\phi} \rho_m C_{pm} \Delta T, \quad (\text{A.48})$$

$$\Theta = u \beta, \quad (\text{A.49})$$

where

$$\alpha_i = \rho_l x_i f_l + \rho_v y_i f_v, \quad (\text{A.50})$$

$$\beta = \rho_l H_l S_l + \rho_v H_v S_v. \quad (\text{A.51})$$

The Rankine-Hugoniot condition for binary systems states

$$\frac{u^u \alpha_1^u - u^d \alpha_1^d}{G_1^u - G_1^d} = \frac{u^u \alpha_2^u - u^d \alpha_2^d}{G_2^u - G_2^d}, \quad (\text{A.52})$$

$$\frac{u^u \alpha_1^u - u^d \alpha_1^d}{G_1^u - G_1^d} = \frac{u^u \beta^u - u^d \beta^d}{\Gamma^u - \Gamma^d}, \quad (\text{A.53})$$

where the superscript “u” stands for the upstream condition of the shock, and the superscript “d” the downstream condition.

We assume that all the variables upstream of the shock are known. The unknowns that remain to be solved are vapor phase saturation, S_v^d , and local flow velocity, u^d , downstream of the shock. One way to solve the problem is by using the Newton-Ralpson method. Objective functions can be formulated from the Rankine-Hugoniot conditions as

$$\mathcal{F}_1(S_v^d, u^d) = \frac{F_1^u - F_1^d}{G_1^u - G_1^d} - \frac{F_2^u - F_2^d}{G_2^u - G_2^d}, \quad (\text{A.54})$$

$$\mathcal{F}_2(S_v^d, u^d) = \frac{F_1^u - F_1^d}{G_1^u - G_1^d} - \frac{\Theta^u - \Theta^d}{\Gamma^u - \Gamma^d}. \quad (\text{A.55})$$

For each iteration, the following system must be solved,

$$\begin{pmatrix} \frac{\partial \mathcal{F}_1}{\partial S_v^d} & \frac{\partial \mathcal{F}_1}{\partial u^d} \\ \frac{\partial \mathcal{F}_2}{\partial S_v^d} & \frac{\partial \mathcal{F}_2}{\partial u^d} \end{pmatrix} \begin{pmatrix} \Delta S_v^d \\ \Delta u^d \end{pmatrix} = - \begin{pmatrix} \mathcal{F}_1 \\ \mathcal{F}_2 \end{pmatrix}, \quad (\text{A.56})$$

where the Jacobian matrix can be evaluated as

$$\begin{aligned} \frac{\partial \mathcal{F}_1}{\partial S_v^d} &= -\frac{1}{G_1^u - G_1^d} \frac{\partial F_1^d}{\partial S_v^d} + \frac{F_1^u - F_1^d}{(G_1^u - G_1^d)^2} \frac{\partial G_1^d}{\partial S_v^d} \\ &\quad + \frac{1}{G_2^u - G_2^d} \frac{\partial F_2^d}{\partial S_v^d} - \frac{F_2^u - F_2^d}{(G_2^u - G_2^d)^2} \frac{\partial G_2^d}{\partial S_v^d}, \end{aligned} \quad (\text{A.57})$$

$$\begin{aligned} \frac{\partial \mathcal{F}_1}{\partial S_v^d} &= -\frac{1}{G_1^u - G_1^d} \frac{\partial F_1^d}{\partial S_v^d} + \frac{F_1^u - F_1^d}{(G_1^u - G_1^d)^2} \frac{\partial G_1^d}{\partial S_v^d} \\ &\quad + \frac{1}{\Gamma^u - \Gamma^d} \frac{\partial \Theta^d}{\partial S_v^d} - \frac{\Theta^u - \Theta^d}{(\Gamma^u - \Gamma^d)^2} \frac{\partial \Gamma^d}{\partial S_v^d}, \end{aligned} \quad (\text{A.58})$$

$$\frac{\partial \mathcal{F}_1}{\partial u^d} = -\frac{\alpha_1^d}{G_1^u - G_1^d} + \frac{\alpha_2^d}{G_2^u - G_2^d}, \quad (\text{A.59})$$

$$\frac{\partial \mathcal{F}_2}{\partial u^d} = -\frac{\alpha_1^d}{G_1^u - G_1^d} + \frac{\beta^d}{\Gamma^u - \Gamma^d}. \quad (\text{A.60})$$